Analysis of the Wake of Tandem Floating Wind Turbines

Suzanne Hendriks

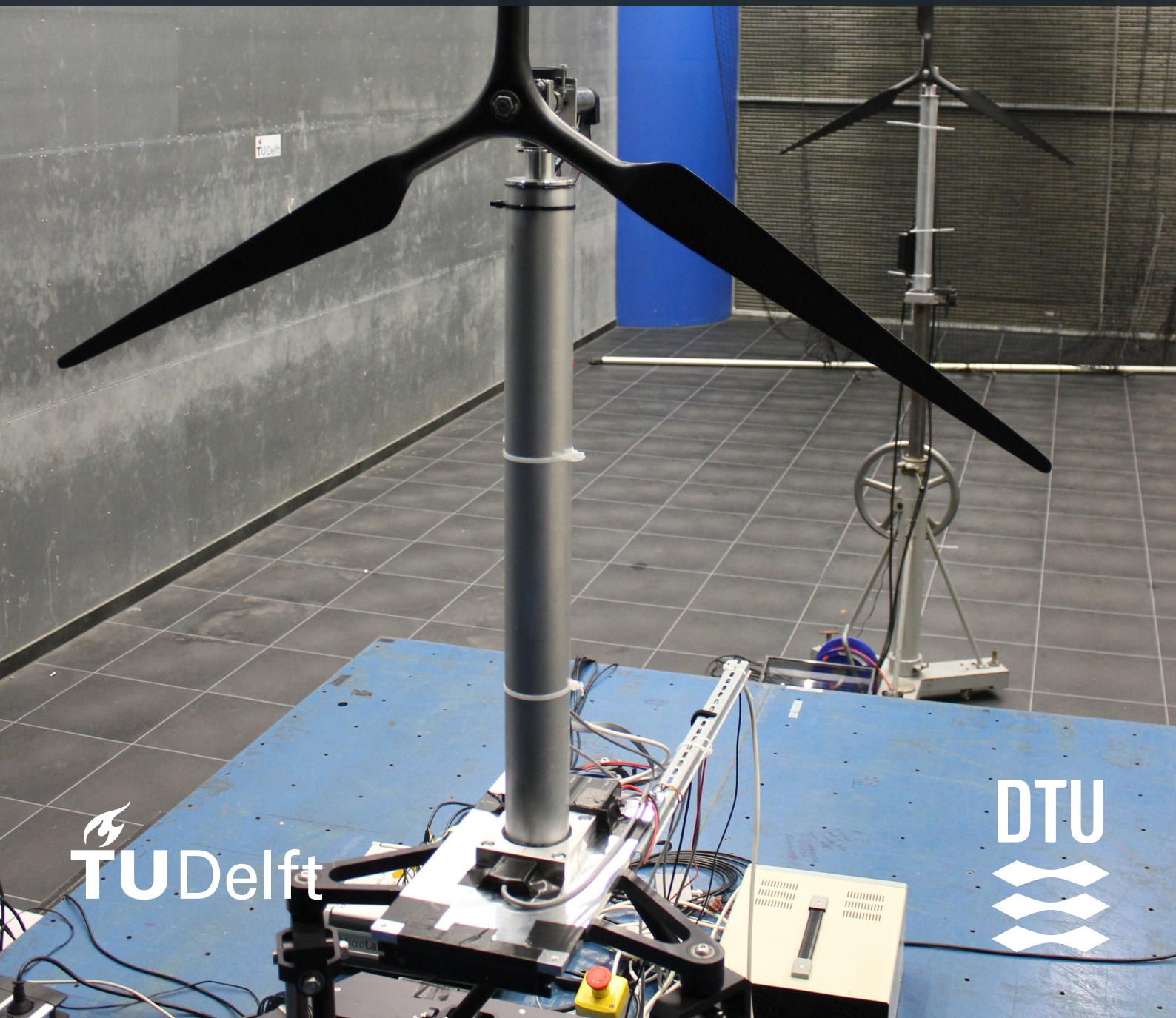

TU Delft

DTU

Analysis of the Wake of Tandem Floating Wind Turbines

Thesis report

by

Suzanne Hendriks

to obtain the degree of Master of Science
at the Delft University of Technology and
at Technical University of Denmark
to be defended publicly on 27 September 2024 at 14:30

Thesis committee:

Chair:	Daniele Ragni
Supervisors:	Axelle Viré
	Knud Erik Meyer
	Federico Taruffi
External examiner:	Simon Watson
Place:	Faculty of Aerospace Engineering, Delft
Project Duration:	November, 2023 – September, 2024
Student number TU Delft:	4831357
Student number DTU:	s223689

An electronic version of this thesis is available at `http://repository.tudelft.nl/`.

Faculty of Aerospace Engineering · Delft University of Technology
Department of Civil and Mechanical Engineering · Technical University of Denmark

Copyright © Suzanne Hendriks, 2024
All rights reserved.

Abstract

In this thesis, the effect of a surging and pitching motion of a floating wind turbine on its wake as well as the effect of a surging, pitching and yawing motion on a stationary downstream turbine are analysed. Two experiments are conducted in order to address both points. The turbine models used are scale models of the DTU 10 MW turbine, and the upstream turbine is placed onto a kinematic robot which can move in all 6 degrees of freedom. The first objective is studied using Particle Tracking Velocimetry and the second objective using load cell measurements. It is found that pitch has a larger effect on the flow field in the wake than surge and that the effects of low frequency motion are more visible than those of high frequency motion. Moreover, it is found that the tracing particles are concentrated in specific areas, affecting the accuracy of the results. In future research, it should be examined why this is the case and how it can be improved. Additionally, low frequency pitch and surge had the greatest effect on the loads. A clear sinusoidal motion is visible and the mean thrust, torque, and power is increased. The effect of the high frequency motions is not visible in the results. In future studies, the wake behind a downstream turbine can also be examined using Particle Tracking Velocimetry. Moreover, the downstream turbine can also be moving rather than standing still and more movements of the turbine can be examined.

Summary

Increasing the amount of energy obtained from renewable energy sources, such as solar and wind power, is necessary to help limit the increase in global temperature. Offshore wind energy plays a big role in this, however, there is not enough shallow water available where stationary wind turbines can be placed. Therefore, floating wind turbines can be used to reach this target, as these can be placed in deep water.

By switching to floating wind turbines, the traditional offshore wind farm design gains a dynamic component. The two most significant motions for platforms housing Floating Offshore Wind Turbines (FOWTs) are acknowledged to be pitch and surge [1]. These motions alter the forces acting on the turbine, as well as its wake. When designing a wind farm, it is relevant to know what the effect of the wakes of wind turbines are.

To study these effects, two main research questions are created: *What does the flow field in the wake of a turbine look like when it is moving with a sinusoidal pitch or a sinusoidal surge motion?* and *How does applying surge, pitch, and yaw to the upstream turbine impact the loads on the downstream turbine?* To answer the first research question, a Particle Tracking Velocimetry set-up is created. The turbine is placed onto a kinematic robot, which is able to move in all 6 Degrees of Freedom (DoF). Helium Filled Soap Bubbles (HFSB) are added to the flow as tracer particles and two Light Emitting Diode (LED) lights are used to illuminate them. DaVIS10 is used for both the recording and post-processing of the tests. To answer the second research question, a second turbine is placed behind the original turbine. The second turbine is identical to the first turbine, but it is placed onto a static stand rather than a kinematic robot. The turbine is positioned at various locations downstream, varying both the downstream and lateral locations. The loads are measured with a load cell.

It was found that pitch has a larger effect on the flow field in the wake than surge and that the effects of low frequency motion are more visible than those of high frequency motion. Moreover, it is found that the tracing particles are concentrated in specific areas, affecting the accuracy of the results. In future research, it should be examined why this is the case and how it can be improved.
Additionally, low frequency pitch and surge have the greatest effect on the loads. A clear sinusoidal motion is visible and the mean thrust, torque, and power are increased. The effect in the case of low frequency yaw motion was less, but still present. The effect of the high frequency motions is not visible in the results.

In future studies, the wake behind a downstream turbine can also be examined using Particle Tracking Velocimetry (PTV). Moreover, the downstream turbine can also be moving rather than standing still and more movements of the turbine can be examined.

All in all, the thesis provides a start for further research into the wakes of floating wind turbines.

Acknowledgements

I would like to thank my supervisors, Federico Taruffi, Knud Erik Meyer and Axelle Viré for their support, knowledge, and guidance during my thesis.
Moreover, I would like to thank Peter Duyndam for helping in the wind tunnel and Hasse Dekker for answering my questions regarding DaVIS10.
Lastly, I would like to thank my friends and family for their support.

Suzanne Hendriks
Delft, September 2024

Contents

Nomenclature

$\boldsymbol{B}$ Number of Blades 6

$\boldsymbol{C_T}$ Thrust Constant 5

$\boldsymbol{C_d}$ Drag Coefficient 5

$\boldsymbol{C_l}$ Lift Coefficient 5

$\boldsymbol{C_n}$ Normal Coefficient 5

$\boldsymbol{C_t}$ Tangential Coefficient 5

D Rotor Diameters 2, 3, 6–9, 20, 22, 28, 30, 33, 39, 40, 64, 70, 71, 78, 79, 81

$\boldsymbol{F}$ Prandtl's tip loss correction 5, 6

$\boldsymbol{M_r}$ Moment 6

$\boldsymbol{N}$ Number of Particles 55

$\boldsymbol{P}$ Power 6

$\boldsymbol{T}$ Thrust 6

V Wind Speed 2, 4, 28

V_{rel} Relative Wind Speed 5

α Angle of Attack 4, 5

β Twist Angle 4, 5

$\frac{\boldsymbol{\Delta V}}{\boldsymbol{U_0}}$ Normalized velocity variation 22, 28

ω Rotational Speed 4, 6

$\overline{\boldsymbol{x}}$ Mean 55

ϕ Flow Angle 4, 5

$\boldsymbol{\rho}$ Density 5

$\boldsymbol{a'}$ Axial Induction factor 5

$\boldsymbol{a}$ Induction factor 5

$\boldsymbol{c}$ Chord 5

$\boldsymbol{d}$ Drag 5

$\boldsymbol{l}$ Lift 5

$\boldsymbol{p_n}$ Normal Force 5, 6

$\boldsymbol{p_t}$ Tangential Force 5, 6

p pressure 2

$\boldsymbol{r}$ radial position 6

$\boldsymbol{s}(\overline{\boldsymbol{x}})$ Standard Deviation 55

Abbreviations

CFD Computational Fluid Dynamics 9, 80

DNS Direct Numerical Simulation 9

DoF Degrees of Freedom iii, 6, 7, 18, 28, 33, 77, 80, 81

f Frequency 22, 28, 33

FOV Field of View 14, 18–20, 24, 79

FOWT Floating Offshore Wind Turbine iii, 1, 4, 6, 7, 13

HAWT Horizontal Axis Wind Turbine 1

HFSB Helium Filled Soap Bubbles iii, 1, 6, 8, 9, 13, 17, 22, 77

HWA Hot Wire Anemometry 8

IM In Plane Motion 22, 28, 33

IPR Iterative Reconstruction of Volumetric Particle Distribution 12

LED Light Emitting Diode iii, 9, 17–19, 21, 23, 25, 46, 78, 80

NREL National Renewable Energy Laboratory 6, 7

OJF Open Jet Facility 14

PIV Particle Image Velocimetry 7–12, 17

PSD Power Spectral Density 34, 65, 75

PTV Particle Tracking Velocimetry iii, ix, xxi, 1, 12–14, 18, 19, 21, 22, 28, 34, 77, 79

R Rated 30, 33

RPM Radians per Minute 28, 45

SPIV Stereoscopic Particle Image Velocimetry 8, 11

STB Shake the Box 12, 13, 21, 26

TSR Tip Speed Ratio 6, 59

VAWT Vertical Axis Wind Turbine 1

WTM Wind Turbine Model 14, 33

List of Figures

List of Tables

1

Introduction

In 2015, 196 parties adopted the Paris Agreement. The goals of this agreement are to maintain “the increase in the global average temperature to well below 2 °C above pre-industrial levels” and pursue efforts “to limit the temperature increase to 1.5 °C above pre-industrial levels” [2]. An important element of this agreement is to increase the amount of energy obtained from renewable energy, such as solar and wind power. In 2019, the European Commission shared the Green Deal, in which it is stated that at least 60 GW should come from offshore wind energy [3]. To achieve such an amount of offshore wind energy, many more wind turbines must be realised. However, current wind turbine foundations are only economically attractive in shallow water and there are not enough shallow waters to achieve the targets set by the EU. Therefore, floating wind can contribute to reaching this target [4].

By switching to floating wind turbines, the traditional offshore wind farm design gains a dynamic component. The two most significant motions for platforms housing FOWTs are acknowledged to be pitch and surge [1]. These motions alter the forces acting on the turbine, and will change its wake as well. When designing a wind farm, it is relevant to know what the effect of the wakes of wind turbines are. This has been studied for fixed Horizontal Axis Wind Turbines (HAWTs) and Vertical Axis Wind Turbines (VAWTs), however, the effect of the wake of FOWTs have been studied less[1].

This takes us to the main objective of this thesis: investigating the impact of rotational and translational motions on the wake of a floating turbine. The velocity of the wake will be measured with PTV using HFSB whilst the loads will be measured using load cells. PTV experiments are not only useful for quantifying the velocities in the wake, but they will also visualise it. As the renewable energy sector searches for sustainable solutions, it is vital to experimentally validate the effect of floating wind turbines on one another. Research can eventually help in creating efficient wind park layouts, which will aid the (economic) viability of floating wind turbine technology.

1.1. Report structure

The report is structured as follows. Chapter 1 gives relevant background knowledge on wakes, loads, and particle image velocimetry as well as the current state of the art. The experimental set-up is discussed in Chapter 2. Next, the results of the first experiment will be presented in Chapter 3 and the results of the second experiment in Chapter 4. Lastly, conclusions will be drawn and recommendations will be given in Chapter 5.

1.2. Wakes

What are wakes?

A wind turbine extracts energy from the wind, it generates electricity by reducing the kinetic energy of the wind. This means that the velocity behind the turbine is lower than the velocity in front of the turbine. The region behind the turbine that is lower in velocity is called the wake. In this region, the turbulence levels are also higher, which causes an increase in fatigue loads [5]. When a turbine is placed in the vicinity of another turbine, less power will be generated as it is positioned in a low velocity wind region. Therefore, fixed offshore wind turbines are usually spaced 5-10 D (wind turbine diameters) apart from each other [6] [7].

An example of a wake is visualised in Figure 1.1. The wake is visualised using a stream tube which expands as the velocity decreases.

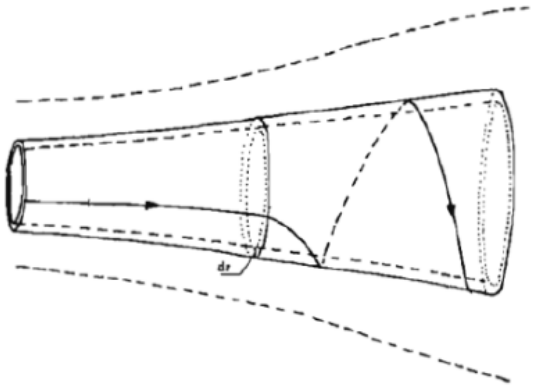

Figure 1.1: An expanding wake [8]

Near and far wake

The wake can be split into the near, intermediate and far wake. The size of these zones is determined by the rotor diameter, however the exact size can vary. Usually the near wake is defined as the first 1 to 5 D [7] [9] and the far wake starts after 5 to up to 50 D [9], [10]. The properties of these zones are characterized by the pressure p and wind speed U , and the turbulence intensity, as shown in Figure 1.2.

The near wake is the area just after the wind turbine. The pressure increases and the velocity decreases, due to the momentum and mass conservation laws. The turbine geometry, as well as other initial conditions, dominate this area. This causes both tip vortices and rotational effects.

The far wake is the furthest away from the rotor, the pressure here is constant, and the centreline velocity will reach the free stream velocity. Two definitions exist for the far wake. The classical turbulent wake theory, in this theory the wake is the point where the flow has achieved 'self similar behaviour'. The far wake will not begin until 30 to 50 D downstream of the turbine. For wind energy studies, however, a different definition is used. The far wake is usually the point where the mean velocity deficit profiles get a Gaussian shape, or where the effect of the rotor is not noticeable any more. The far wake can therefore already start at 3 to 5 D away from the turbine [10]. In this thesis, we will use the latter definition.

The intermediate is the area in between the far and near wake. The pressure is already constant. The velocity is also constant, but still lower than the free stream velocity. In wind farms, wind turbines

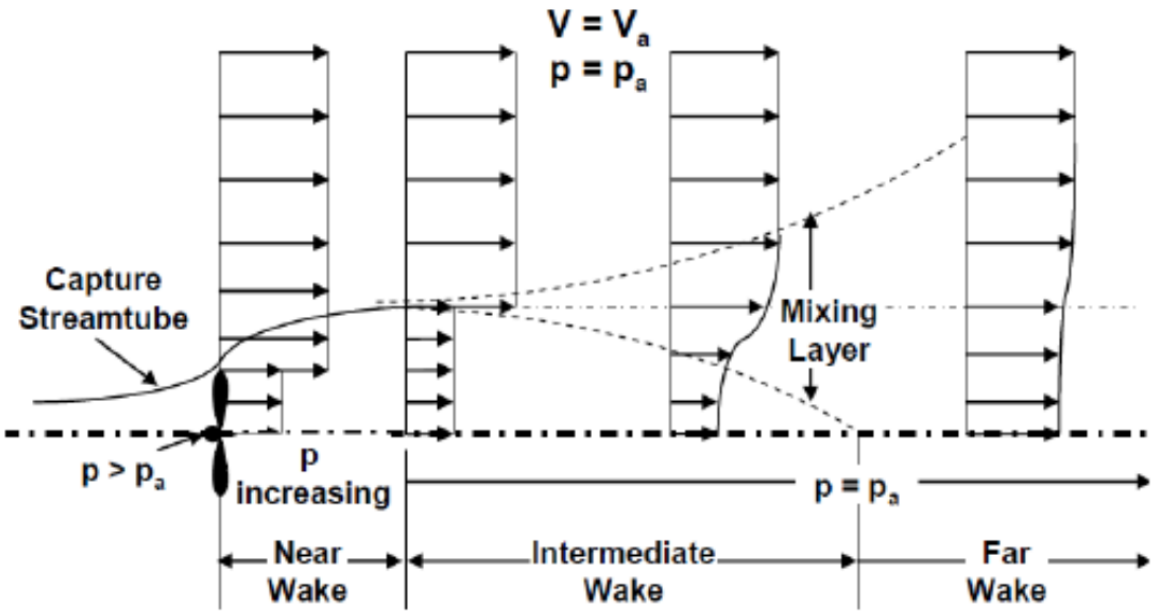

Figure 1.2: Near, intermediate, and far wake [8]

usually are located within 5 to 10 D apart from each other. However, the optimal distance from a purely technical point of view would be around 15 D [8]. For space and economic considerations, this distance is significantly reduced in practice. Therefore, it makes sense to look at the far wake.

Tip and root vortices

In the near wake, the tip vortices are noteworthy. The pressure difference between the pressure and suction sides of the rotor blades causes these vortex structures. Rotating systems such as wind turbines, propellors, or rotors produce vortices in their wake. A horizontal wind turbine produces a vortex at the tip and at the root of each blade, which will rotate in opposite to the wind turbine. The vortices influence the near wake and their breakdown influences the far wake. Meaning it has consequences for downwind turbines in wind farms regarding the loads and performance [11].

Wake meandering

The motions of the wake, with respect to the wake centreline, are called the meandering of the wake. It is believed to be caused by the large eddies in the atmospheric boundary layer [12]. It was found that for floating turbines, the wake meandering had the most impact at below rated wind speeds. Moreover, it did not really impact the fatigue loading in the mooring line tension and tower base fore-aft bending moment since this primarily relied on the velocity deficit. It did, however, affect both the fatigue loads caused by the yaw moment at the tower top and the fatigue loads caused by out of plane blade root moments [13].

Wind farm wake reducing concepts

By studying the wake effect, it will become possible to place the turbines in such a way that other turbines experience less wake and a larger amount of power is generated. There are several ways in which the wake effect can be reduced.

The annual revenue of a wind farm can be reduced by up to 20% depending on the placement of the turbines and the effect of their wakes.There are several concepts to reduce these wake effects. **Axial induction control**: The goal of this concept is to decrease the power production from the upstream turbine causing the axial induction factor to be lower. This will result in a lower velocity and momentum deficit in the wake, meaning that the downstream turbine can get a higher power output. In this concept, it is vital to weigh the power gain from the second turbine to the power loss from the first turbine.

Wake redirection: In this concept, the yaw angle of the upstream turbine is altered, causing the wake to overlap less with the downstream turbine. The downstream will therefore have a higher inflow wind speed, leading to a higher power output. In this concept, it is necessary to weight the gain from the power gain from the downstream turbine to the power loss by yaw misalignment from the upstream turbine.

Rotor reposition: This concept is specifically for a FOWT as it is possible to change the location of a turbine. The idea is to change the position of a wind turbine to decrease the overlap area [14].

1.3. Loads

Velocity triangle

A section of a wind turbine blade with its corresponding velocity triangle is shown in Figure 1.3. The relative velocity can be decomposed into axial and tangential components. The axial velocity is dependent on the free stream velocity, U, while the tangential velocity is influenced by the rotational speed, ω . The flow angle, ϕ , is visualised, this is the sum of the angle of attack, α and the twist angle β [15] [16].

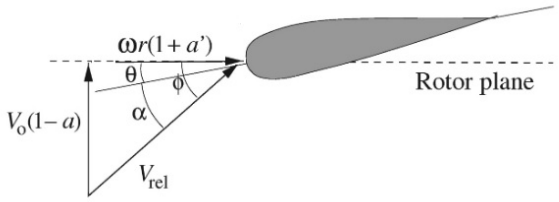

Figure 1.3: Velocity triangle [17]

The tangential and normal forces acting on the rotor plane are decomposed from the lift and drag force, as visible in Figure 1.4. Power and thrust can be calculated from these two forces, respectively, from Equation 1.1 and Equation 1.2 [15] [16] [17].

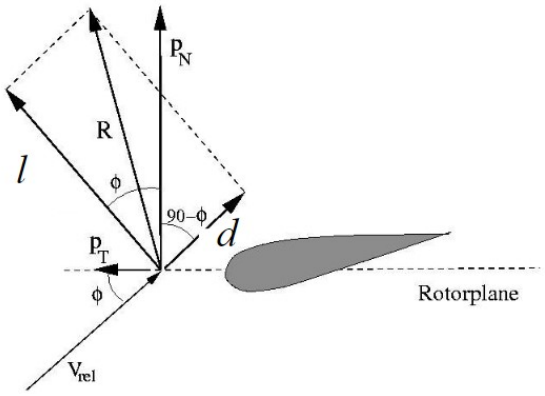

Figure 1.4: Loads on an airfoil [17]

$$l = \frac{1}{2}\rho {V_{rel}}^2 c C_l(\alpha) \tag{1.1}$$

$$d = \frac{1}{2}\rho {V_{rel}}^2 c C_d(\alpha) \tag{1.2}$$

From the inflow angle, lift and drag, the normal and tangential coefficients can be calculated, using Equation 1.3 and Equation 1.4. These can then be used to calculate the tangential and normal force Equation 1.5 and Equation 1.6. These forces can be decomposed into a normal and tangential force, Equation 1.4 and Equation 1.3 [17].

$$C_t = C_l sin(\phi) - C_d cos(\phi) \tag{1.3}$$

$$C_n = C_l cos(\phi) + C_d sin(\phi) \tag{1.4}$$

$$p_t = \frac{1}{2}\rho {V_{rel}}^2 c C_t \tag{1.5}$$

$$p_n = \frac{1}{2}\rho {V_{rel}}^2 c C_n \tag{1.6}$$

Equation 1.7 and Equation 1.8 show the induction factor and the tangential induction factor, respectively [17].

$$a = \frac{1 - u/V_0}{2} = \frac{1 - u/V_0}{2} \tag{1.7}$$

$$a' = \frac{1}{\frac{4F \sin\phi \cos\beta}{\beta C_x} - 1} \tag{1.8}$$

Next, Equation 1.9 can be used to calculate the thrust constant [18].

$$C_T = \begin{cases} 4a(1-a)F & a \leq \frac{1}{3} \\ \left(1.816 - 4\sqrt{1.816} - 1)(1-a)\right) F & a > 1 - \frac{\sqrt{1.816}}{2} \end{cases} \tag{1.9}$$

where Prandtl's tip loss correction is denoted by F.

Next, the forces must be integrated over the whole blade as seen in Equation 1.10 and Equation 1.11 to find the power and thrust.

$$P = \omega M_r = \omega B \int (r p_t) dr \tag{1.10}$$

$$T = B \int (p_n) dr \tag{1.11}$$

where M_r is the moment, B is the number of blades and r is the radial position [17] [19].

1.4. State-of-the-art

In this section, the literature will be discussed. The current understanding is summarised, and the knowledge gaps are highlighted. This includes the wakes of FOWTs and the effect of the wake of a wind turbine on another. In order, we will discuss 1) Numerical studies on floating turbines; 2) Numerical studies on tandem floating turbines; 3) Experimental studies on floating turbines; and 4) Experimental methodology using HFSB.

1.4.1. Numerical studies on floating turbines

Hakjin Lee and Duk-Joo Lee [20] studied the effect of platform motions on aerodynamic performance and unsteady wake evolution of a floating wind offshore wind turbine. The 6 DoF (heave, sway, surge, yaw pitch and roll) were enforced on the National Renewable Energy Laboratory (NREL) 5 MW turbine. The non-linear vortex lattice method and the vortex particle method were combined. Additionally, the floating turbine was compared with a bottom-fixed turbine. They concluded that the motions in the streamwise direction, i.e. surge and pitch, had a noteworthy effect on the power and thrust output. The unsteady evolution of the wake, relative to the bottom-fixed turbine, resulted from all degrees of freedom. This phenomenon could lead to an unsteady inflow wind for a wind turbine positioned farther downstream.

Binron Wen et al. [21] studied the effect of platform pitching on the power performance of an FOWT, using the Free Vortex Method. They compared the pitching with the non-pitching case as well as pitching with different amplitudes and frequencies at a Tip Speed Ratio (TSR) of 7 and the effect of a reduced frequency. They found that when the platform pitches, an additional wind shear is added to the rotor, meaning that the wind farm power could be increased. At a design TSR of 7, the pitching case yields a higher power output, albeit with a lower mean power coefficient and increased power fluctuation. If the reduced frequency increases, mean power output increases if the tip speed ratio is high and decreases if the tip speed ratio is low. The mean power coefficient experiences a reduction across nearly all tip speed ratios.

1.4.2. Numerical studies on tandem floating wind turbines

Razeiha et al. [22] found that the power and thrust coefficients were dominated by the surge motion and oscillated with a quasi-steady sinusoidal motion. The transient power and thrust coefficients of the upstream rotor with imposed surge motions were negatively correlated to those of the downstream rotor. Huang et al. [23] found that the power for a turbine $5D$ downstream of the upstream turbine was 36%

lower than that of the upstream one and the thrust was 66% lower. The platform motions had more effect on the power than on the thrust. Xue et al. [24] found that the power loss of the downstream rotor can be 60%, 55% and 30% when varying the wind speed from 8 m/s to 10 m/s to 12 m/s, respectively. They also found that the power increased significantly when the distance between the turbines increased, this was especially noteworthy around rated wind speed.

The wake of the FOWT also becomes more complicated when a downstream turbine is added. Razeiha et al. [22] found that the velocity deficit in the wake was comparable to a fixed rotor, but the motion of the wake was more unsteady. This unsteadiness causes the wake of the downstream motion to be very different. However, the wake recovers faster when subjected to a surging motion, as the unsteadiness caused more vertical mixing. Huang et al. [23] also found that the wake became more complicated and the wind speed deficit behind the downstream FOWT was more severe, causing the increase of the power input of the downstream FOWT. Xue et al. [24] found that the wake recovery was not influenced as much by wake shear as by turbulence intensity. Apart from power loss, the downstream turbine also experienced more power fluctuations, which is a problem for the connection to the grid. Inflow conditions caused variations in the pitch and surge motions of the platform. This caused problems regarding the stability of the FOWT. Moreover, the power fluctuated a lot when the wake inflow conditions were varied, causing problems in wind power forecasting and increasing costs as the energy needs to be stored.

Lastly, Huang et al. [23] found that the downstream rotor was found to have more unsteady blade tip vortices. Xue et al. [24] found that the platform motions of the downstream turbine exhibited severe turbulence under some inflow conditions. If the rotor was under the right half wake inflow condition, the FOWT suffered the most severe wake.

Arabgolarcheh et al. [25] examined the wake interactions within offshore wind farms by analysing how the movement of the upstream turbine influences the loads and performance of the downstream wind turbine. The downstream turbine is placed $3D$ away. They used a Navier-Stokes actuator line model within OpenFOAM® and the NREL 5 MW turbine as a reference turbine. The study revealed that variations in peak-to-peak thrust and power are influenced by incorporating the discrete characteristics of the blades. While discrete tip vortices under stable conditions disperse within the initial two diameters downstream of the rotor, the motion of the platform can reshape them into a distinct wake pattern resembling discrete ring structures. Analysis of the frequency spectra of the parameters indicated a notable influence from these motion-induced discrete rings.

1.4.3. Experimental studies on floating turbines

Belvasi et al [26], studied the effect of imposed pitch, surge and 3 DoF (pitch, surge, heave) on the far-wake meandering of a FOWT. Stereoscopic particle velocimetry is used with oil as a seeding particle to examine the far wake at $8.125D$. The time series and normalised available power of the far wake in time and frequency domains were then studied. They found that there was no visible effect on the mean far-wake recovery when imposing the motions on the FOWT. Moreover, the velocity statistics of the wake were not influenced by imposed motions.However, the frequency characteristics were influenced by the imposed motions, this was visible in both the streamwise characteristics and spectral content of the far-wake.

Fontanella [27] also performed Particle Image Velocimetry (PIV) experiments with a single FOWT. They studied the effect of imposed surge on the unsteady aerodynamics of a FOWT. To study the aerodynamic response of the turbine, the thrust force is measured. Hot wire measurements were used to study the near

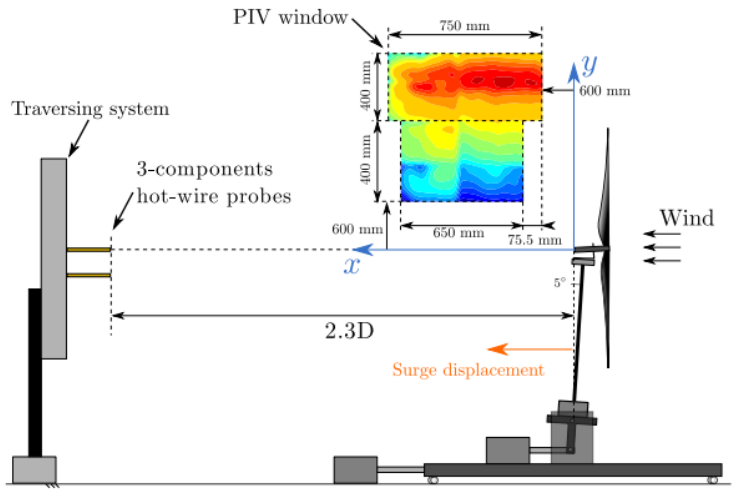

Figure 1.5: PIV setup with coordinate system by Fontanella [28]

wake and the blade tip vortex was visualised using PIV. For the Hot Wire Anemometry (HWA), a traversing system was created and the measurements were done along this system in both the YZ plane and the XZ plane. In the YZ plane the measurements were done 2.3D downwind of the turbine, starting at 1.6 m below the hub height until 1.6 m above the hub height, in increments of 0.1 m between measurements. In the XZ plane, the measurements start at 2.18 m until 5.48 m, which is 2.3D, downwind of the hub. The increments in this case were 0.33 m. For the PIV experiment, the measurements were done in the XZ plane (as defined in Figure 1.5). The measurements were done between 0.6 and 1.35 m downwind of the rotor in the x direction and 0.6 to 1.39 m in the z direction, where 0 m would be the hub height. It was found that up to a reduced frequency of 0.5 the experimental results corresponded to the quasi-steady predictions. Moreover, the average hub height velocity deficit from the case with imposed surge motion does not vary from that of the fixed case. The increase of the wake spectral content is however proportional to the maximum surge velocity. The largest increase is found in the outside region of the rotor when it is in rated conditions. The PIV experiments showed that the travel speed of the blade-tip vortex was altered by the surge motion.

Rockel et al.[29] aimed to investigate the influence of pitch motion on the wake of a wind turbine. Stereoscopic Particle Image Velocimetry (SPIV) was used to do the measurements and the results were compared with existing models. The hub height of the scale model was 25 cm. They found that the pitch of the platform and the oscillations in the streamwise directions have a strong impact on the wake's shape and the velocity magnitudes.

1.4.4. Experimental studies using Helium Filled Soap Bubbles

In 1963 Walcott already used HFSB to visualise air flow in a parachute [30]. Later, Kerho and Bragg [31] focused their research on the accuracy of bubbles that were (almost) neutrally buoyant, as produced by a commercially accessible system. They found that using HFSB is not accurate for quantitative measurements and should only be used qualitatively, unless the buoyancy of the tracers is neutral which is difficult to achieve with the commercially available generation system used.

In 2009, Kuhn [32] created a tomographic PIV system to measure large-scale flow structures in air.

They concluded that the optical characteristics of HFSB have no significant influence on the measurement accuracy. In 2009, Bosbach [33] also managed to do a PIV experiment on a large scale when doing an experiment on a full scale double aisle aircraft cabin mock up.

Scarano [34] studied the flow-tracing fidelity of HFSB for low speed aerodynamics. The velocity around a cylinder was studied. They found that HFSB can be applied quantitatively. In 2017, the tracing fidelity of HFSB in concentrated vortices was studied by Caridi et al. [35]. The velocity measurements are usually hard to perform, as tracers are often heavier than air. Using neutrally buoyant HFSB gave results corresponding to literature. In 2018, Faleiros [36] studied the tracing fidelity in turbulent boundary layers. For turbulent boundary layers above about two bubble diameters from the wall, it was discovered that HFSB can be used to calculate the mean velocity and turbulent fluctuations.

Van der Hoek [37] investigated the dynamic behaviour of the wake of a wind turbine, while influenced by helix excitation. He used tomographic PIV with HFSB as a seeding element. An experiment by Heckmeier was expanded. The PIV data was averaged on both the azimuthal angle of the rotor and the phase of the helix in order to quasi-time-resolve the data. This study not only focuses on the validation of the helix approach, but it also focuses on shedding more light on the working principles of PIV for future testing. The experiment was done at TU Delft's Open Jet facility. Two turbines were placed $5D$ away from each other. The HFSB were created by a seeding rake, which was placed at the outlet of the open jet. The HFSB were lit by two LaVision LED Flashlights and recorded by four cameras in a tomographic PIV setup. The total volume that was recorded was 2.1x0.7x0.7 m^3, which was created by getting seven smaller volumes. The setup was based on a previous study done by van der Hoek [37]. Five improvements were made, including being able to move the cameras, adding another camera, doing multiple tests of the same control action, increasing the distance to the HFSB seeder and increasing the length of the measurement domain in order to capture more of the wake. The seeding of the HFSB was not uniform, meaning that the PIV measurements were not suitable for dynamic analysis.

1.5. Particle Image Velocimetry

To understand the Particle Tracking Velocimetry technique, first PIV will be elaborated upon. PIV is a technique where the velocity of a flow can be measured by adding particles to a flow. These particles are illuminated by a laser and scatter the light. The individual particles can then be followed by taking snapshots with a camera. The velocity and vorticity of the particles can then be deduced from the correlation of the images [38].

To determine the properties of a flow, Computational Fluid Dynamics (CFD) is often used. These methods depend on the modelling of turbulence, as Direct Numerical Simulation (DNS) requires too much computational power. Nowadays, CFD and wind tunnel tests are used interactively. Wind tunnel tests can help verify the CFD simulations. As CFD becomes more and more advanced, experimental techniques, such as PIV, must also become more developed.

Setup

Flow seeding

The flow is seeded with tracer particles. These particles must follow the flow, and they should scatter enough light in order to be visible. Moreover, they must not be toxic, hazardous, corrosive, or reactive, and they should naturally evaporate. It is important to choose the right size of particles, smaller particles will follow the flow better, but larger particles will scatter the light better. Tracer particles are often around a micrometer in size and are created from materials with a higher density than air. The problem is that with particles larger than 3 micrometres, the particles will not follow the flow properly and lag behind, causing the velocity measurements to be inaccurate. On the other hand, small articles will have trouble scattering enough light and the domain of the test section can hardly exceed 100 cm^3 [38].

Powder-based seeding

Powder used for PIV are usually metal oxides. They have high melting points, are unreactive and relatively cheap. As powders incline to cluster together, special seeding techniques must be used.

Liquid-based seeding

Liquids used for PIV are often oils, the seeding droplets are created using a Laskin atomizer.

Soap bubble seeding

Soap bubbles seeding is beneficial as they scatter more light, meaning a larger volume can be illuminated [38].

Magnification

The thin lens equation can be used to calculate the characteristics of the imaging system. Equation 1.12 shows the relation between the focal length, f, the distance to the image, d_i, and the distance to the object d_o, which is the airfoil in this case.

$$\frac{1}{f} = \frac{1}{d_i} + \frac{1}{d_o} \tag{1.12}$$

The magnification is the ratio between the field of view and the image on the sensor plane, and is calculated as shown in Equation 1.13.

$$M = \frac{d_i}{d_o} = \frac{\text{sensor size}}{\text{imaged object size}} = \frac{\text{pixel size} \times \text{number of pixels in the width sensor}}{\text{FOV}_{\text{width}}} \tag{1.13}$$

The intercept theorem, as demonstrated in Equation 1.14, may then be used to connect the distance to the image and the distance to the object to the magnification factor. Here, H_i represents the height of the image on the sensor, and H_o is the height of the field of view height.

$$\frac{H_i}{d_i} = \frac{H_o}{d_o} \tag{1.14}$$

Consequently, Equation 1.15 provides the relationship between the image distance, object distance, and magnification factor.

$$\frac{d_i}{d_o} = \frac{H_i}{H_o} = M \tag{1.15}$$

This relation can be substituted in Equation 1.12, by replacing d_i by $d_o M$, as shown in Equation 1.16 in order to find an expression for d_0 by rearranging the equation.

$$\frac{1}{f} = \frac{1}{d_o M} + \frac{1}{d_o} \tag{1.16}$$

The f-stop is necessary to get a good particle image. Two criteria are used to compute the aperture. The first criterion is provided in Equation 1.17, where M is the magnification factor, δz is the focal depth, Δz is the laser sheet thickness, $f_\#$ is the f-stop, and λ is the laser wavelength. It says that the focal dept must be greater than the thickness of the laser sheet.

$$\delta z = 4.88 \lambda f_\# \left(\frac{M+1}{M} \right)^2 \geq \Delta z \tag{1.17}$$

The second criterion says that in order to guarantee sub-pixel accuracy, the ideal particle diameter, d_τ, which is determined by Equation 1.18, with d_p being the particle diameter without taking light diffraction, should be roughly 2-3 pixels. Moreover, Equation 1.19 provides the f-stop as a function of the diffraction diameter, d_{diff}.

$$d_\tau = \sqrt{(M\, d_p)^2 + (d_{\text{diff}})^2} \tag{1.18}$$

$$f_\# = \frac{d_{\text{diff}}}{2.44 \lambda (1+M)} \tag{1.19}$$

By rearranging Equation 1.18 an expression for the diffraction diameter can be obtained, as presented in Equation 1.20. Furthermore, substituting this in Equation 1.19, results in Equation 1.21, which can be used to calculate the f-stop based on the particle image diameter criterion [39] [40].

$$d_{\text{diff}} = \sqrt{d_\tau^2 - (M d_p)^2} \tag{1.20}$$

$$f_\# = \frac{\sqrt{d_\tau^2 - (M d_p)^2}}{2.44 \lambda (1+M)} \tag{1.21}$$

1.6. Types of PIV

Planar PIV

Planar PIV has one camera, this camera is orthogonal to the laser sheet. The output consists of two velocity components in a 2D domain.

Stereoscopic PIV

SPIV has two cameras, and the output consists of three velocity components in a 2D domain.
When using planar PIV, only two velocity components are measured. When using SPIV, two cameras are

used to capture three velocity components in a 2D domain. To capture three velocity components in a 3D domain, tomographic PIV can be used. At least three cameras are required for this, and the volume measured must be reconstructed.

Tomographic PIV

Tomographic PIV operates in the 3D domain. Several cameras are used to have different views on the illuminated tracers, these are reconstructed using optical tomography. The method used most commonly is MART [41].

Algebraic techniques are applicable. It is possible to solve a set of linear equations iteratively. The discretization of the particle distribution volume results in a 3D array of cubic voxel elements with intensity E in (X, Y, Z). The dimension of a cubic voxel element is similar to that of a pixel, as both require correct discretization. It has a uniform on-zero value within and zero outside. Furthermore, it is simple to expand cross-correlation inquiry from a pixel to a voxel [41].

There are several limitations regarding tomographic PIV. The velocity measurements can be influenced by ghost particles, in particular when many particles are present in the images. When using cross-correlation, averages over interrogation volumes are used, smoothing out changes in velocity, However, this can cause up to 1.4 pixels per time step velocity errors in turbulent boundary layers. There are methods that reduce this problem, but none that can fix it completely.
Additionally, the representation of particles in a voxel space introduces errors, which are then amplified by noise and lighting problems.
Lastly, a lot of computational power and storage space is necessary for tomographic PIV. [42]

1.7. Particle Tracking Velocimetry

3D PTV

Given tomographic PIVs constraints and computational demands, it is critical to have direct knowledge of particle locations in space. The velocity and acceleration of particles can be determined by tracking particles over time and applying temporal filtering. When using this approach, called three-dimensional particle tracking velocimetry (3D PTV), no spatial averaging is needed and the number of things to calculate is reduced. A downside is that dense particle images can lead to interference and inaccuracies in the tracking of particles [42].

New techniques

A technique to overcome the limitations of 3D PTV was designed by Wieneke in 2013, it was called the Iterative Reconstruction of Volumetric Particle Distribution (IPR) method. This was the first method which was based on particle positions alone. However, it still had problems regarding ghost particles [42].

Next, Shake the Box (STB) was constructed, based on tomographic PIV and IPR. It predicts particle distributions in future time-steps based on trajectories that are already known. This is why in dense particle fields, the processing is still fast and the ghost particles are minimal. A main feature of STB is that it does not handle each snapshot individually when reconstructing 3D particle distributions, but it incorporates temporal and spatial information. STB uses velocity information to make an estimation of the distribution

of the particles, after which it corrects errors using image matching, thus reversing the usual evaluation process [42].

The two main ideas behind the STB methods are that particles do not leave the measurement volume, and knowing the path of a particle will help predict its position in the next time-step [42].

Existing tracks are extended, and new ones are added when necessary for every time step in a sequence of images. However, in the beginning not everything is known about most particle tracks, meaning that the methods must converge to a stable solution through three phases: initialisation, convergence and converged state. Reconstruction becomes easier when more true tracks are found and the new particles that enter the volume are balanced with particles exiting the volume [42].

1.8. Synthesis

Numerical studies have been done on tandem floating wind turbines and experimental studies have been done on single floating wind turbines. However, not many experiments have been done on tandem rotors, especially PTV experiments with HFSB.

Numerical studies have contributed to the advancement of knowledge of tandem floating wind turbines, whereas most experimental studies have been on single floating wind turbines. Therefore, the gap in the research concerns experimental validation of the wake of floating tandem rotors. Numerical simulations have provided data on the performance of FOWTs. However, as numerical models require simplifications and assumptions, it is important to supplement these models with experimental studies. Using HFSB as tracing particles for PTV will provide a new approach to study the wake.

1.9. Research questions

Multiple experimental studies have been done on the wake of a floating wind turbine, and multiple numerical studies have been done on tandem floating wind turbines. However, not much is done yet on experimental tandem wind turbines.

1. **What does the flow field in the wake of a turbine look like when it is moving with a sinusoidal pitch or a sinusoidal surge motion?**
   (a) How does the wake of a turbine compare when it is moving with a surge motion vs when it is moving with a pitch motion?
   (b) What is the difference between the velocity field behind the upstream turbine when it is moving with low frequency (2 Hz) sinusoidal motion vs when it is moving with a high frequency (5 Hz) sinusoidal motion?
2. **How does applying surge, pitch, and yaw to the upstream turbine impact the loads on the downstream turbine?**
   (a) How do the loads on the downstream turbine change when the upstream turbine is moving with a low frequency (2 Hz) or a high frequency (5 Hz) motion?
   (b) How do the loads on the downstream turbine change when the downstream turbine is positioned at different locations in the downstream direction?
   (c) How do the loads on the downstream turbine change when the downstream turbine is positioned at different locations in the lateral direction?

2

Methodology

In this section, the methodology of the two separate experiments will be discussed. First, the details of the wind tunnel, which was used to do the experiments, will be discussed. Subsequently, the scale model used during the experiments will be described. Then, the PTV experiment, conducted to determine the flow field behind a floating wind turbine, will be described. This includes the materials, Field of Views (FOVs), calibration and test matrix. Lastly, the experiment conducted to determine the loads on a downstream turbine will be elaborated upon.

2.1. Wind tunnel and scale model overview

First, the experimental setup will be elaborated upon. This section will discuss the wind tunnel used for the experiments. Additionally, the scale model used in the experiments will be presented. This overview will provide a foundation for the explanation of the methodology of the two experiments conducted for this thesis.

2.1.1. Wind tunnel

For all experiments the Open Jet Facility (OJF) at the University of Technology Delft was used, visualised in Figure 2.1. The OJF is a state-of-the-art wind tunnel with dimension of 13m (width) by 8m (height). In the OJF a wind velocity of 120 km/hr (or 33.3 m/s) can be achieved using its 500 kW fan (number 1). After this, a long diffuser and two rows of corner vanes (number 2) turns the air 180 degrees, a short diffuser then leads the air to the settling chamber (number 3). Five fine mesh screens are located in this chamber, reducing the turbulence and the velocity deviations. Next, the air will be blown into a test section (number 5) via a contraction (number 4). Afterwards, a cooling radiator (number 6) will cool the air and then the air will be transported back to the ventilator [43].

2.1.2. Scale model of the wind turbine

To conduct this study, a scale model of a wind turbine is used, shown in Figure 2.2. The Wind Turbine Model (WTM) is a 1:148 scaled version of the DTU 10 MW reference wind turbine, designed to operate at a velocity scale of 3, it has three blades, a fixed pitch and the rotor model is upwind.
The blades are scaled such that the thrust force can be reproduced correctly, rather than geometrically scaling the blades of the model. This is done such that the aerodynamic performance is not impaired by

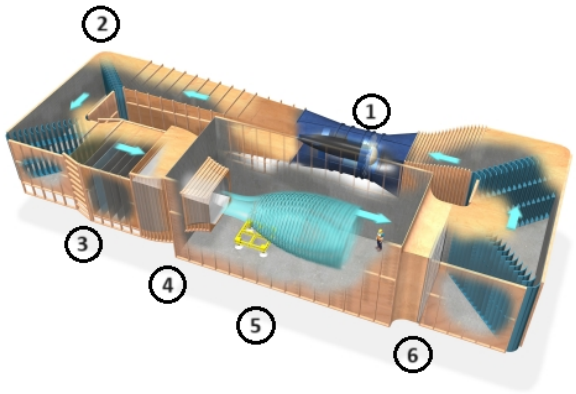

Figure 2.1: The Open Jet Facility at TU Delft where the experiments were conducted [43]

low Reynolds numbers. The aim of this study is to investigate the thrust of floating offshore wind turbines. Therefore, it is important to be able to reproduce the thrust forces on the (scaled) blades and translate the results to a full-scale wind turbine. The wind turbine is a fixed-pitch model, ensuring the performance to

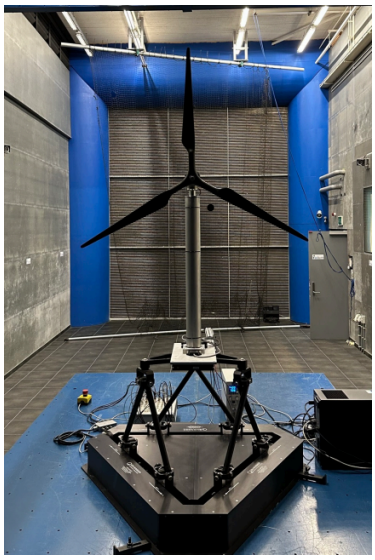

Figure 2.2: The scale model placed on top of the hexapod in the Open Jet Facility

be consistent. If the blades are able to pitch, it has the potential to lead to the operating conditions being different or the blades having different angles.
The airfoil chosen for the wind turbine is the SD7031 airfoil. This airfoil has a low-thickness profile, which is fitting for the low-Reynolds application. This means that the airfoil used it not the same as the airfoils used in the original wind turbine.
A servomotor with a gearbox is powering the rotor. An Oldham coupling is used to connect the rotor to the shaft. A servo drive is used to speed control the servomotor and a braking resistor is used to dissipate the generated power.
The tower is a cylinder made of aluminium with a high stiffness, ensuring the deflection of the rotor-nacelle assembly. The tower first for-aft mode should be far from the rotor's 1P and 3P frequencies, to ensure that the test is not effected by deflections and vibrations. The first for-aft mode is at 12.5 Hz, which is more

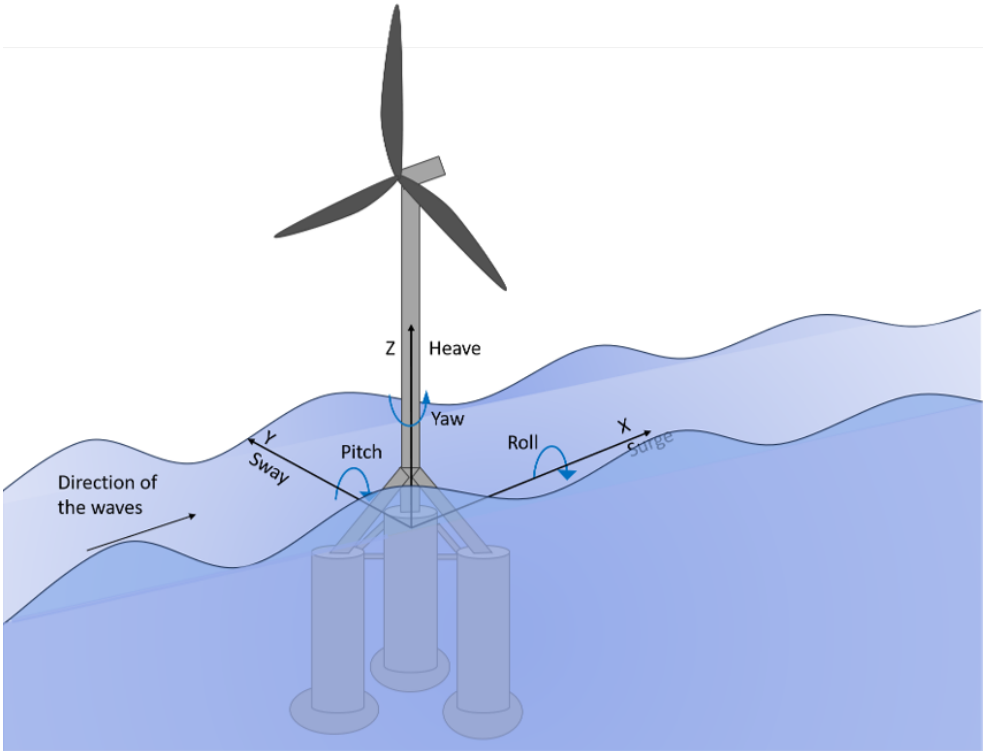

Figure 2.3: The six degrees of freedom

than double the highest frequency of the motion.
The wind turbine model is mounted on a parallel kinematic robot, the Quanser Hexapod, a commercially available hexapod which can move in six degrees of freedom: surge, sway, heave, pitch, roll, and yaw [44]. The six degrees of freedom are visualised in Figure 2.3.

The second turbine is an exact copy of the first turbine. It will be positioned at several positions downwind of the first turbine and placed onto a fixed stand rather than the kinematic robot.
A comparison of the variables between the full scale wind turbine and the scale model used are shown in Table 2.1 and parameters of the model are shown in Table 2.2.

Table 2.1: Comparison of the variables between the full scale wind turbine and the scale model used [44]

Parameter	Full Scale	Model Scale	Unit
Cut-in speed	4	1.33	m/s
Rated speed	11.4	3.8	m/s
Cut-out speed	25	8.33	m/s
Minimum rotor speed	6	296	rpm
Maximum rotor speed	9.6	473.6	rpm
Rated thrust	1619	0.012	kN
Rated torque	10738	0.529	kNm

Table 2.2: Parameters of the scale model [44]

Parameter	Value	Unit
Rotor diameter	1.2	m
Hub height	0.8	m
Blade pitch angle	0	deg
Tilt angle	0	deg
Nacelle mass	1.03	kg
Rotor mass	0.58	kg

2.2. Particle Tracking Velocimetry of the wake of one turbine

Next, the experimental setup of the first experiment will be elaborated upon. The first experiment concerns one wind turbine, where its wake will be examined. The method to examine the wake will be discussed, the equipment will be presented, and the set-up will be explained. After this, the test section will be elaborated upon and the test matrix will be discussed.

2.2.1. Equipment

To visualise the bubbles in the flow, seeding particles are used. Specifically, Helium Filled Soap Bubbles (HFSB) are used, which are released by a seeding rake placed at the end of the nozzle. These bubbles travel downstream. At the test section, they are illuminated by the LaVision LED Flashlights and recorded by four Photron FASTCAM SA1.1 cameras. The frame rate of these cameras is 5000 frames/s and the resolution at which it operates is 1024 by 1024 pixels. The LaVision PUT-X timing device is used to synchronise the four cameras.

A PIV software called DaVIS is used for image acquisition. This software has four main functions; it can be used to control the illuminations and acquisition settings, to analyse the images, to post process the data (including but not limited to the velocity vector statistics, mean, vorticity, streamlines), and to display the data [37].

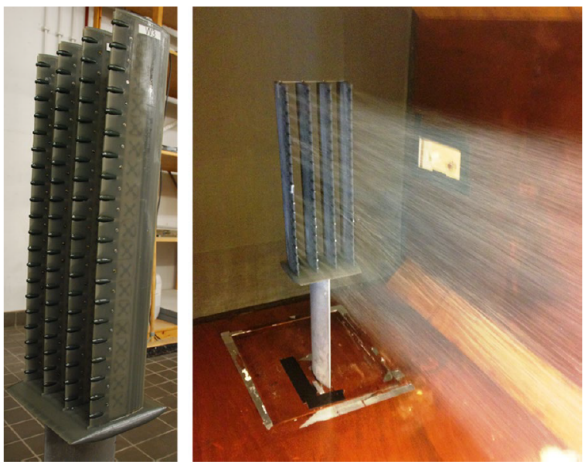

Figure 2.4: The TU Delft seeding rake [38].

Figure 2.5: The cameras used [45].

Figure 2.6: The LEDs used [46].

2.2.2. Set-up

The full setup is visualised in Figure 2.7. The turbine is placed on the earlier mentioned Quanser Hexapod. This is commercially available and is able to enforce all 6 DoF. The turbine is attached to a servomotor, which is a Maxon EC-4pole 30 200W with a Maxon GP 32 C 5.8:1 gearbox. A Maxon DSR 70/30 braking resistor is used to be able to dissipate the power that will be generated. An ATI mini45 SI-290-10 load cell is placed between the tower top and nacelle. It can measure the forces and torques of the rotor. MEMS TE Connectivity 4030-002-120 triaxial accelerometers are placed between the tower base and nacelle. These can measure the translational acceleration [37].

The PTV setup is mounted onto aluminium profiles. The cameras are placed such that the appropriate FOV is captured, and the LEDs are located in the centre.

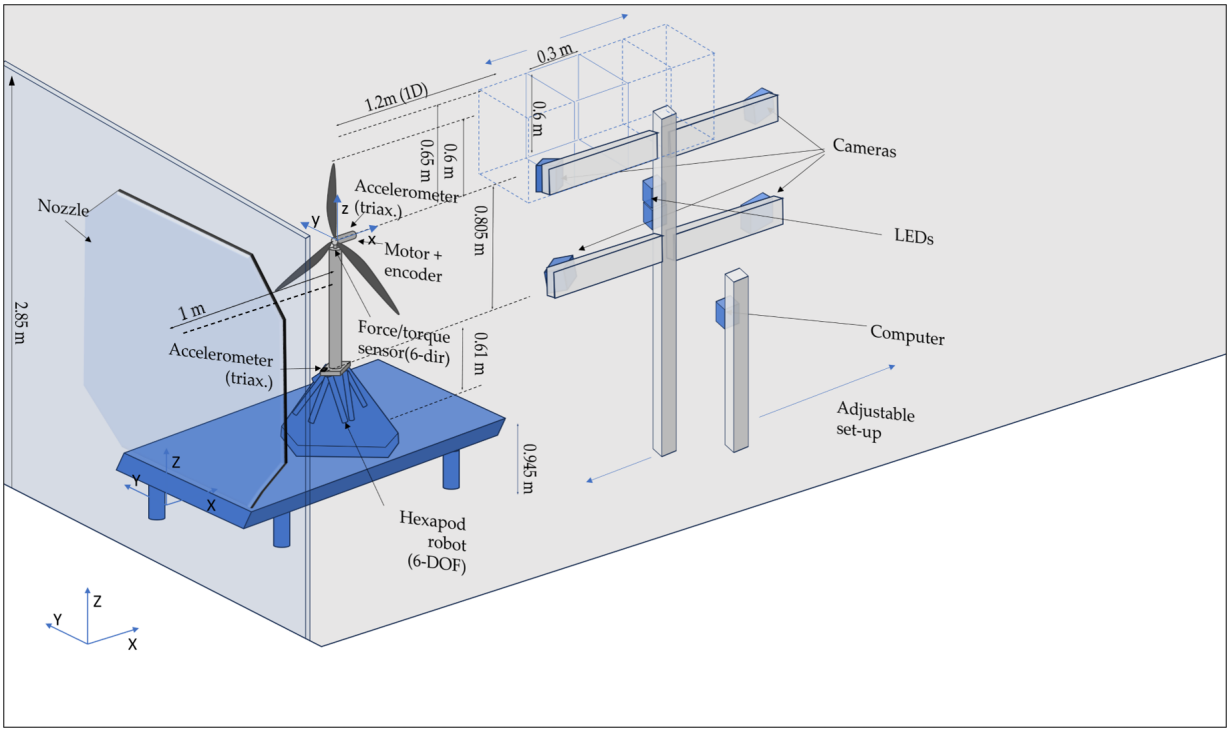

Figure 2.7: Set-up of the PTV experiment done on a single turbine

The full setup for the PTV is shown in Figure 2.8. The four cameras, 2 LEDs and FOV are highlighted.

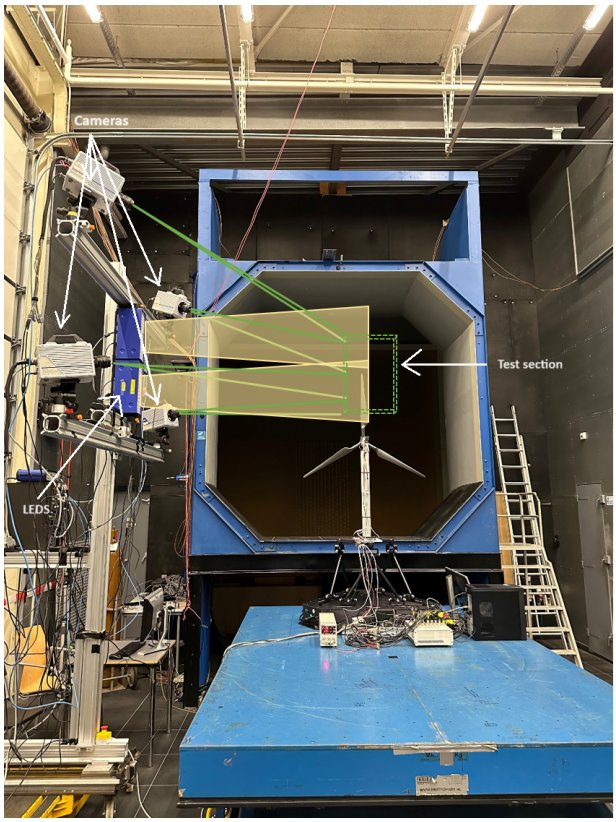

Figure 2.8: Visualisation of the 3D PTV test section in the wind tunnel

2.2.3. Test section

The field of view that was captured by the cameras was 300 mm by 470 mm by 650 mm. To create a larger test section and to capture more of the wake, the camera setup was moved to four different locations. The camera setup was centred at 1 D , 1.25 D , 1.5 D , and 1.75 D (rotor diameters), respectively. This is the distance between the back of the top blade and the centre of the test section. This was chosen such that there was also some overlap between the Field of Views. A visualisation of the FOVs can be found in Figure 2.9. A 2D representation is added in Figure 2.10.

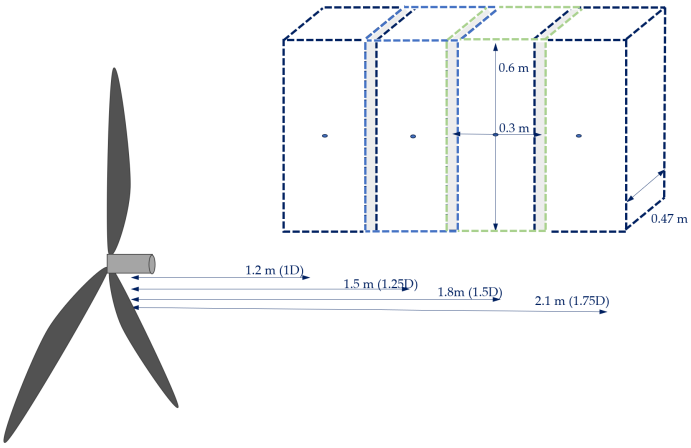

Figure 2.9: Field of View, 3D

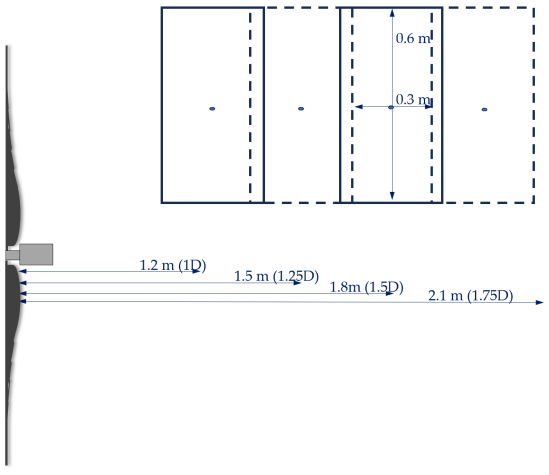

Figure 2.10: Field of View, 2D

2.2.4. Acquisition procedure

Next, the procedure in which the data was acquired will be explained. This process is further detailed below.

Preparation

1. **Installation**

   - **Measurement of distances:** Before the parts were installed, the distances necessary were measured to ensure all the equipment was placed accurately. This step is important to ensure that the data was collected accurately and that the experiment can be repeated in the future.
   - **Installation of the turbine:** The robot was securely attached to the blue table located in the wind tunnel. The turbine was mounted onto this kinematic robot. The kinematic robot can be used to simulate motions in 6 degrees of freedom.
   - **Installation of the PTV system:** The PTV is necessary to capture the wake of the turbine. The system consists of cameras, LEDs, amongst others. The system is installed on beams, positioned such that the correct test section is captured. The test section is explained in Section 2.2.3.
   - **Relocating the PTV system:** After each set of the tests, the system has to be repositioned in order to capture a larger area of the wake, as explained in Section 2.2.3. This movement was done carefully such that all necessary points were covered.

2. **Calibration**

   - **PTV system calibration:** The Particle Tracking Velocimetry PTV system was calibrated using a calibration plate. A picture was taken of the plate and loaded onto DaVIS10, where the calibration steps were followed as per the manual. This is shown in Figure 2.11. Both days the calibration was redone, this picture is the calibration of day two (Figure 2.12).

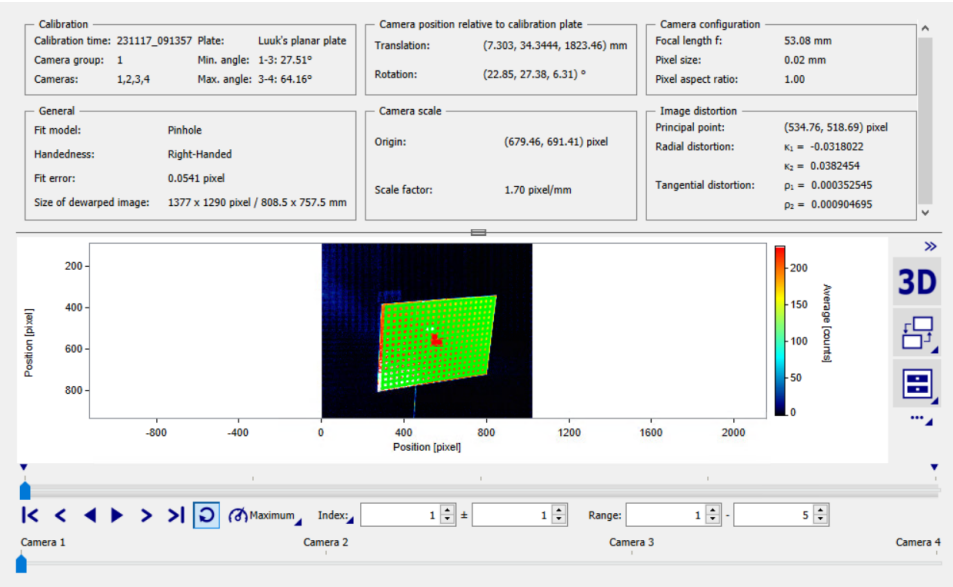

Figure 2.11: Screenshot of the calibration page in DaVIS10

   - **Convergence:** It was made sure that the particles converged when doing STB. As explained in Section 1.7, the particle tracks must converge to be able to have a stable solution.

3. **Robot calibration**

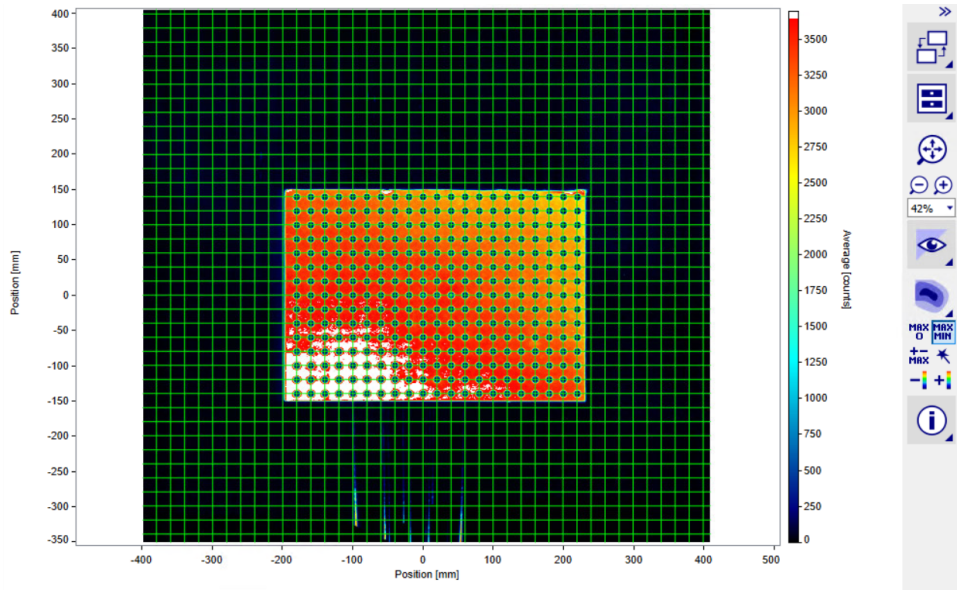

Figure 2.12: Screenshot of the calibration plate in DaVIS10

- **Hexapod calibration:** The hexapod was calibrated using a Simulink model, provided by the manufacturer. The calibration was performed after every test in which the hexapod was used. This calibration is necessary to ensure precise positioning during the experiments.

Data acquisition

1. **Positioning of the wind turbine**
   - **Positioning turbine:** The turbine was positioned 1 m behind the nozzle.
   - **Positioning PTV system:** The PTV set-up was initially positioned such that it was centred at a distance of $1D$ behind the turbine. It was then moved in increments of $0.25D$ until it was positioned at a distance of $1.75D$ behind the rotor. This movement allowed for capturing a larger part of the wake, some overlap between the test sections were present to ensure no data was lost.
   - **Types of tests:** At each position, four different tests were done. The motion of the wake was captured when the rotor was moving with low frequency pitch, high frequency pitch, low frequency surge and high frequency surge motion. These frequencies were chosen based on findings from previous studies [44].
   - **Test matrix:** As four different tests were done at four different locations, a total of 16 test cases were conducted. This test matrix can be found in Table 2.3. The In Plane Motion (IM) Frequency (f), and amplitude of the motion is added as well as the normalized velocity variation ($\frac{\Delta V}{U_0}$) to the table. The normalized velocity variation is the change in velocity divided by the inflow velocity. The magnitudes of these values are derived from the experiments done in March 2023 [44].
2. **Seeding**
   - **Seeding:** The seeding generator, as pictured in Figure 2.4, was placed in the wind tunnel. First, the wind tunnel was turned on, after which the turbine and finally the seeding generator was turned on. The seeding generator is used to spread the HFSB into the flow.

3. **Acquisition**

   - **Acquisition:** The LEDs were turned on, and the pictures were taken and stored.

Post-processing

1. **Background filtering**

   - **Subtract time filter function:** First, the background must be filtered to ensure that only the particles are visible. The minimum is subtracted with a filter length of 9 images, see Figure 2.13.

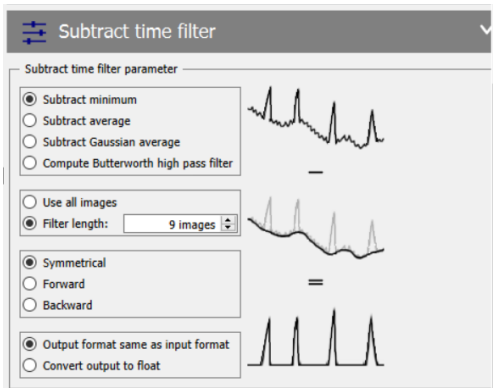

Figure 2.13: The *subtract time filter* parameters used in DaVIS10

2. **Binning**

   - **Binning**: The option binning in DaVis10 is used to create the average flow fields. In this option, one larger pixel is created by summing the intensities of several regular pixels.
     Two types of binning exist, namely hardware and software. In software binning, the intensities are summed after digitisation. This is what is used in this case.
     Higher image rates are often present when binning because the transferred data size is diminished.
   - **The effect of bin size**: The bin size is defined in terms of voxels in DaVIS10. One voxel is a 3D element, the size of a pixel. If the bins are too large, the means are not taken accurately. This may lead to a loss of information and an inaccurate presentation of the data. On the other hand, if the bins are too small, there may not be enough particles within each bin to provide enough information to accurately depict the flow field. It is therefore vital to choose a bin size balancing accuracy and reliability.
   - **The effect of overlap**: DaVis 10 allows for the bins to overlap. The overlap causes the resolution to increase without decreasing the bin size. In this way, more bins containing particle tracks can be found.
   - **Bin size in millimetres**: Since there are 1024 pixels in each direction (as discussed in Section 2.2.1), the voxel size in the X direction is $\frac{300}{1024} = 0.29mm$, in the Y direction it is $\frac{470}{1024} = 0.46mm$ and in the Z direction it is $\frac{600}{1024} = 0.59mm$. This means that when a bin size of 32x32x32 voxels is used, the bin size in mm in the X direction is $32 \cdot \frac{300}{1024} = 9.4mm$, in the Y direction $32 \cdot \frac{470}{1024} = 14.7mm$, and in the Z direction is $32 \cdot \frac{300}{1024} = 18.8mm$.

- **Bin size**: In Figure 2.14 to Figure 2.16 the low frequency surge is plotted with three different bin sizes. It can be clearly observed that with a reduced bin size, the data becomes clearer, but more noise is present. The 32x32x32 voxel ($9.4 \times 14.7 \times 18.8mm$) bin size is chosen as a compromise between the lack of information in the 64x64x64 voxel ($18.8 \times 29.4 \times 37.5mm$) case and the presence of noise in the 16x16x16 voxel ($4.7 \times 7.3 \times 9.4mm$) case. Additionally, an overlap can also be chosen. If e.g. a bin size of 32x32x32 voxel ($9.4 \times 14.7 \times 18.8mm$) is chosen with 50% overlap, the effective bin size will be 16x16x16 voxel ($4.7 \times 7.3 \times 9.4mm$).

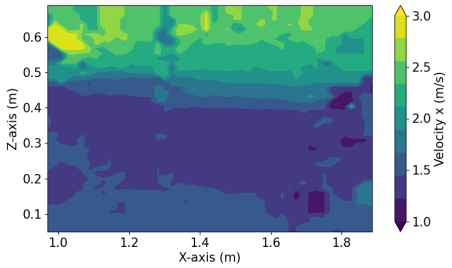

Figure 2.14: Surge low frequency mean with 16x16x16 voxel ($4.7 \times 7.3 \times 9.4mm$) bin size and 0% overlap

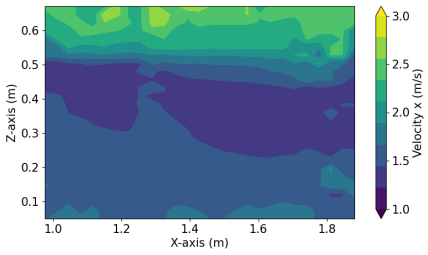

Figure 2.15: Surge low frequency mean with 32x32x32 voxel ($9.4 \times 14.7 \times 18.8mm$)bin size and 0% overlap

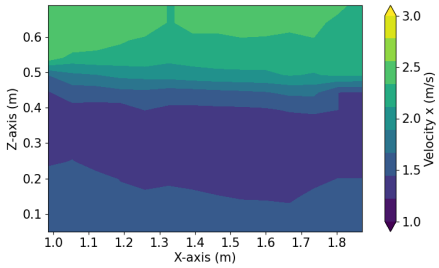

Figure 2.16: Surge low frequency mean with 64x64x64 voxel ($18.8 \times 29.4 \times 37.5mm$)6 bin size and 0% overlap

- **Overlap percentages**: In Figure 2.17 to Figure 2.20 the low frequency surge is plotted with four different overlap percentages and a 32x32x32 voxel ($9.4 \times 14.7 \times 18.8mm$) bin size. Again, it is clearly visible that increasing overlap percentages cause the detail to increase. However, the noise will also increase. Another key observation is that there are issues with the stitching of the images. It can be clearly observed where the different FOVs are stitched together, namely at around 1.3, 1.6 and 1.9 m. The largest issue can be seen between the first FOV and the second. It seems like the second, third, and fourth are a few centimetres lower than the first. This could be due to a measurement error or an uncertainty in the measuring equipment used to measure the height of the cameras. The test of the first FOV was also on another day than the tests of the other FOVs, which could be a cause of the errors.
- **Overlap percentages - number of particles**: Figure 2.21 to Figure 2.24, the effect of different overlap percentages on the number of particles is shown. The maximum number of particles for 12.5% and 25% is the same, as is the maximum number of particles for 50% and 75%.

However, there are more areas with more particles when the overlap percentage increases. This increase is particularly noticeable in the most left FOV. There are far fewer particles in this area than in other areas, especially when the overlap percentage is 12.5%. Though it looks like there are no particles in the dark blue areas, the minimum number of particles per bin is at least two. The particles are not evenly distributed, influencing the accuracy. Possible reasons for this included that 1) the flow field pushed the bubbles to these locations and 2) the bubbles were spread more evenly, but the LED lights did not light the full test section, meaning that bubbles were not recorded due to a lack of light. This is also discussed in Section 3.5 and Section 5.2.1. The 50% overlap was chosen again as a compromise between the detail and noise present.

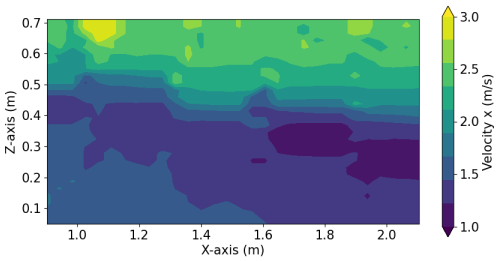

Figure 2.17: Surge low frequency mean with 32x32x32 bin size and 12.5% overlap

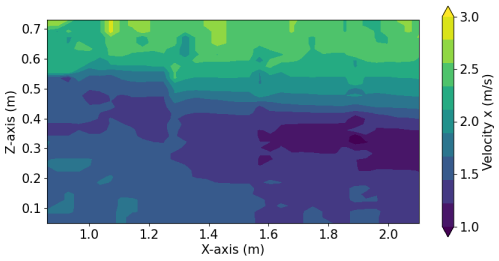

Figure 2.18: Surge low frequency mean with 32x32x32 bin size and 25% overlap

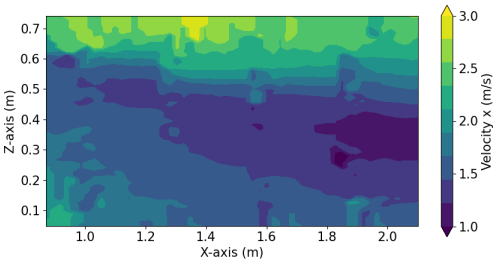

Figure 2.19: Surge low frequency mean with 32x32x32 bin size and 50% overlap

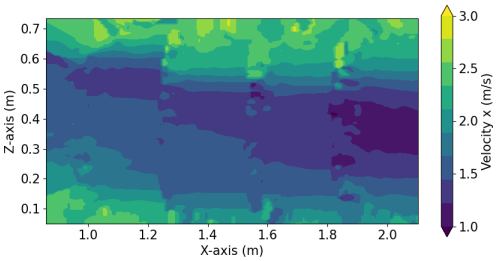

Figure 2.20: Surge low frequency mean with 32x32x32 bin size and 75% overlap

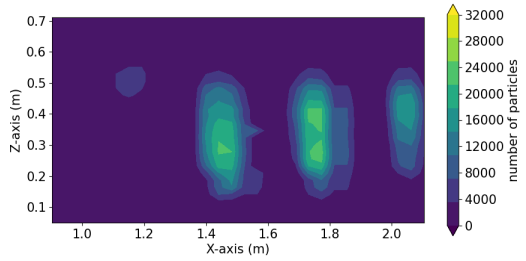

Figure 2.21: Surge 2 Hz frequency - number of particles - 32x32 bin size and 12.5% overlap

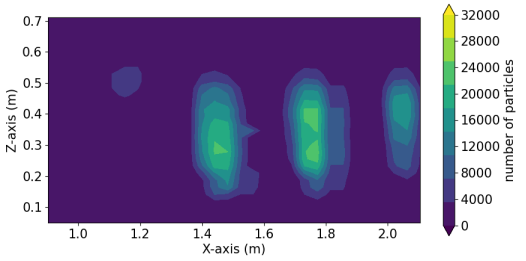

Figure 2.22: Surge 2 Hz frequency - number of particles - 32x32 bin size and 25% overlap

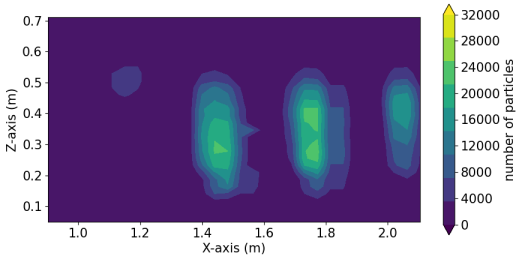

Figure 2.23: Surge 2 Hz frequency - number of particles - 32x32 bin size and 50% overlap

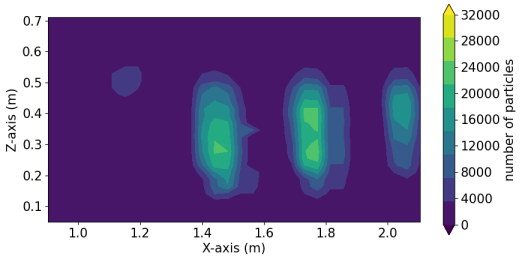

Figure 2.24: Surge 2 Hz frequency - number of particles - 32x32 bin size and 75% overlap

3. **Shake the Box (STB)**

   - **STB**: The Shake the Box function in DaVIS 10 was used to find the velocities. The parameters can be found in Figure 2.25

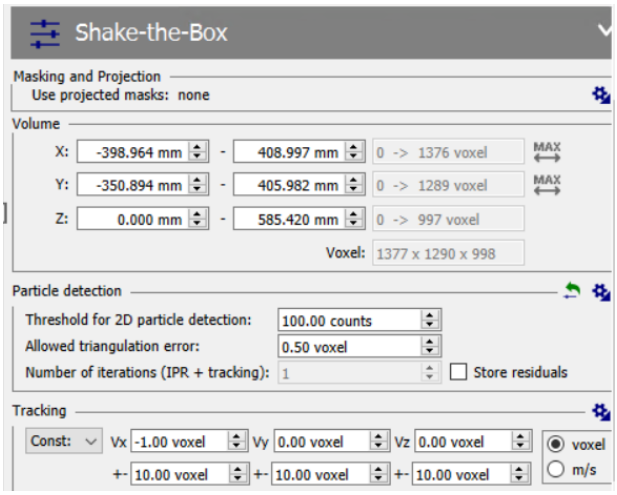

Figure 2.25: The *Shake the Box* parameters used in DaVIS10

4. **Plotting**

   - **Post-processing**: The data was first loaded and then a grid was created onto which the data could be projected. This was done because the data was a list rather than a 3D grid. Next, the data was interpolated onto this grid. The grid size of location 2 and location 3 were 25x25x25

and 35x35x35 data points, respectively, as there were fewer particles present at these locations. The locations are explained in Chapter 3. This was then plotted.

- **XZ plane**: In Figure 2.26 an example is shown of a plot. A wind turbine is positioned as reference. The origin is the hub of the wind turbine. In Figure 2.27 only the test section is plotted. In future sections, only the test section will be plotted for clarity.
- **YZ plane**: In Figure 2.28 an example is shown of a plot. A wind turbine is positioned as reference. The origin is the hub of the wind turbine. In Figure 2.29 only the test section is plotted. In future sections, only the test section will be plotted for clarity.
- **XY plane**: In Figure 2.30 an example is shown of a plot. A wind turbine is positioned as reference. The origin is the hub of the wind turbine. In Figure 2.31 only the test section is plotted. In future sections, only the test section will be plotted for clarity.

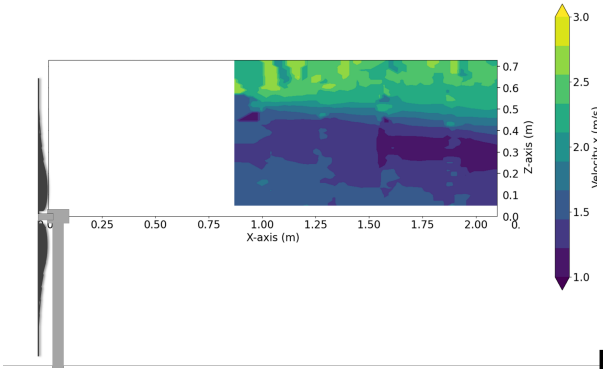

Figure 2.26: A mean velocity plot including the blades as reference - lateral view

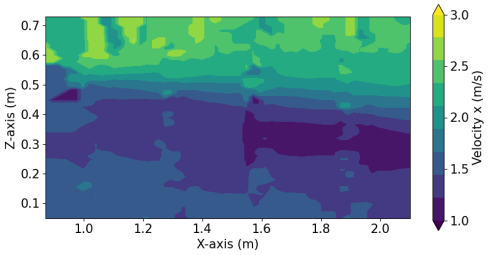

Figure 2.27: An example of how the mean velocity plots will be shown in later plots

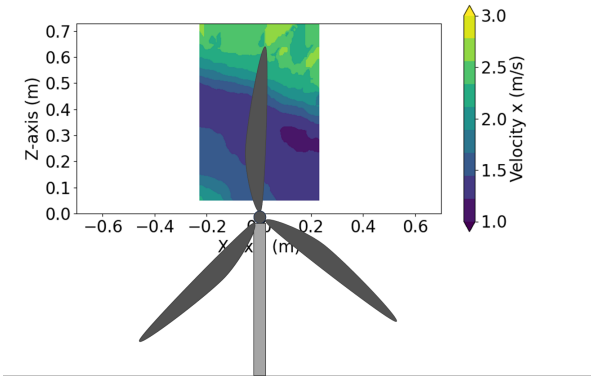

Figure 2.28: A mean velocity plot including the blades as reference - front view

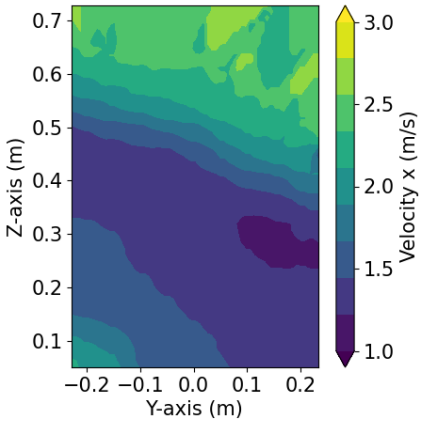

Figure 2.29: An example of how the mean velocity plots will be shown in later plots

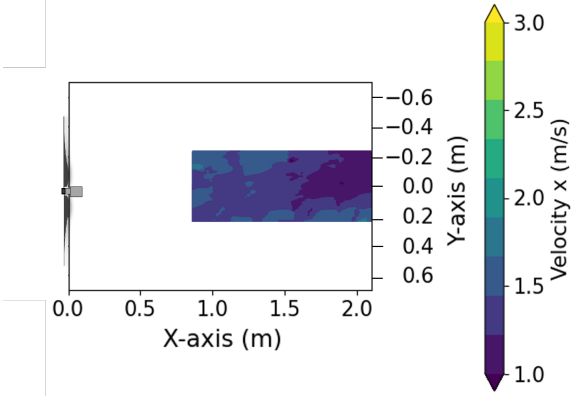

Figure 2.30: A mean velocity plot including the blades as reference - front view

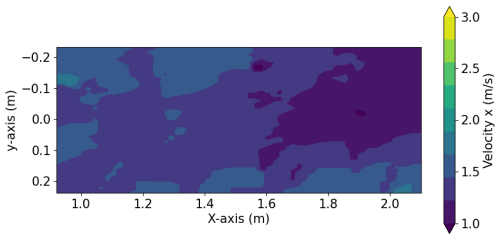

Figure 2.31: An example of how the mean velocity plots will be shown in later plots

Table 2.3: Test cases - PTV

#	D	motion	DoF	$\frac{\Delta V}{U_0}$	IM f	Amplitude	U	Radians per Minute (RPM)
1	1	sine	surge	0,05	2	15.9 [mm]	4	480
2	1	sine	surge	0,05	5	6.4 [mm]	4	480
4	1	sine	pitch	0,05	2	0.84 [deg]	4	480
4	1	sine	pitch	0,05	5	0.34 [deg]	4	480
5	1,25	sine	surge	0,05	2	15.9 [mm]	4	480
6	1,25	sine	surge	0,05	5	6.4 [mm]	4	480
7	1,25	sine	pitch	0,05	2	0.84 [deg]	4	480
8	1,25	sine	pitch	0,05	5	0.34 [deg]	4	480
9	1,5	sine	surge	0,05	2	15.9 [mm]	4	480
10	1,5	sine	surge	0,05	5	6.4 [mm]	4	480
11	1,5	sine	pitch	0,05	2	0.84 [deg]	4	480
12	1,5	sine	pitch	0,05	5	0.34 [deg]	4	480
13	1,75	sine	surge	0,05	2	15.9 [mm]	4	480
14	1,75	sine	surge	0,05	5	6.4 [mm]	4	480
15	1,75	sine	pitch	0,05	2	0.84 [deg]	4	480
16	1,75	sine	pitch	0,05	5	0.34 [deg]	4	480

2.3. Loads on the downstream turbine

Next, the experimental setup of the second experiment will be elaborated upon. The second experiment concerns two turbines, where the loads on the second wind turbine are examined. The additional turbine will be discussed, the set-up will be shown, and the test matrix will be explored.

2.3.1. Equipment

The additional equipment used for the second experiment is explained in this section. The additional load cell, turbine, and turbine stand are discussed.

Load cells

An ATI mini45 SI-290-10 load cell is placed between the tower top and nacelle. This load cell is visualised in Figure 2.32.

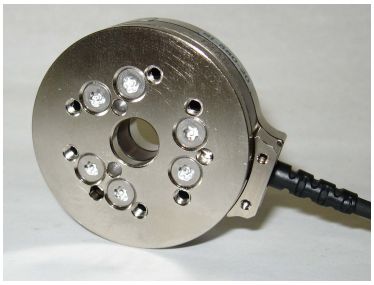

Figure 2.32: The ATI mini45 SI-290-10 load cell [47]

Additional turbine

In the second set of experiments, an additional turbine was added. The turbine is identical to the original turbine. This turbine is stationary, meaning it will be placed on top of a stand rather than on the hexapod. A load cell identical to the one on the first turbine will be placed on this turbine as well.

Turbine stand

The downstream turbine is stationary, meaning it does not have to stand on a kinematic robot but rather on a stationary stand. On one side, the turbine was attached using bolts and nuts and on the other side using clamps. The stand could be adjusted in height, it was put such that the two turbines were at the same height, and relocated at different positions in the wake.

2.3.2. Set-up

The setup of the loads experiment containing two wind turbines is shown in Figure 2.35. The second turbine will be placed downstream of the first turbine on several locations, as visualised in Figure 2.36. The upstream turbine will be placed on top of the hexapod identical to the earlier experiments. The measurements were done using load cells. The force measured in the X direction was considered the thrust, the moment measured in the X direction was considered the torque. The torque multiplied by the rotational speed of the turbine was considered the power. The torque and power were also measured with the motor and then converted to the rotor side, these values can be compared to the values measured by the load cell.

Figure 2.33: Downstream turbine positioned on top of the stand used.

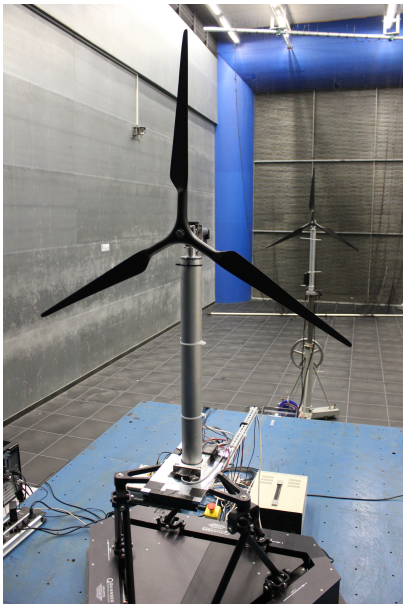

Figure 2.34: Both turbines, with a full view of the stand in the background.

Preparation

1. **Installation**
    - The second turbine was varied in downwind distance and at 3.5D it was also varied in lateral distance. It was only moved to one side. The locations are visualised in Figure 2.36. In total, there were 5 distances.
    - The wind speed of the wind tunnel was set to the rated (R) conditions, i.e. 4 m/s, and the wind turbines were either off or also set to rated conditions.
    - The hexapod was either off, or moving with a surge, pitch, or yaw motion with either a frequency of 2 Hz or 5 Hz. These are in total 8 different cases per distance.
    - In total, 40 different cases were done for the loads experiment, i.e. 8 different hexapod cases at 5 different distances. The test matrix is shown in Table 2.4.
2. **Calibration**
    - The load cells were zeroed whenever the turbine was moved.
3. **Robot calibration**
    - The hexapod was calibrated using a script that came along with the hexapod after each test.

Data acquisition

1. **Load cell**
    - An ATI mini45 SI-290-10 load cell is placed between the tower top and nacelle. These were used to measure the forces and moments. The torque and power were also measured using the motor. These outputs were saved in a .mat file.

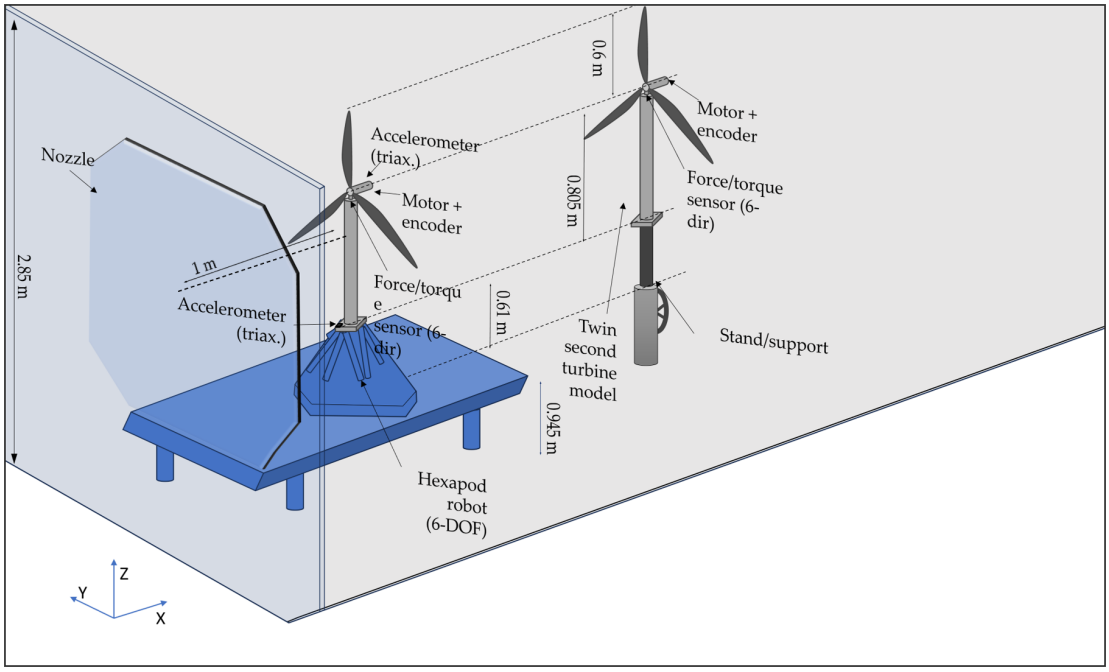

Figure 2.35: Set-up of the loads experiment done on the downstream turbine

Post-processing

1. **Loading data and applying filter**
    - The data files were loaded using a Matlab script and a Butterworth filter was applied.
2. **Time averaging**
    - After determining the number of periods and organizing them into a matrix, the average was calculated. The up and down movement of each sinusoid was synchronised, to make comparing the different cases more intuitive.
3. **Plotting**
    - The data was plotted in one figure. The process is also visualised in Figure 2.37.

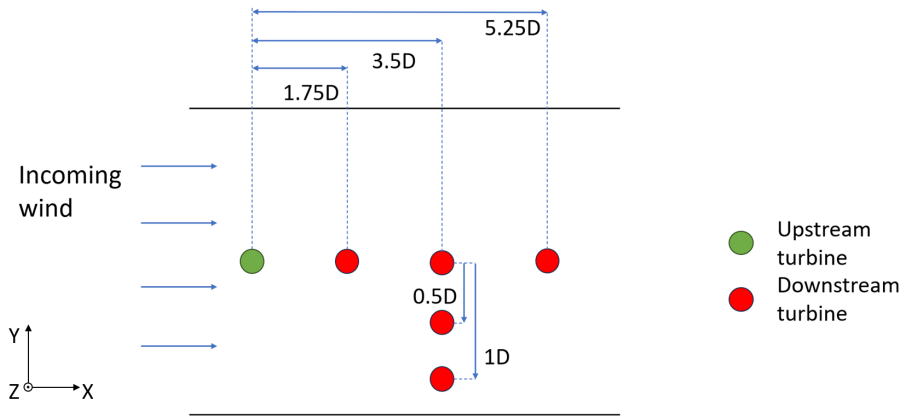

Figure 2.36: Visualisation of how the downstream turbine was placed at various positions

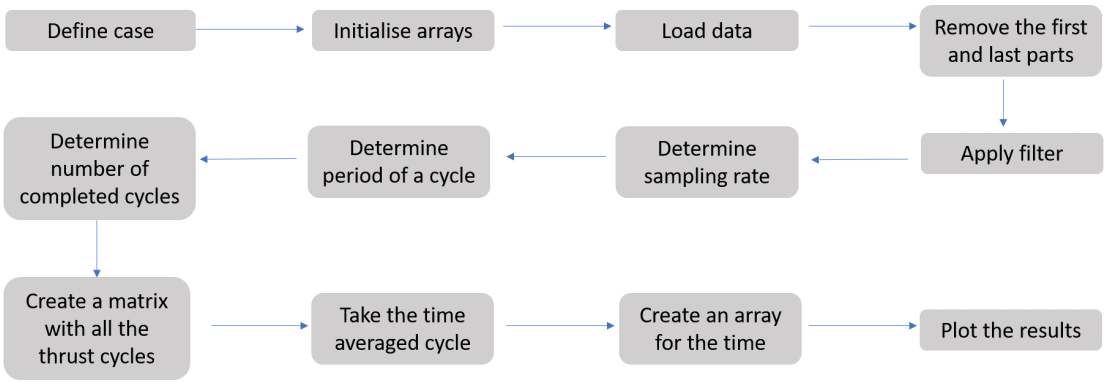

Figure 2.37: Flowchart indicating how the code was set up for creating the plots

Table 2.4: Test matrix of the loads experiment

#	Uref	WTM 1	IM DoF	IM f	Amplitude	WTM 2	pos downwind	pos lateral
1	Rated (R)	Off				R	1.75D	0
2	R	R				R	1.75D	0
3	R	R	Surge	2	15.9 [mm]	R	1.75D	0
4	R	R	Surge	5	6.4 [mm]	R	1.75D	0
5	R	R	Pitch	2	0.84 [deg]	R	1.75D	0
6	R	R	Pitch	5	0.34 [deg]	R	1.75D	0
7	R	R	Yaw	2	1.51 [deg]	R	1.75D	0
8	R	R	Yaw	5	0.61 [deg]	R	1.75D	0
9	R	Off				R	3.5D	0
10	R	R				R	3.5D	0
11	R	R	Surge	2	15.9 [mm]	R	3.5D	0
12	R	R	Surge	5	6.4 [mm]	R	3.5D	0
13	R	R	Pitch	2	0.84 [deg]	R	3.5D	0
14	R	R	Pitch	5	0.34 [deg]	R	3.5D	0
15	R	R	Yaw	2	1.51 [deg]	R	3.5D	0
16	R	R	Yaw	5	0.61 [deg]	R	3.5D	0
17	R	Off				R	3.5D	0.5D
18	R	R				R	3.5D	0.5D
19	R	R	Surge	2	15.9 [mm]	R	3.5D	0.5D
20	R	R	Surge	5	6.4 [mm]	R	3.5D	0.5D
21	R	R	Pitch	2	0.84 [deg]	R	3.5D	0.5D
22	R	R	Pitch	5	0.34 [deg]	R	3.5D	0.5D
23	R	R	Yaw	2	1.51 [deg]	R	3.5D	0.5D
24	R	R	Yaw	5	0.61 [deg]	R	3.5D	0.5D
25	R	Off				R	3.5D	1D
26	R	R				R	3.5D	1D
27	R	R	Surge	2	15.9 [mm]	R	3.5D	1D
28	R	R	Surge	5	6.4 [mm]	R	3.5D	1D
29	R	R	Pitch	2	0.84 [deg]	R	3.5D	1D
30	R	R	Pitch	5	0.34 [deg]	R	3.5D	1D
31	R	R	Yaw	2	1.51 [deg]	R	3.5D	1D
32	R	R	Yaw	5	0.61 [deg]	R	3.5D	1D
33	R	Off				R	5.25D	0
34	R	R				R	5.25D	0
35	R	R	Surge	2	15.9 [mm]	R	5.25D	0
36	R	R	Surge	5	6.4 [mm]	R	5.25D	0
37	R	R	Pitch	2	0.84 [deg]	R	5.25D	0
38	R	R	Pitch	5	0.34 [deg]	R	5.25D	0
39	R	R	Yaw	2	1.51 [deg]	R	5.25D	0
40	R	R	Yaw	5	0.61 [deg]	R	5.25D	0

3

Results: Particle Tracking Velocimetry

The results will be split into two sections, as two experiments were conducted. In this section, the results of the PTV will be discussed, while the results of the load tests done on the tandem turbines will be discussed in Chapter 4. First, the mean velocity plots of the wake of the turbine will be discussed. Next, the vorticity will be elaborated upon. After this, the Power Spectral Density (PSD) plots will be shown. Finally, the number of particles per bin and the uncertainties are discussed.

3.1. Different planes

In this chapter, the results will be presented as discussed in Section 2.2.4. There are six planes that will be discussed. These planes are shown in Figure 3.1 to create a visual understanding of which results are where.

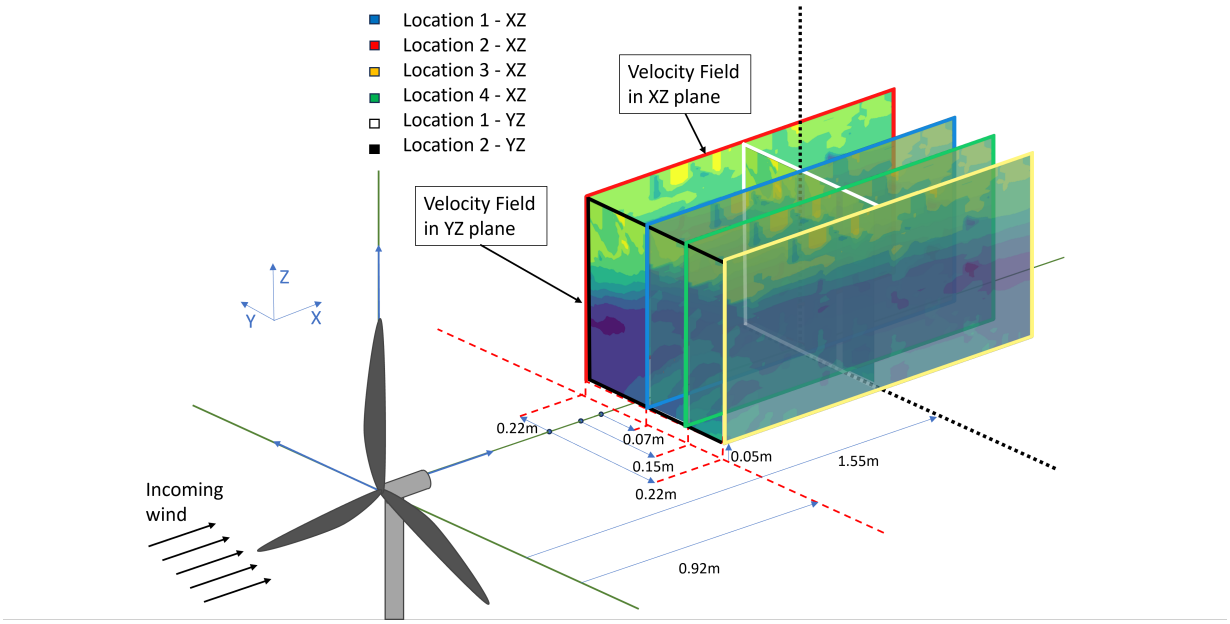

Figure 3.1: Various planes and their locations

3.2. Particle Tracking Velocimetry - Mean

Location 1

The mean velocity plots for the wake of the upstream turbine for different pitch and sway frequencies are shown in Figure 3.2 to Figure 3.5. The maximum velocity, as demonstrated in these plots, is constant across all the scenarios, namely 3.0 m/s. The highest velocities are observed at the tip of the blade, which could be attributed to tip vortices. Furthermore, the velocity is slightly higher near the root of the blade, this could be due to root vortices.

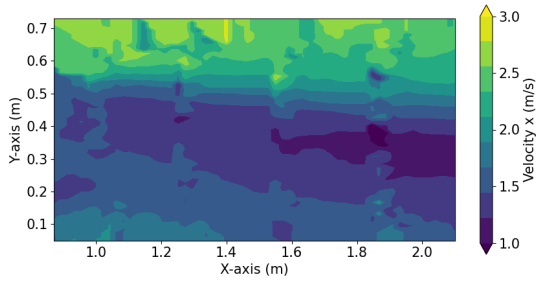

Figure 3.2: Mean velocity of the wake at location 1 when the upstream turbine is moving with a 2 Hz pitch motion

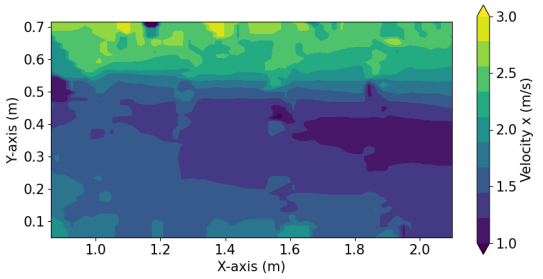

Figure 3.3: Mean velocity of the wake at location 1 when the upstream turbine is moving with a 5 Hz pitch motion

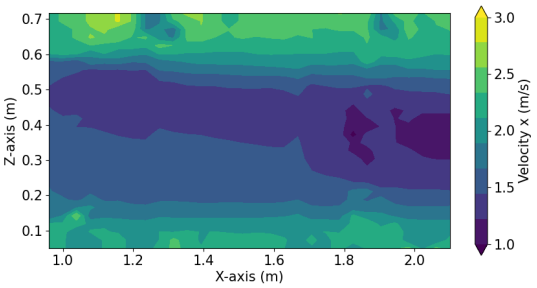

Figure 3.4: Mean velocity of the wake at location 1 when the upstream turbine is moving with a 2 Hz surge motion

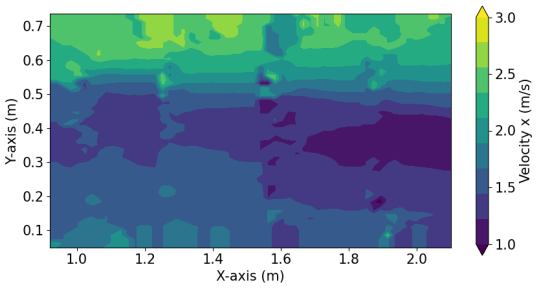

Figure 3.5: Mean velocity of the wake at location 1 when the upstream turbine is moving with a 5 Hz surge motion

The region containing the largest velocity reduction is located just below the area affected by the tip vortices, rather than at the centre of the rotor. This deficit is present further downstream as well and gradually extends toward the root of the blade, particularly in the case of pitch.
Something to notice is that the velocities within the flow field are all consistently lower than the free stream velocity of 4 m/s. This is expected, one would typically expect the air to reach the free stream velocity outside the blade's wake, however only a small part beyond the blade is measured. The blade goes up to 0.65 metres and the measurement area stops at 0.7 metres, i.e. not enough for the free stream velocity to be measured.

Some differences between pitch and surge motions are visible. Despite having the same maximum

velocity of 3.0 m/s in all cases, the velocity distribution varies somewhat between the scenarios.
In the high frequency pitch case, overall, there are more areas with higher velocities. A reason for this could be that the higher frequency movement adds more motion to the flow, leading to an increased velocity. When considering both pitch cases, the low velocity region starts at the top left and continues to the bottom right of the plot. This means that the low velocity area starts in the near wake close to the tip of the blade and extends to the centre of the rotor further downstream. This could be due to the angle the rotor makes, however to verify this a measurement with a rotor that is standing still should be done to be able to compare it.
When considering the surge cases, the low frequency case also demonstrates this pattern. However, it is slightly more extreme in this case. In the high frequency case, the low velocity region stays around the centre of the blade. Possibly, this is because when the surge frequency is high, the air does not have time to move in that direction and the surge movement causes it to stay at the centre of the blade.

Another reason could be that the turbine is less efficient to remove energy from the wind when it undergoes a sinusoidal pitch or surge motion. This seems to be more the case with pitch than with surge. Which is logical, because when the turbine is moving with a pitch motion, the angle of attack of the blades will be suboptimal.

Location 2

In Figure 3.6 to Figure 3.9 the mean velocities at location 2 are visualised. The main difference between location 1 and 2 is that the velocity at the root is slightly higher at location 2. The increase in velocity suggests that the flow field characteristics are different between the two planes, which makes sense as location 1 is centred and location 2 is where the turbine blades go up. The high velocity region at the tip of the blade also starts at a higher Z coordinate, this could be because the turbine blade is moving upwards, influencing the velocity distribution.

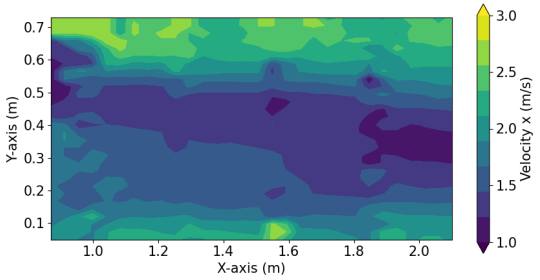

Figure 3.6: Mean velocity of the wake at location 2 when the upstream turbine is moving with a 2 Hz pitch motion

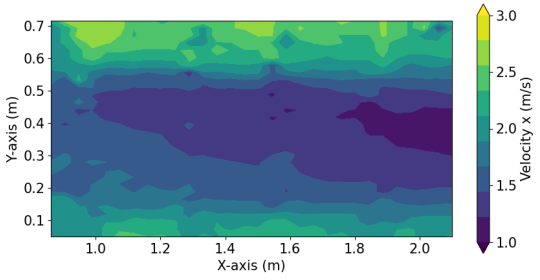

Figure 3.7: Mean velocity of the wake at location 2 when the upstream turbine is moving with a 5 Hz pitch motion

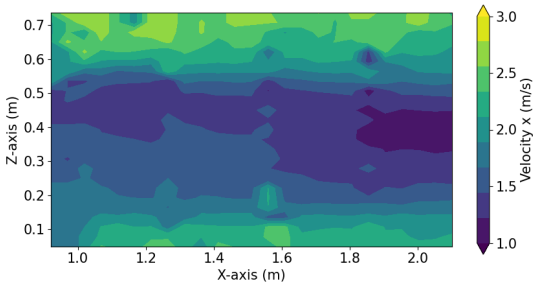

Figure 3.8: Mean velocity of the wake at location 2 when the upstream turbine is moving with a 2 Hz surge motion

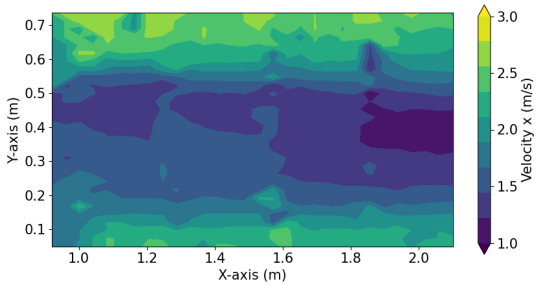

Figure 3.9: Mean velocity of the wake at location 2 when the upstream turbine is moving with a 5 Hz surge motion

Location 3

The velocity profiles at location 3 are shown in Figure 3.10 to Figure 3.13. The profiles are less clear here, this could be because there are fewer particles visible. This is further detailed in Section 3.5. The flow field looks more fragmented, making it harder to analyse the characteristics of the flow. It can be observed, however, that the velocity is not much higher at the root region. Additionally, the high velocity region starts at a lower Z coordinate. This could be due to the blade moving downward, as it is opposite to what is observed at location 2. It should be noted that since there are fewer particles here, it could also be due to a decrease in accuracy.

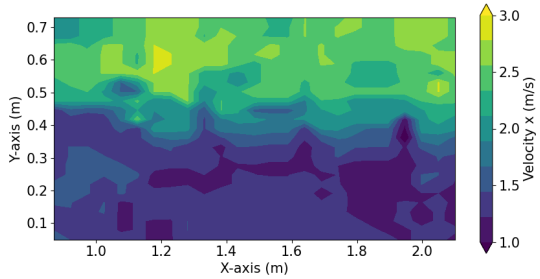

Figure 3.10: Mean velocity of the wake at location 3 when the upstream turbine is moving with a 2 Hz pitch motion

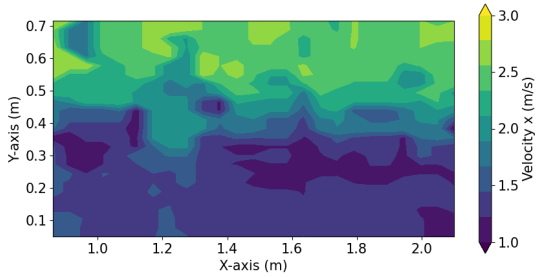

Figure 3.11: Mean velocity of the wake at location 3 when the upstream turbine is moving with a 5 Hz pitch motion

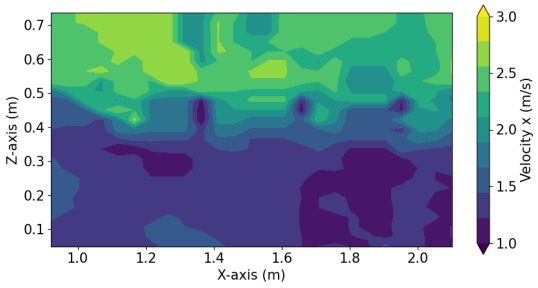

Figure 3.12: Mean velocity of the wake at location 3 when the upstream turbine is moving with a 2 Hz surge motion

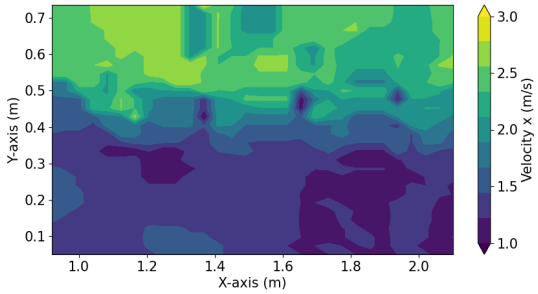

Figure 3.13: Mean velocity of the wake at location 3 when the upstream turbine is moving with a 5 Hz surge motion

Location 4

In Figure 3.14 to Figure 3.17 the velocity profiles at location 4 are shown. At this location, the characteristics are in between that of location 1 and 3, which is what is expected as it is a plane located in between those two planes. It seems like the particle count is higher than at location 3, as the velocities look less like a patchwork. The velocity at the root is slightly higher again, but still lower than at location 1. The velocity at the root is especially higher in the case of LF surge, this could indicate that at HF surge and both pitch cases the flow mixes better, as discussed earlier.

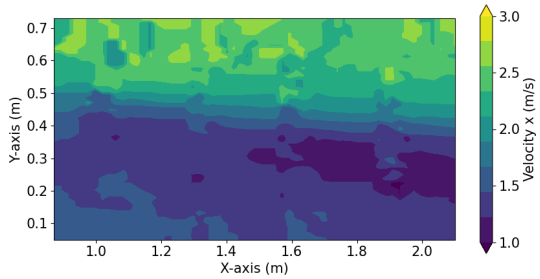

Figure 3.14: Mean velocity of the wake at location 4 when the upstream turbine is moving with a 2 Hz pitch motion

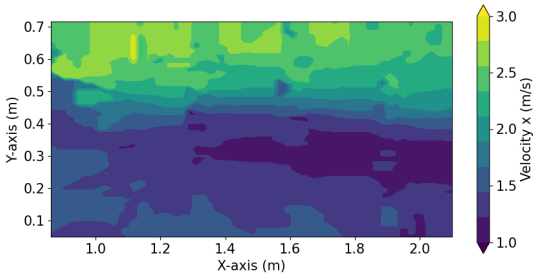

Figure 3.15: Mean velocity of the wake at location 4 when the upstream turbine is moving with a 5 Hz pitch motion

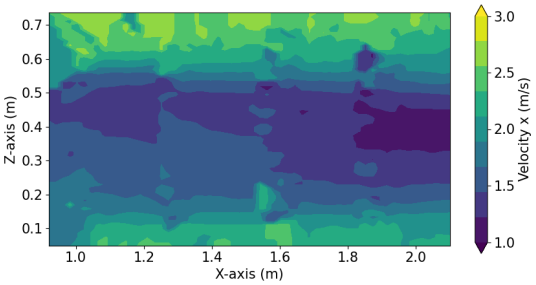

Figure 3.16: Mean velocity of the wake at location 4 when the upstream turbine is moving with a 2 Hz surge motion

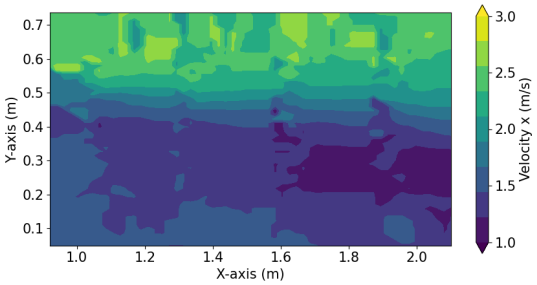

Figure 3.17: Mean velocity of the wake at location 4 when the upstream turbine is moving with a 5 Hz surge motion

Mean velocity in the YZ plane

In Figure 3.18 to Figure 3.21, the mean velocities are shown in the YZ plane (i.e. perpendicular to the previous plots at x= 0m) at 1.55 m behind the turbine. It is visible that near the root the velocities are slightly higher, possibly due to root vortices. In the middle section it is the lowest and above the tip of the blade it is the highest due to tip vortices.

The velocity plane is not symmetrical around Y=0, which is what was expected. One reason for this could be that the hub is actually aligned with Y = -0.23 m. Another reason could be that since the blades are rotating, on one side the blade goes up and on the other side it goes down, causing the plot to be asymmetrical.

These results also correspond to the earlier discussed plots. At location 2, the high velocity region at the root of the blade was clearly visible, whereas at location 3, this was not visible.

In the wake, the area where the velocity is low seems to be greater at low frequency motions than at high frequency motions, especially in the case of surge. The high frequency plots also seem to have more details at the location where the tip vortices are expected to be found.

It is also very evident that there are not as many particles everywhere. These are 2D plots at a location with relatively many particles. The YZ plots are measurements at the location with a relatively large number of seeding particles reducing the errors in the measurements, which ultimately lead to smoother plots.

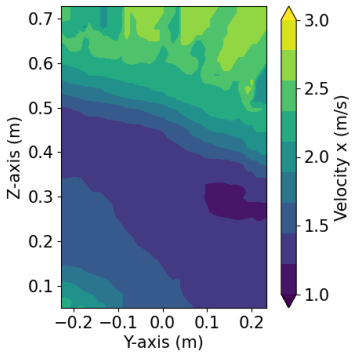

Figure 3.18: Mean velocity of the wake when the upstream turbine is moving with a 2 Hz pitch motion - YZ plane - X location is 1.55 m behind the upstream rotor

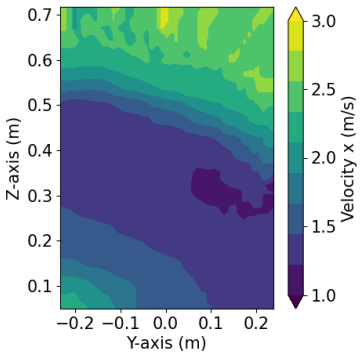

Figure 3.19: Mean velocity of the wake when the upstream turbine is moving with a 5 Hz pitch motion - YZ plane - X location is 1.55 m behind the upstream rotor

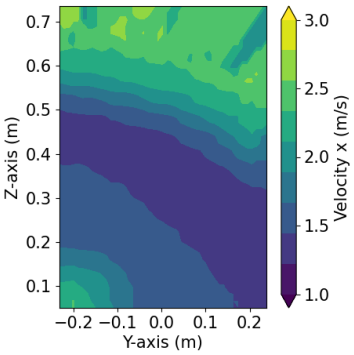

Figure 3.20: Mean velocity of the wake when the upstream turbine is moving with a 2 Hz surge motion - YZ plane - X location is 1.55 m behind the upstream rotor

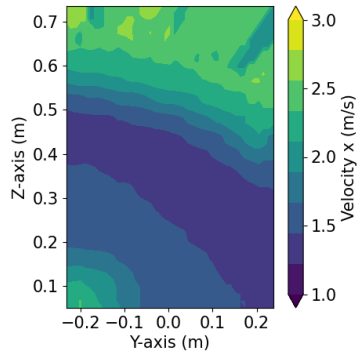

Figure 3.21: Mean velocity of the wake when the upstream turbine is moving with a 5 Hz surge motion - YZ plane - X location is 1.55 m behind the upstream rotor

Figure 3.22 to Figure 3.25 are examples of where there are few particles. These planes are $0.92D$ behind the rotor. It is evident that the areas with certain velocities are not as smooth. It is still evident that there is a higher velocity in the top / top right and lower at the bottom / bottom left.

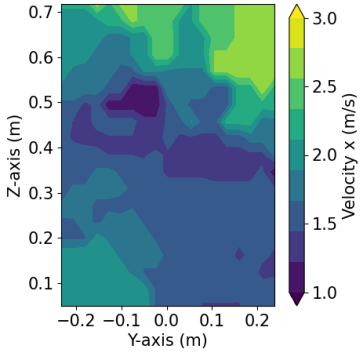

Figure 3.22: Mean velocity of the wake when the upstream turbine is moving with a 2 Hz pitch motion - YZ plane - X location is 0.92 m behind the upstream rotor

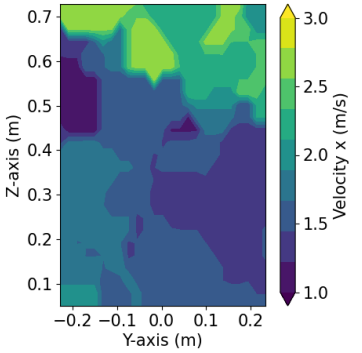

Figure 3.23: Mean velocity of the wake when the upstream turbine is moving with a 5 Hz pitch motion - YZ plane - X location is 0.92 m behind the upstream rotor

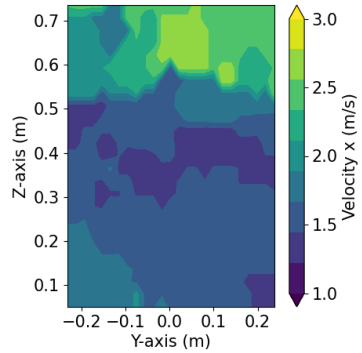

Figure 3.24: Mean velocity of the wake when the upstream turbine is moving with a 2 Hz surge motion - YZ plane - X location is 0.92 m behind the upstream rotor

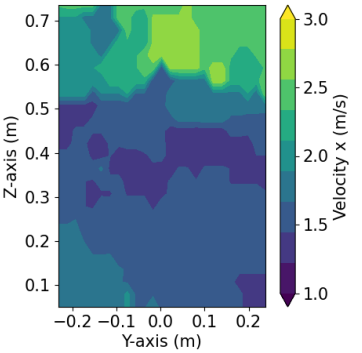

Figure 3.25: Mean velocity of the wake when the upstream turbine is moving with a 5 Hz surge motion - YZ plane - X location is 0.92 m behind the upstream rotor

3.3. Particle Tracking Velocimetry - Vorticity

In this section, the vorticity will be compared at several locations. First, several XZ planes will be discussed. First, the XZ plane aligned with the hub is shown, after which the XZ planes at the edges of the test sections will be discussed. Next an XZ plane at a quarter of the test section is explored, and finally a YZ plane 0.92 D behind the rotor is discussed.

Vorticity at location 1

First, the vorticity at the mid-plane is compared. The vorticity in the four cases is quite similar, except for the surge low-frequency case, where the vorticity is significantly lower. Interestingly, the vorticity is not lower at a low frequency pitch. This could indicate that the pitch motion has more effect on the wake. Furthermore, the vorticity peaks are further downstream in the high frequency cases. This suggests that at higher frequencies, the vortices travel further.

Figure 3.26 to Figure 3.29 visualise the vorticity magnitude for the four cases. In the low frequency surge case, the vorticity is clearly lower, and the other cases are deemed to be similar. The downstream locations of the peaks are also visible, showing the variation in behaviour due to the frequencies.

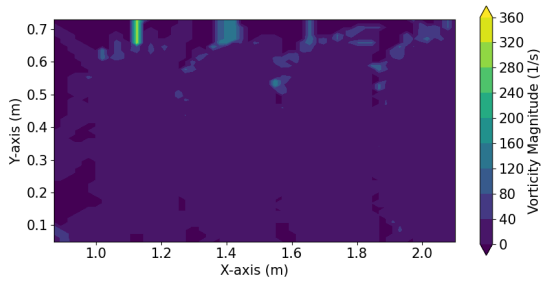

Figure 3.26: Vorticity magnitude of the wake when the upstream turbine is moving with a 2 Hz pitch motion - 2D plot at location 1

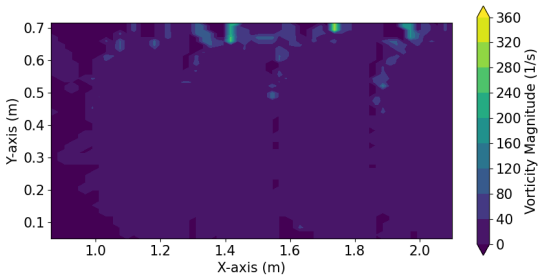

Figure 3.27: Vorticity magnitude of the wake when the upstream turbine is moving with a 5 Hz pitch motion - 2D plot at location 1

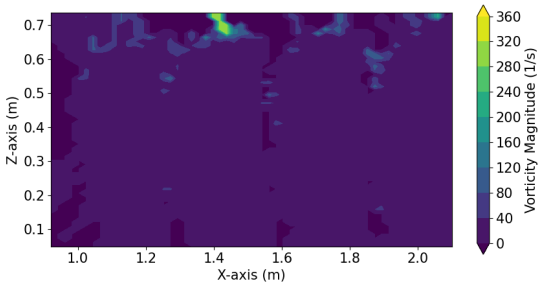

Figure 3.28: Vorticity magnitude of the wake when the upstream turbine is moving with a 2 Hz surge motion - 2D plot at location 1

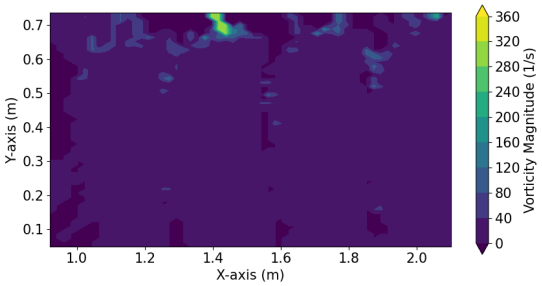

Figure 3.29: Vorticity magnitude of the wake when the upstream turbine is moving with a 5 Hz surge motion - 2D plot at location 1

Vorticity at location 2

When looking at the vorticity at a plane at the edge (Figure 3.30 to Figure 3.33), more variations become apparent between low and high frequencies. The maximum vorticity at low frequency is noticeably lower than the vorticity at high frequency. Besides this, there are more locations where the vorticity is not zero at low frequency. This implies that the flow is more scattered and less concentrated, whereas at high frequency cases, the vorticity seems to be more concentrated and higher in terms of magnitude.
Additionally, there seem to be root vortices present here as well, as opposed to location 1. This is especially the case for the low frequency cases.
It should be noted that the vorticity circles around the places where more particles are found, i.e. the vorticity is higher when there are few particles. This could be because the airflow pushes the helium filled soap bubbles towards the locations with less vorticity.

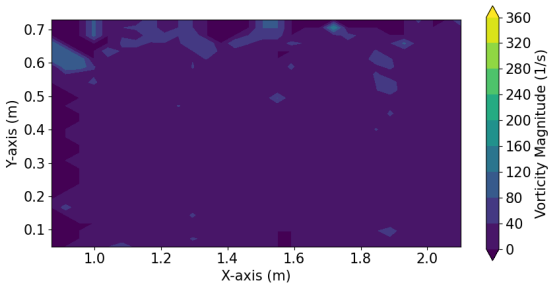

Figure 3.30: Vorticity magnitude of the wake when the upstream turbine is moving with a 2 Hz pitch motion - 2D plot at location 2

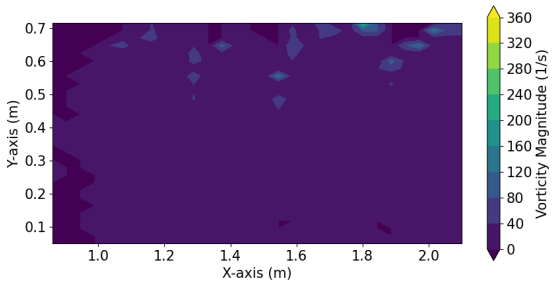

Figure 3.31: Vorticity magnitude of the wake when the upstream turbine is moving with a 5 Hz pitch motion - 2D plot at location 2

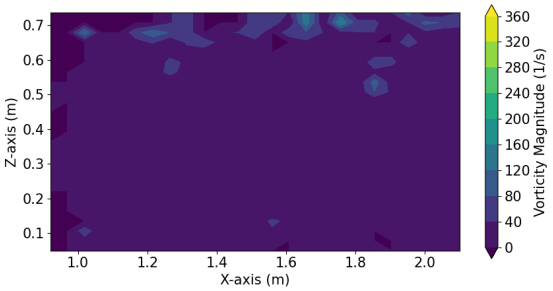

Figure 3.32: Vorticity magnitude of the wake when the upstream turbine is moving with a 2 Hz surge motion - 2D plot at location 2

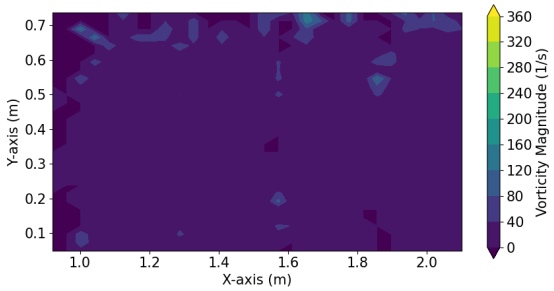

Figure 3.33: Vorticity magnitude of the wake when the upstream turbine is moving with a 5 Hz surge motion - 2D plot at location 2

Vorticity at location 3

On the other side of the test section, the vorticity plots look very different (Figure 3.34 to Figure 3.37). The vorticity is now lower in case of the high frequency. This could be attributed to the particles being more concentrated on the one side than the other. One reason this happened is because the wake moves towards the other side of the y plane.

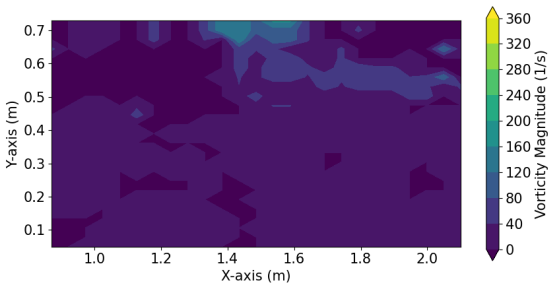

Figure 3.34: Vorticity magnitude of the wake when the upstream turbine is moving with a 2 Hz pitch motion - 2D plot at location 3

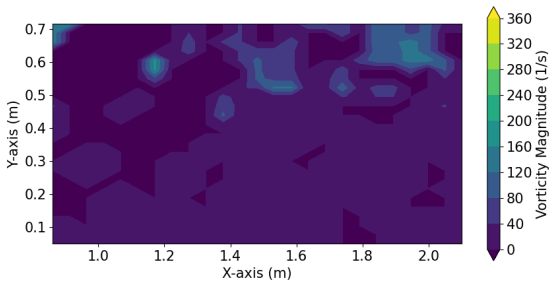

Figure 3.35: Vorticity magnitude of the wake when the upstream turbine is moving with a 5 Hz pitch motion - 2D plot at location 3

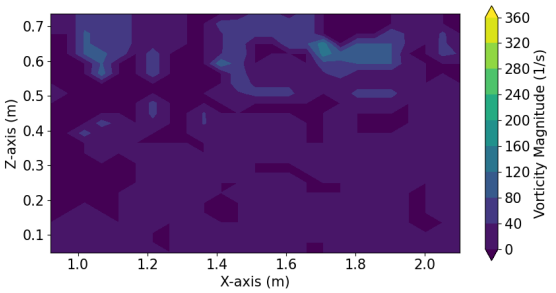

Figure 3.36: Vorticity magnitude of the wake when the upstream turbine is moving with a 2 Hz surge motion - 2D plot at location 3

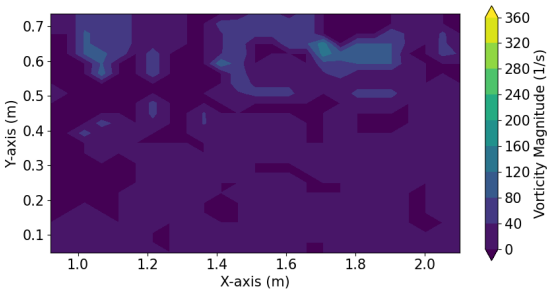

Figure 3.37: Vorticity magnitude of the wake when the upstream turbine is moving with a 5 Hz surge motion - 2D plot at location 3

Vorticity at location 4

The vorticity at location four is different again Figure 3.38 to Figure 3.41. It should be noted again that the vorticity seem to be present mostly around the areas with high number of particles. The tip vortices are present again, as well as some root vortices. The vortices are higher again when the frequency is higher, though there are more higher spots when the frequency is lower. This could indicate that the vortices travel further at higher frequency.

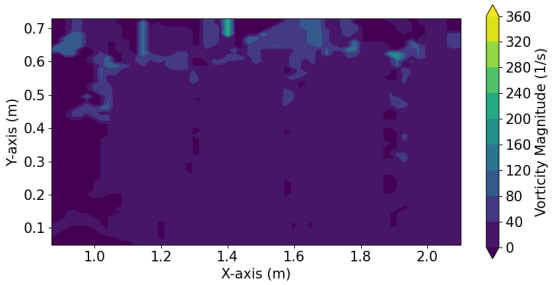

Figure 3.38: Vorticity magnitude of the wake when the upstream turbine is moving with a 2 Hz pitch motion - 2D plot at location 4

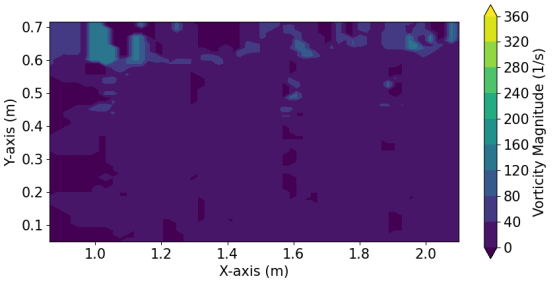

Figure 3.39: Vorticity magnitude of the wake when the upstream turbine is moving with a 5 Hz pitch motion - 2D plot at location 4

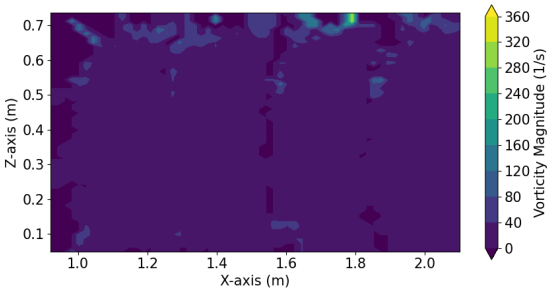

Figure 3.40: Vorticity magnitude of the wake when the upstream turbine is moving with a 2 Hz surge motion - 2D plot at location 4

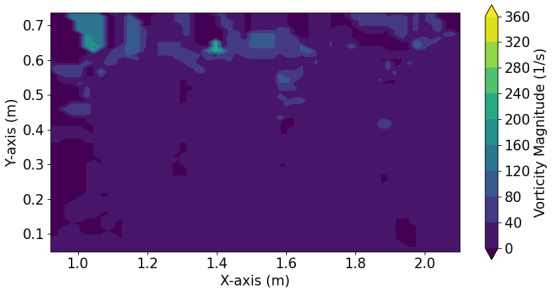

Figure 3.41: Vorticity magnitude of the wake when the upstream turbine is moving with a 5 Hz surge motion - 2D plot at location 4

Vorticity in the YZ plane

The vorticity in the YZ plane at 1.55 m behind the turbine is shown in (Figure 3.42 to Figure 3.45). These plots are at a plane perpendicular to the previous plots. The vorticity is the highest at the tip. The root vortices are not visible. The vorticity is the lowest at the surge LF case, indicating this has the least effect on the vorticity in the wake.

The maximum magnitude of the others are the same, but the low frequency pitch has the most areas with high vorticity.

It would be expected that the vorticity is somewhat symmetrical around Y = 0 m. However, this is not the case. This finding does, however, align with the results found in Figure 3.2.

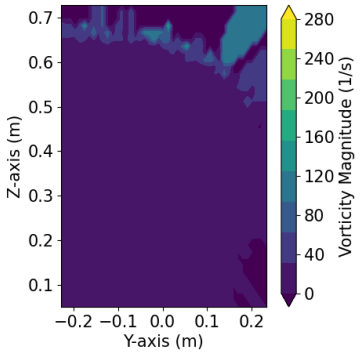

Figure 3.42: Vorticity of the wake when the upstream turbine is moving with a 2 Hz pitch motion - YZ plane - Location 1

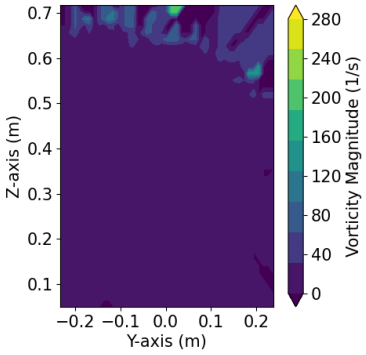

Figure 3.43: Vorticity of the wake when the upstream turbine is moving with a 5 Hz pitch motion - YZ plane - Location 1

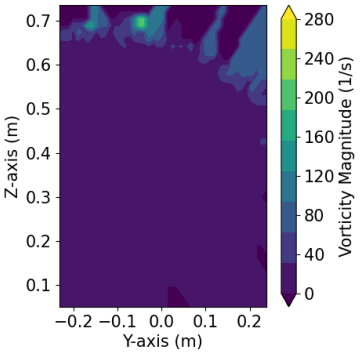

Figure 3.44: Vorticity of the wake when the upstream turbine is moving with a 2 Hz surge motion - YZ plane - Location 1

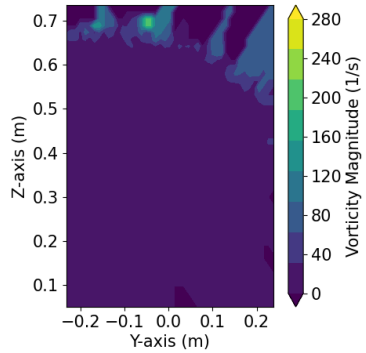

Figure 3.45: Vorticity of the wake when the upstream turbine is moving with a 5 Hz surge motion - YZ plane - Location 1

In Figure 3.46 to Figure 3.49, the vorticity at 0.92 m behind the rotor is shown. Again the results are less clear as the particle count is lower.There are some higher vorticity magnitude patches at the top right, especially in the pitch cases. This could suggest that pitch has a greater influence on the vorticity. Both surge plots look very similar.

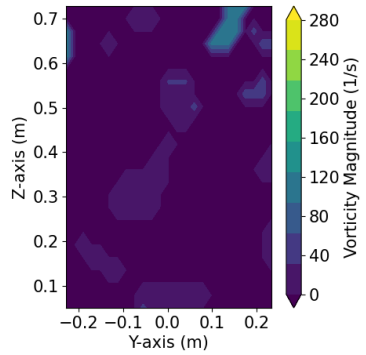

Figure 3.46: Vorticity of the wake when the upstream turbine is moving with a 2 Hz pitch motion - YZ plane - Location 2

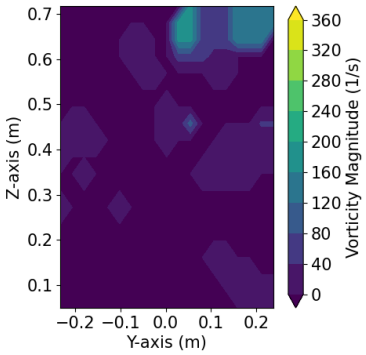

Figure 3.47: Vorticity of the wake when the upstream turbine is moving with a 5 Hz pitch motion - YZ plane - Location 2

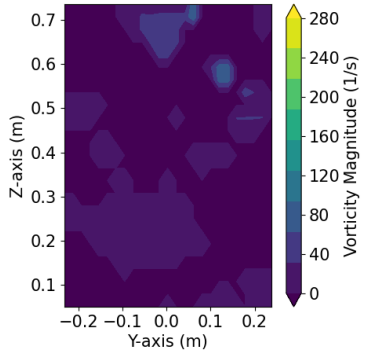

Figure 3.48: Vorticity of the wake when the upstream turbine is moving with a 2 Hz surge motion - YZ plane - Location 2

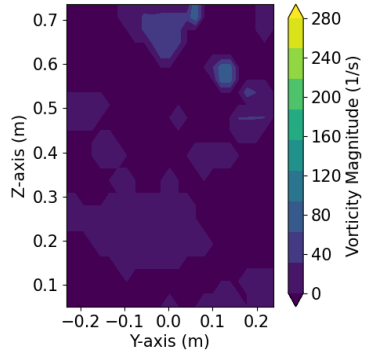

Figure 3.49: Vorticity of the wake when the upstream turbine is moving with a 5 Hz surge motion - YZ plane - Location 2

3.4. Particle Tracking Velocimetry - Power Spectral Density

The PSD are shown in Figure 3.50 to Figure 3.53. The low frequency pitch, high frequency pitch and high frequency surge look very similar. There is a peak at 2 Hz. At low frequency surge, there is no peak at 2 Hz, but there is one at 8 Hz. 8 Hz corresponds to the RPM of the two turbines. However, the peaks at low frequency surge are much smaller than the peaks at the other frequencies.

A 2 Hz peak is expected to be seen in the wake in the low frequency cases, and a 5 Hz is expected to be seen in the wake in the high frequency cases, however as this is not the case, this should be looked at again.

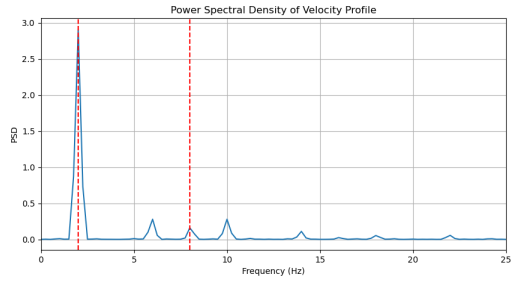

Figure 3.50: PSD of the velocity in the X direction of the wake when the upstream turbine is moving with a 2 Hz pitch motion at the tip of the blade, 1.5D downstream, toward the right edge in the Y plane

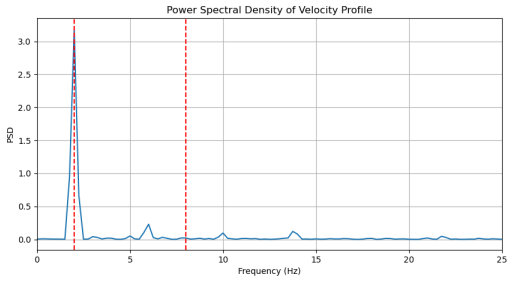

Figure 3.51: PSD of the velocity in the X direction of the wake when the upstream turbine is moving with a 5 Hz pitch motion at the tip of the blade, 1.5D downstream, toward the right edge in the Y plane

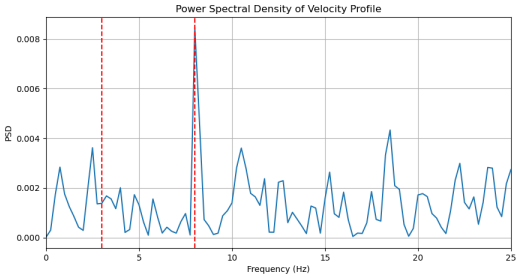

Figure 3.52: PSD of the velocity in the X direction of the wake when the upstream turbine is moving with a 2 Hz surge motion at the tip of the blade, 1.5D downstream, toward the right edge in the Y plane

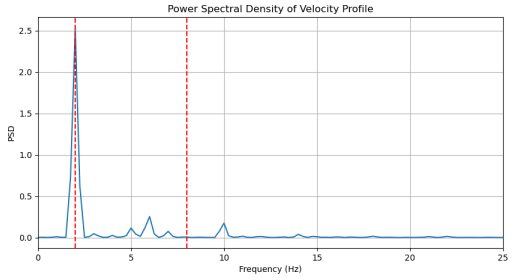

Figure 3.53: PSD of the velocity in the X direction of the wake when the upstream turbine is moving with a 5 Hz surge motion at the tip of the blade, 1.5D downstream, toward the right edge in the Y plane

3.5. Particle concentrations

There are four regions where the number of particles is higher. The number of particles becomes lower in the surrounding areas, but it does not reach zero. This uneven distribution suggests that the particles are not spreaded well, which potentially leads to a reduced measurement accuracy. Additionally, the number of particles amongst the various Y planes also varies. The highest number of particles can be found at the middle plane and the lowest in the positive Y planes. This was also noticeable during the experiments. A possible reason for this is that the flow field pushed the bubbles to these locations. It could also be the case that the bubbles were spreaded more evenly, but the LED lights did not light the full test section, meaning that bubbles were not recorded due to a lack of light.

The uneven distribution of the particles has some consequences. In areas where the particle concentration is high, the data may be more trustworthy. On the other hand, the data may be less trustworthy in areas with a lower particle count, potentially resulting in incorrect interpretations of the data. It may be necessary to analyse why the difference in particle count was so large to increase the accuracy of the test. Moreover, the difference in the amount of particles between the various y-planes could be caused by the differences in the flow field at these locations. It could be that the regions with lower concentrations have fewer particles because of how the flow in the wake is constructed, i.e. it contains more turbulence. The same goes for the areas containing more particles, the flow may be more stable there. Nevertheless, understanding the real reasons behind these concentration differences is important.

Location 1

At this location, the number of particles is the highest amongst the four locations in the XZ plane (visible in Figure 3.54 to Figure 3.57). The four regions where the particle concentrations are higher are clearly visible. This corresponds to what was earlier discussed on the velocity plots. The higher particle density allows for a more accurate analysis of the flow. The high number of particles observed here suggests that either the seeding was more effective here, or that the lights are concentrated on this area, rather than on the whole test section.

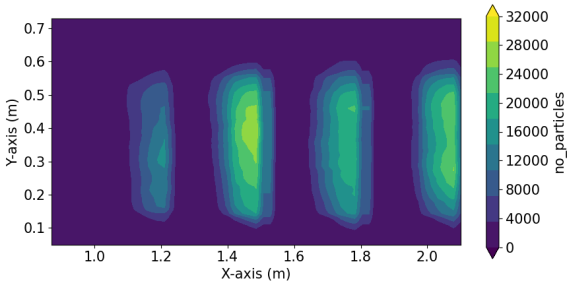

Figure 3.54: Number of particles per bin in the wake when the upstream turbine is moving with a 5 Hz surge motion - 2D plot at location 1

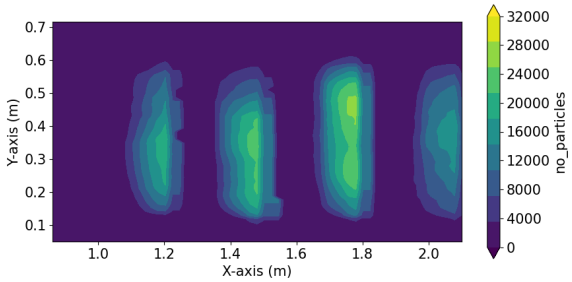

Figure 3.55: Number of particles per bin in the wake when the upstream turbine is moving with a 5 Hz surge motion - 2D plot at location 1

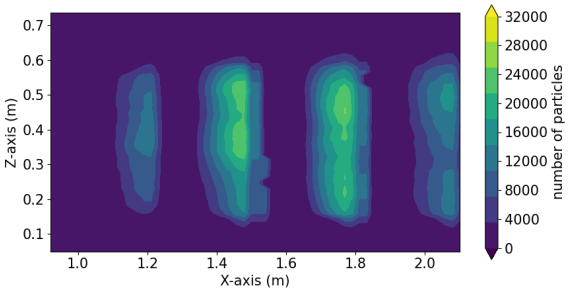

Figure 3.56: Number of particles per bin in the wake when the upstream turbine is moving with a 5 Hz surge motion - 2D plot at location 1

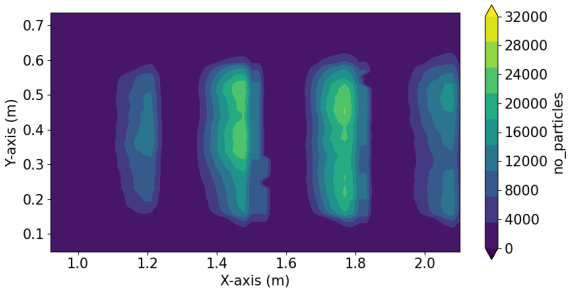

Figure 3.57: Number of particles per bin in the wake when the upstream turbine is moving with a 5 Hz surge motion - 2D plot at location 1

Location 2

In Figure 3.58 to Figure 3.61 the number of particles per bin at location 2 are shown. At this location, the particle count is considerably lower when compared to location 1. The four regions are, however, still visible. In the velocity plots, it was also noticeable that the particle count was lower, as the plots appeared less smooth. The lower particle count could be attributed to flow field interactions or lighting differences between the various locations.

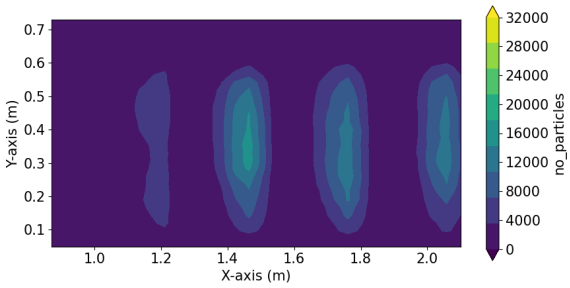

Figure 3.58: Number of particles per bin in the wake when the upstream turbine is moving with a 5 Hz surge motion - 2D plot at location 2

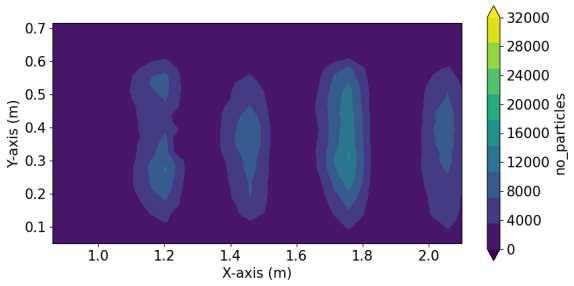

Figure 3.59: Number of particles per bin in the wake when the upstream turbine is moving with a 5 Hz surge motion - 2D plot at location 2

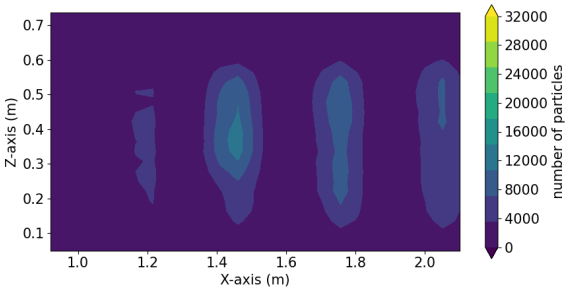

Figure 3.60: Number of particles per bin in the wake when the upstream turbine is moving with a 5 Hz surge motion - 2D plot at location 2

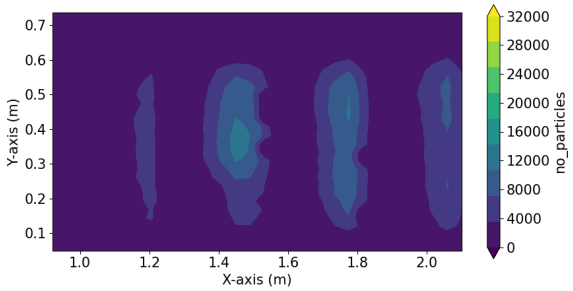

Figure 3.61: Number of particles per bin in the wake when the upstream turbine is moving with a 5 Hz surge motion - 2D plot at location 2

Location 3

The particle count is significantly lower at this location compared to location 1 and 2. This is visualised in Figure 3.62 to Figure 3.65. The number of particles is not equal to zero, but it is low enough that no contours are visible in the plots. This makes it harder to get accurate velocity and vorticity plots, as could also be seen in Section 3.2 and Section 3.3. The low particle count could be due to the flow of the velocity field or inadequate lighting.

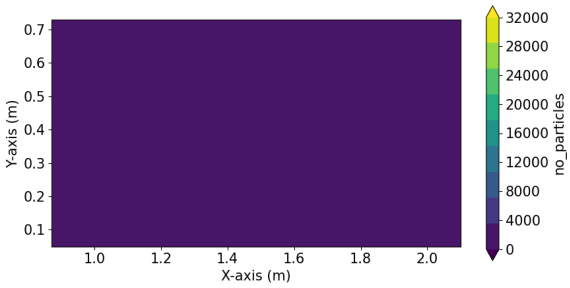

Figure 3.62: Number of particles per bin in the wake when the upstream turbine is moving with a 5 Hz surge motion - 2D plot at location 3

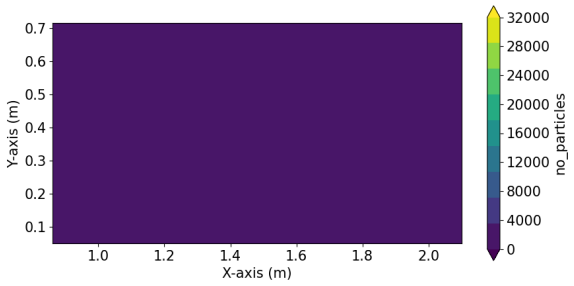

Figure 3.63: Number of particles per bin in the wake when the upstream turbine is moving with a 5 Hz surge motion - 2D plot at location 3

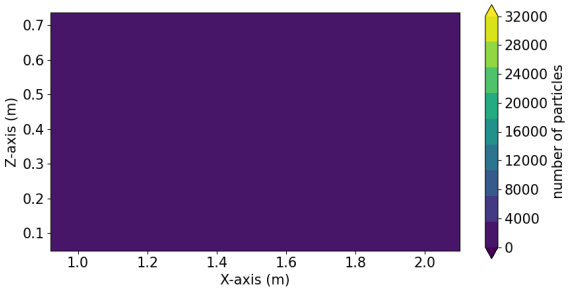

Figure 3.64: Number of particles per bin in the wake when the upstream turbine is moving with a 5 Hz surge motion - 2D plot at location 3

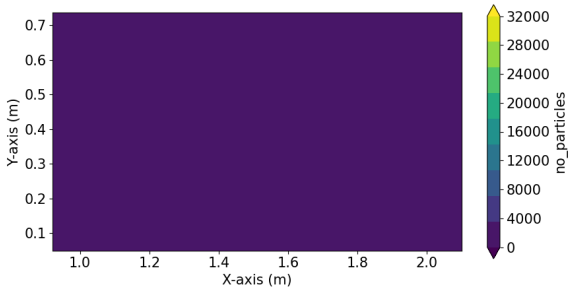

Figure 3.65: Number of particles per bin in the wake when the upstream turbine is moving with a 5 Hz surge motion - 2D plot at location 3

Location 4

In Figure 3.66 to Figure 3.69 the number of particles per bin at location 4 are shown. At this location, the height of the particle count falls in between that of location 1 and 3. While the number of particles per bin is lower than at location 1, it is not as low as in location 3. Three of the four regions are still distinguishable. Interestingly, the test section closest to the wind turbine contains the fewest amount of particles. It should be investigated as to why this is the case. A possibility is that slight variations in the setup could cause the discrepancies, since the first test section was recorded on a different day.

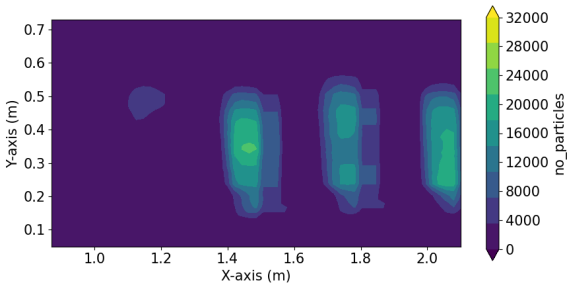

Figure 3.66: Number of particles per bin in the wake when the upstream turbine is moving with a 5 Hz surge motion - 2D plot at location 4

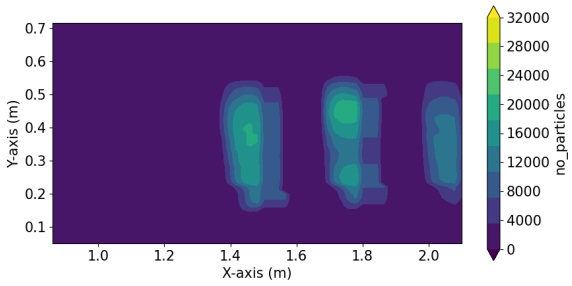

Figure 3.67: Number of particles per bin in the wake when the upstream turbine is moving with a 5 Hz surge motion - 2D plot at location 4

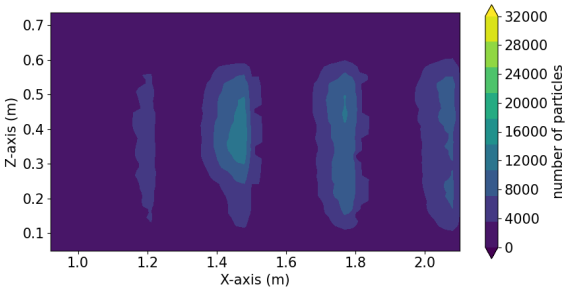

Figure 3.68: Number of particles per bin in the wake when the upstream turbine is moving with a 5 Hz surge motion - 2D plot at location 4

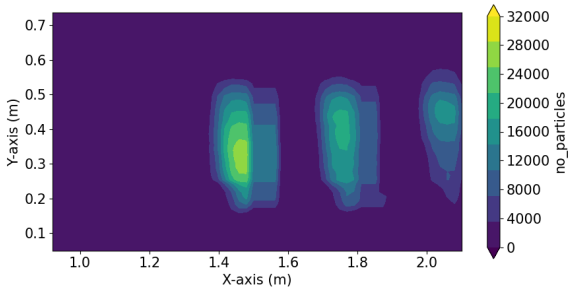

Figure 3.69: Number of particles per bin in the wake when the upstream turbine is moving with a 5 Hz surge motion - 2D plot at location 4

YZ planes

The amount of particles per bin is the largest in the middle-left area. The number is far higher in the surge case than in the other cases. When comparing various planes, there is also a large distinction in number of particles. In Figure 3.70 to Figure 3.73, the number of particles at X = 1.55 m is shown. In Figure 3.74 to Figure 3.77, the number of particles at X = 1.13 m is shown. In the latter figures, the number of particles per bin is much lower. This corresponds to the earlier findings (Figure 3.78 to Figure 3.81), where there were also fewer particles at this distance.

In the YZ planes, it is also clearly visible that the number of particles on the left-hand side are indeed higher than on the right-hand side.

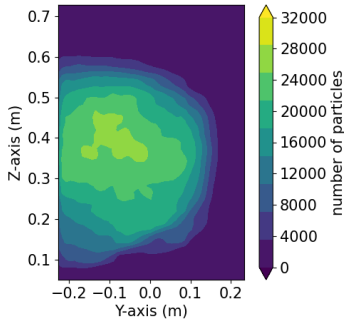

Figure 3.70: Number of particles per bin in the wake when the upstream turbine is moving with a 2 Hz pitch motion - YZ plane- X location is 1.55 m behind the upstream rotor

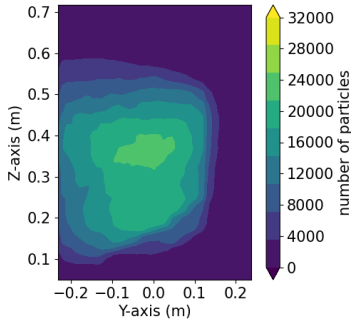

Figure 3.71: Number of particles per bin in the wake when the upstream turbine is moving with a 5 Hz pitch motion - YZ plane- X location is 1.55 m behind the upstream rotor

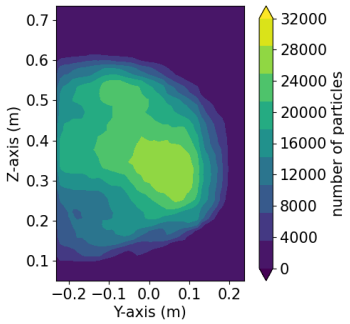

Figure 3.72: Number of particles per bin in the wake when the upstream turbine is moving with a 2 Hz surge motion - YZ plane- X location is 1.55 m behind the upstream rotor

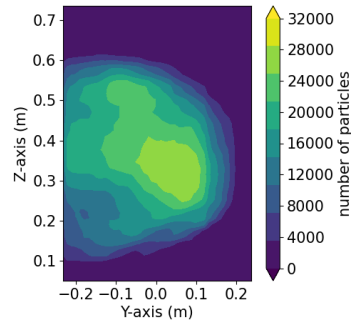

Figure 3.73: Number of particles per bin in the wake when the upstream turbine is moving with a 5 Hz surge motion - YZ plane- X location is 1.55 m behind the upstream rotor

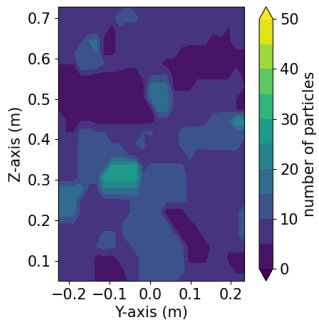

Figure 3.74: Number of particles per bin in the wake when the upstream turbine is moving with a 2 Hz pitch motion - YZ plane- X location is 1.13 m behind the upstream rotor

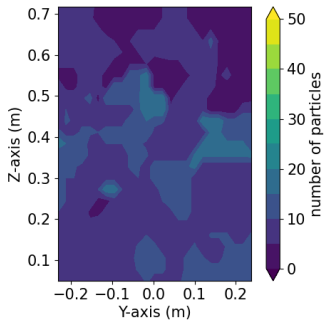

Figure 3.75: Number of particles per bin in the wake when the upstream turbine is moving with a 5 Hz pitch motion - YZ plane- X location is 1.13 m behind the upstream rotor

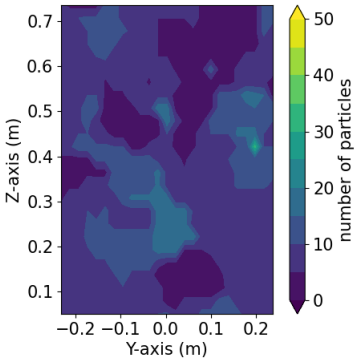

Figure 3.76: Number of particles per bin in the wake when the upstream turbine is moving with a 2 Hz surge motion - YZ plane- X location is 1.13 m behind the upstream rotor

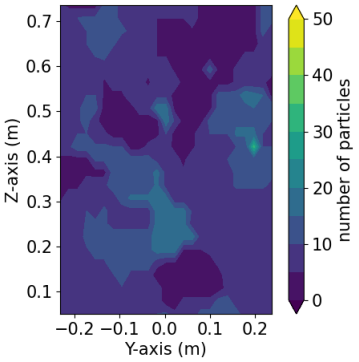

Figure 3.77: Number of particles per bin in the wake when the upstream turbine is moving with a 5 Hz surge motion - YZ plane- X location is 1.13 m behind the upstream rotor

3.6. Particle Tracking Velocimetry - Standard Deviation

Next, the standard deviation will be discussed. When the standard deviation is higher, the inconsistencies in the behaviour of the particles are greater. At locations where the velocity is lower, the standard deviation is lower and at locations where the velocity is higher, the standard deviation is higher. At most locations, it is also very visible where the test sections are stitched together.

Location 1

At location 1, the standard deviation is the lowest close to the wind turbine and it becomes higher further downstream (Figure 3.78 to Figure 3.81). Moreover, it is higher in the tip region, where the velocity is higher. It seems that outside the wake the standard deviation is higher than in the direct wake. The highest standard deviation can be found in the high frequency pitch, albeit only a small part. The high frequency pitch also has the largest region with a low standard deviation. The standard deviation clearly follows the motion of the mean velocities, as shown in Section 3.2.

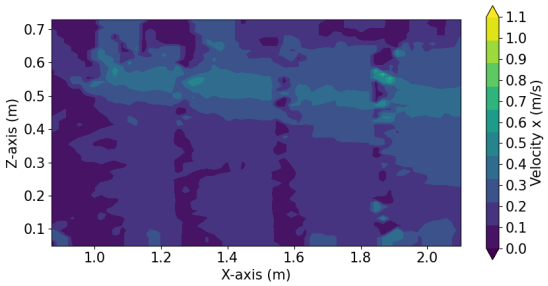

Figure 3.78: Standard deviation of the velocity of the wake when the upstream turbine is moving with a 2 Hz pitch motion - 2D plot at location 1

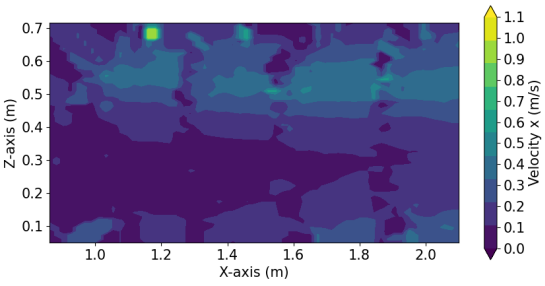

Figure 3.79: Standard deviation of the velocity of the wake when the upstream turbine is moving with a 5 Hz pitch motion - 2D plot at location 1

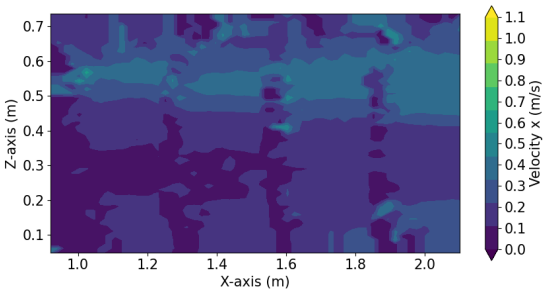

Figure 3.80: Standard deviation of the velocity of the wake when the upstream turbine is moving with a 2 Hz surge motion - 2D plot at location 1

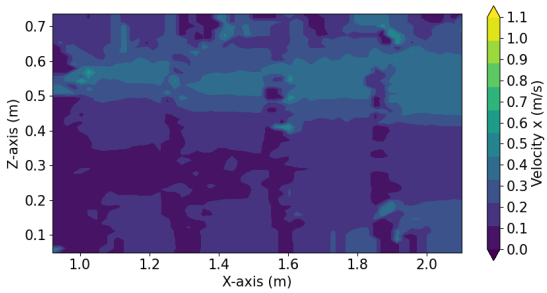

Figure 3.81: Standard deviation of the velocity of the wake when the upstream turbine is moving with a 5 Hz surge motion - 2D plot at location 1

Location 2

The standard deviations at location 2 are shown in Figure 3.82 to Figure 3.85. At this location, the graphs become less detailed again. Apart from that, the standard deviation plots look very similar to those of location 1.

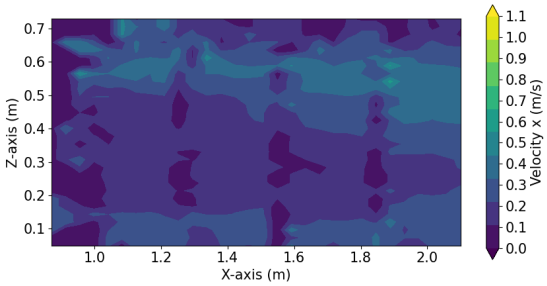

Figure 3.82: Standard deviation of the velocity of the wake when the upstream turbine is moving with a 2 Hz pitch motion - 2D plot at location 2

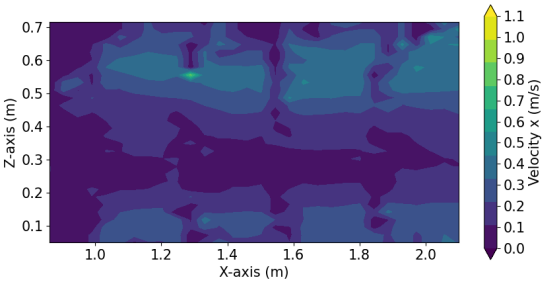

Figure 3.83: Standard deviation of the velocity of the wake when the upstream turbine is moving with a 5 Hz pitch motion - 2D plot at location 2

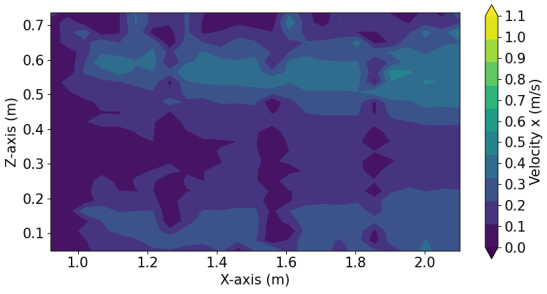

Figure 3.84: Standard deviation of the velocity of the wake when the upstream turbine is moving with a 2 Hz surge motion - 2D plot at location 2

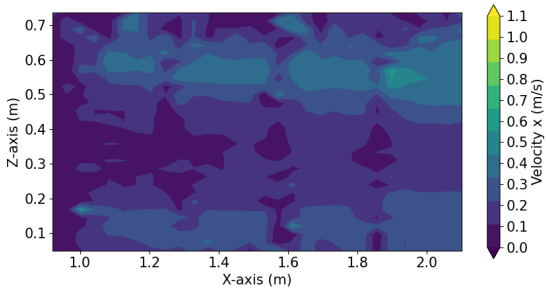

Figure 3.85: Standard deviation of the velocity of the wake when the upstream turbine is moving with a 5 Hz surge motion - 2D plot at location 2

Location 3

At this location, the plots become far less clear due to the decrease in particles per bin (Figure 3.86 to Figure 3.89). This was also visible in earlier sections.

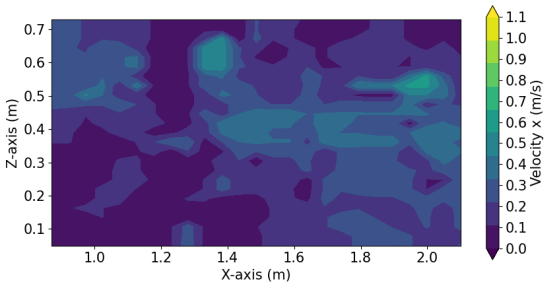

Figure 3.86: Standard deviation of the velocity of the wake when the upstream turbine is moving with a 2 Hz pitch motion - 2D plot at location 3

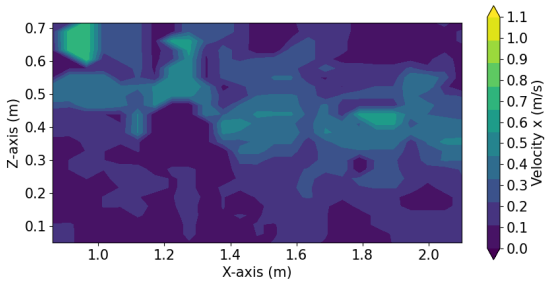

Figure 3.87: Standard deviation of the velocity of the wake when the upstream turbine is moving with a 5 Hz pitch motion - 2D plot at location 3

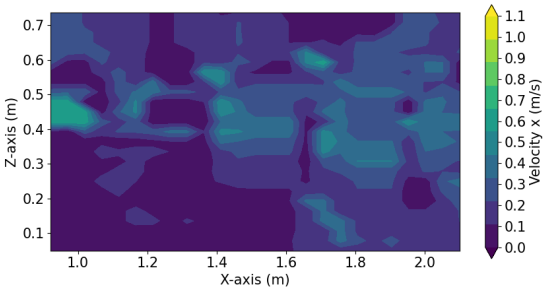

Figure 3.88: Standard deviation of the velocity of the wake when the upstream turbine is moving with a 2 Hz surge motion - 2D plot at location 3

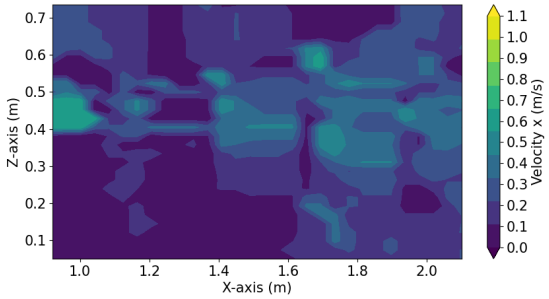

Figure 3.89: Standard deviation of the velocity of the wake when the upstream turbine is moving with a 5 Hz surge motion - 2D plot at location 3

Location 4

The plots are far more detailed in this location again (Figure 3.90 to Figure 3.93). The standard deviation is again higher when the velocity is higher.

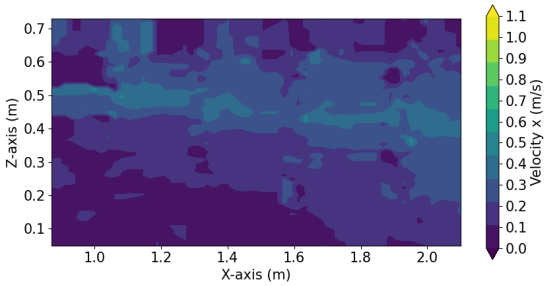

Figure 3.90: Standard deviation of the velocity of the wake when the upstream turbine is moving with a 2 Hz pitch motion - 2D plot at location 4

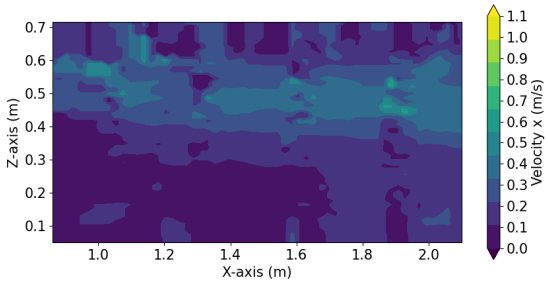

Figure 3.91: Standard deviation of the velocity of the wake when the upstream turbine is moving with a 5 Hz pitch motion - 2D plot at location 4

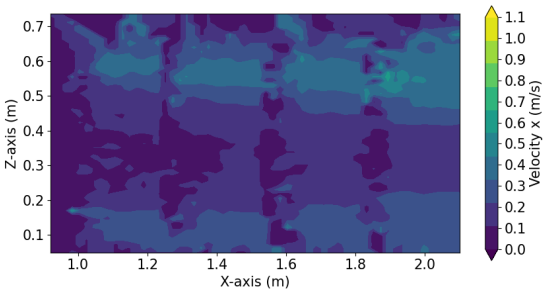

Figure 3.92: Standard deviation of the velocity of the wake when the upstream turbine is moving with a 2 Hz surge motion - 2D plot at location 4

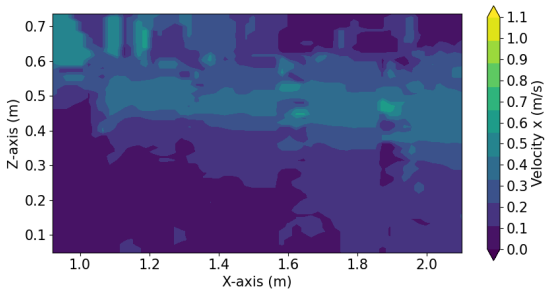

Figure 3.93: Standard deviation of the velocity of the wake when the upstream turbine is moving with a 5 Hz surge motion - 2D plot at location 4

3.7. Particle Tracking Velocimetry - uncertainties

The uncertainties are calculated using Equation 3.1 [48]. The error relative to the free stream velocity is calculated. This is done because when the velocities are very low, the error could be high, whereas this would not really be a problem. The equation requires the number of measurements (N), the standard deviation ($s(\overline{x})$), and the free stream velocity ($\overline{x}$).

$$\epsilon = \frac{s(\overline{x})}{\sqrt{N}\overline{x}} \tag{3.1}$$

Number of measurements

The number of measurements taken was 5000, however, since the measurements are correlated, the number used for N must be lower. To estimate the number of uncorrelated measurements, the total number of measurements (5000) was divided by the number of measurements after which the auto-correlation reached a low value. To find this number, the velocity time series and the autocorrelation of these velocity time series at a few locations was plotted. It can be seen in Figure 3.94 that the function is very periodic. This is because of the rotating blades and moving platform. This is why the x-axis crossing is used as the point where the measurements are not correlated any more. At the outer edges it can be seen that there is some noise. When doing the autocorrelation of these locations, it can be seen that this is uncorrelated. Several points were investigated, the x-axis crossing at each location was in between 62.5 and 65. Therefore, to estimate the error, a value of $\frac{5000}{64} = 78$ was chosen for N.

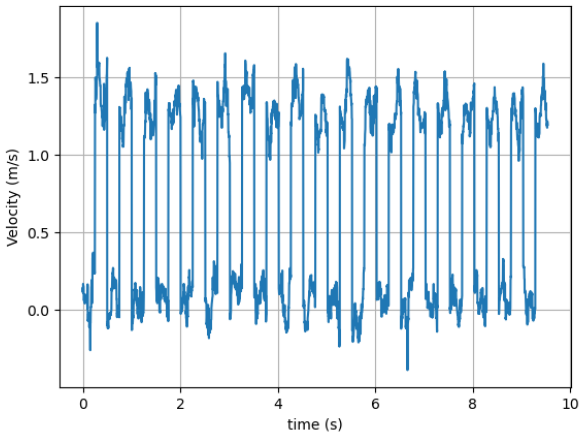

Figure 3.94: Velocity profile in time at one location

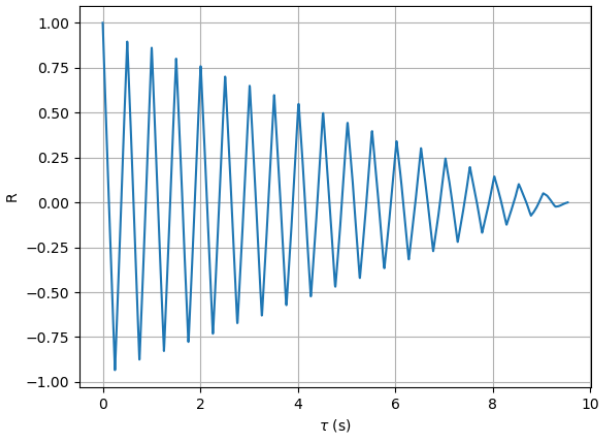

Figure 3.95: Autocorrelation of the velocity profile

Location 1

The error follows the shape of the standard deviation and mean velocities. In general, the error stays below 2%, only in the high frequency pitch case the error goes up to 3.5%. This indicates that the maximum error measured is $\pm 0.14 m/s$, meaning the measurements are quite accurate.

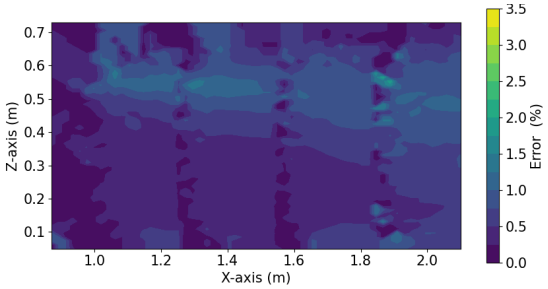

Figure 3.96: Error of the velocity relative to the free stream velocity when the upstream turbine is moving with a 2 Hz pitch motion - 2D plot at location 1

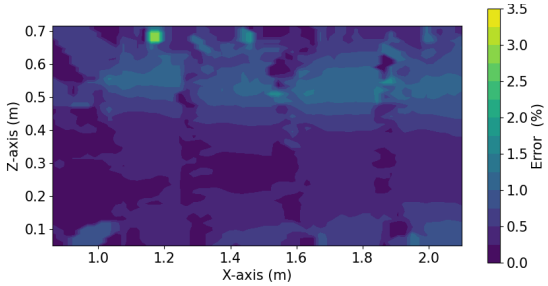

Figure 3.97: Error of the velocity relative to the free stream velocity when the upstream turbine is moving with a 5 Hz pitch motion - 2D plot at location 1

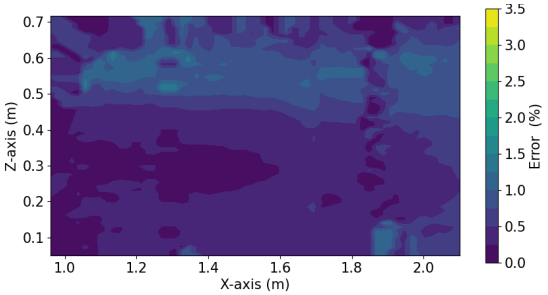

Figure 3.98: Error of the velocity relative to the free stream velocity when the upstream turbine is moving with a 2 Hz surge motion - 2D plot at location 1

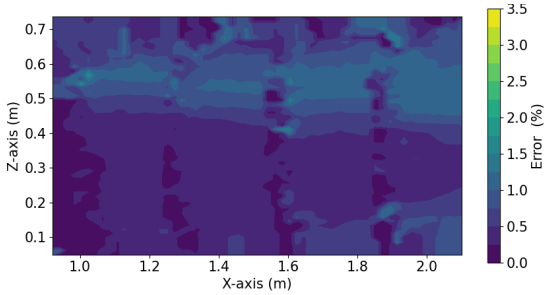

Figure 3.99: Error of the velocity relative to the free stream velocity when the upstream turbine is moving with a 5 Hz surge motion - 2D plot at location 1

Location 2

The error plots look similar to those at location 1. There is a lower peak in the high frequency pitch plot.

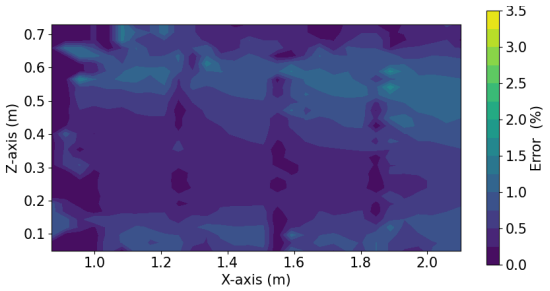

Figure 3.100: Error of the velocity relative to the free stream velocity when the upstream turbine is moving with a 2 Hz pitch motion - 2D plot at location 2

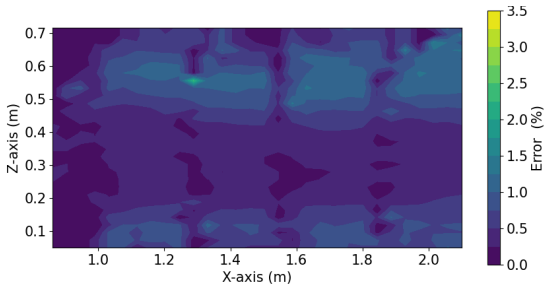

Figure 3.101: Error of the velocity relative to the free stream velocity when the upstream turbine is moving with a 5 Hz pitch motion - 2D plot at location 2

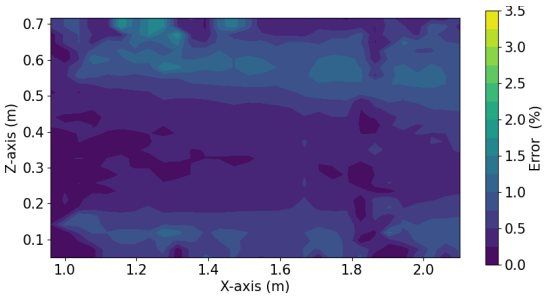

Figure 3.102: Error of the velocity relative to the free stream velocity when the upstream turbine is moving with a 2 Hz surge motion - 2D plot at location 2

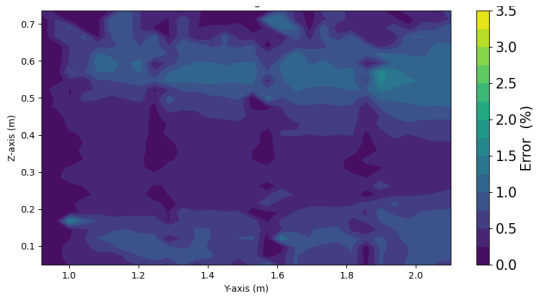

Figure 3.103: Error of the velocity relative to the free stream velocity when the upstream turbine is moving with a 5 Hz surge motion - 2D plot at location 2

Location 3

The error plots look more fragmented, which was also the case in the vorticity, mean, and standard deviation plots. The surge plots have a very low error in the region close to the root of the rotor, this is because the velocity was lower here, and the standard deviation was lower as well.

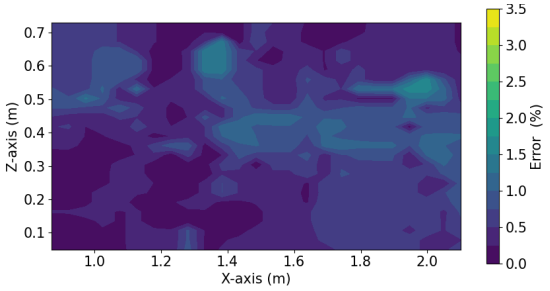

Figure 3.104: Error of the velocity relative to the free stream velocity when the upstream turbine is moving with a 2 Hz pitch motion - 2D plot at location 3

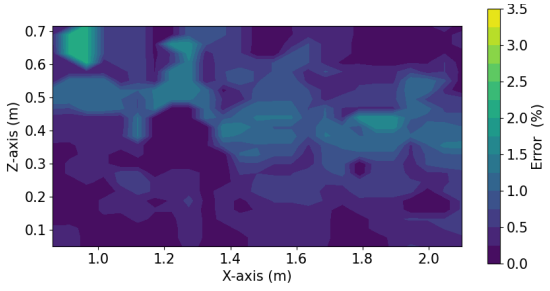

Figure 3.105: Error of the velocity relative to the free stream velocity when the upstream turbine is moving with a 5 Hz pitch motion - 2D plot at location 3

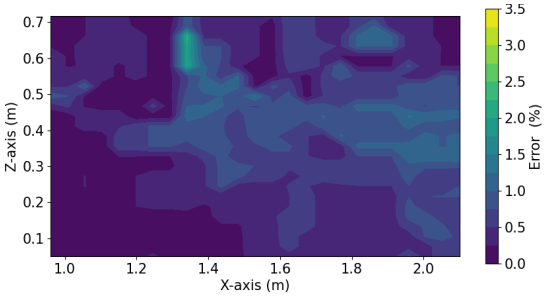

Figure 3.106: Error of the velocity relative to the free stream velocity when the upstream turbine is moving with a 2 Hz surge motion - 2D plot at location 3

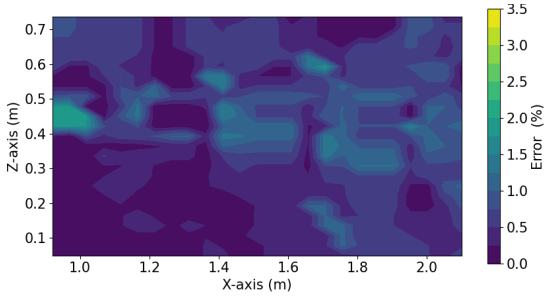

Figure 3.107: Error of the velocity relative to the free stream velocity when the upstream turbine is moving with a 5 Hz surge motion - 2D plot at location 3

Location 4

The error distribution is less fragmented (Figure 3.108 to Figure 3.111), similarly to location 1. There is no peak in the error magnitude in the high frequency pitch plot.

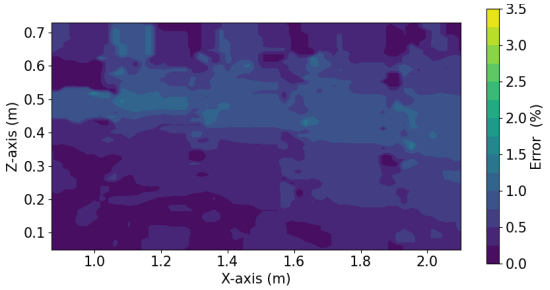

Figure 3.108: Error of the velocity relative to the free stream velocity when the upstream turbine is moving with a 2 Hz pitch motion - 2D plot at location 4

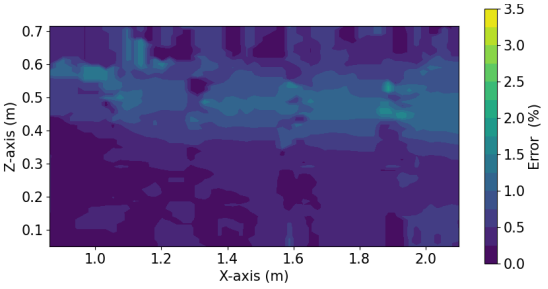

Figure 3.109: Error of the velocity relative to the free stream velocity when the upstream turbine is moving with a 5 Hz pitch motion - 2D plot at location 4

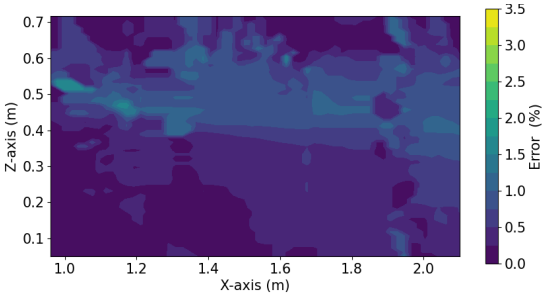

Figure 3.110: Error of the velocity relative to the free stream velocity when the upstream turbine is moving with a 2 Hz surge motion - 2D plot at location 4

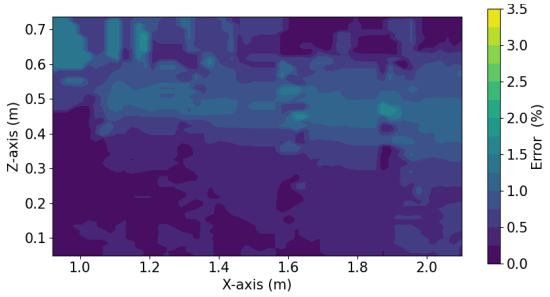

Figure 3.111: Error of the velocity relative to the free stream velocity when the upstream turbine is moving with a 5 Hz surge motion - 2D plot at location 4

4

Results: Effect on downstream turbine

In this section, the results of the experiments regarding the loads on the downstream turbine will be discussed. The thrust and power will be discussed respectively. The data is filtered using a low pass Butterworth filter. First, various cut-off frequencies are compared. Next, the difference in thrust at various locations is discussed. After this, the thrust for the different cases is compared. Lastly, the spectral densities are discussed. Following the thrust, the same is done for the power. The power measured by the load cell is also compared to the power measured by the motor.

4.1. Static tests

First, the aerodynamic performance of the wind turbine model must be verified. The first (upstream) wind turbine model was already verified [44]. This verification is done by doing static tests and creating the thrust and power curve. The results of the test are compared to scaled values of the thrust and power of the DTU 10 MW turbine. The tests were only done until rated wind speed, as the wind turbine model cannot pitch its blades, which is what the DTU 10 MW turbine does after rated wind speed. The results of the experiments are very similar to the theoretical values, especially in the case of thrust, which makes sense as the turbine was scaled down such that the thrust would be the same. The power produced is sightly lower, which could be due to the use of a different, less efficient airfoil [44].

This time, the aerodynamic performance of the second turbine was assessed. The results can be found in Figure 4.3 and Figure 4.4. The discrepancy between these test results and the previous test results is because the TSR is now kept to 7.5 and the previous time the operating conditions of the scaled down DTU 10 MW were used.

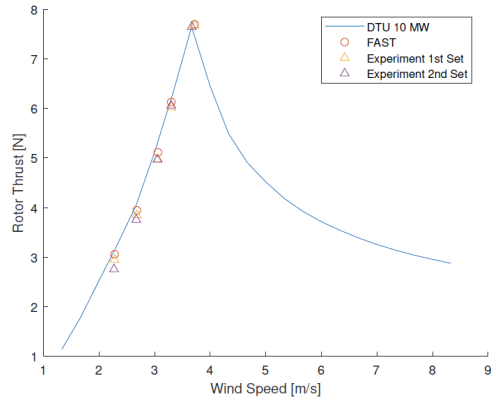

Figure 4.1: The thrust curve of the first wind turbine model as done by [44]

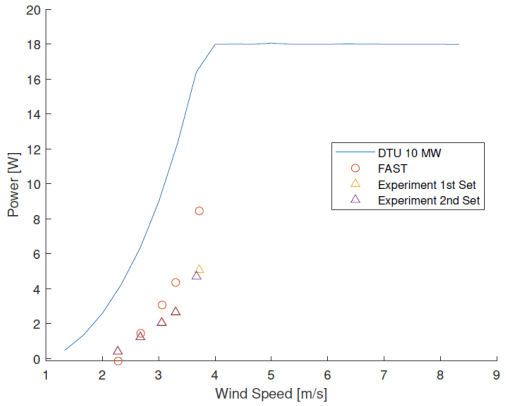

Figure 4.2: The power curve of the first wind turbine model as done by [44]

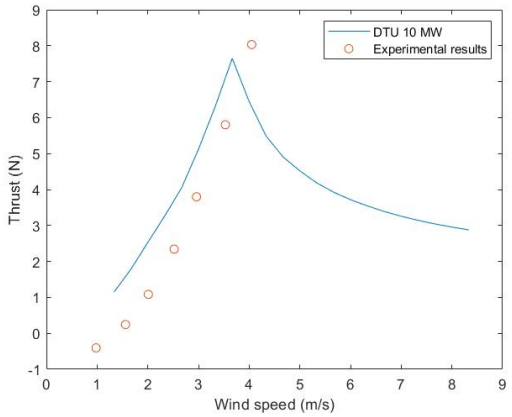

Figure 4.3: The thrust curve of the second wind turbine model

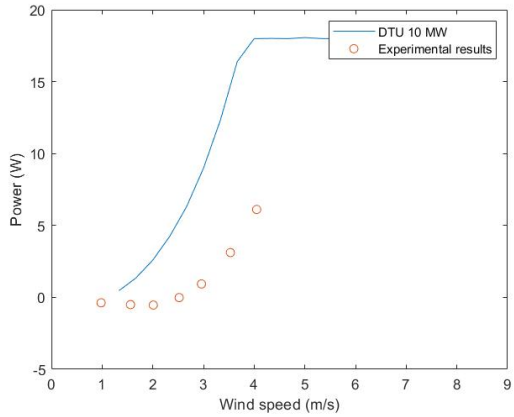

Figure 4.4: The power curve of the second wind turbine model

4.2. Thrust

4.2.1. Thrust - adding a filter

First, the time averaged thrust was plotted without applying a filter to see what the signal looks like originally, including all frequencies and noise, Figure 4.5.

After this, a Butterworth filter was applied with a cut-off frequency of 10 Hz to the data. This filter would cut out all the frequencies above 10 Hz, meaning that all the surge or pitch motion and the rotational speed frequencies are still included, but everything else is excluded.

The graph of the 2 Hz surge motion, Figure 4.6, is now noticeably smoother than the original, meaning that the higher frequencies are effectively filtered out. The graphs of the 5 Hz surge motions now also show a somewhat sinusoidal motion. However, the amplitude is very small, meaning it potentially falls within the error range and it is practically a straight line. Next, the Butterworth filter was applied with a cut-off frequency of 25 Hz (Figure 4.7). This cut-off frequency was chosen under the assumption that the important frequencies would be below 25 Hz. The most important thing that was noticeable, was that the sinusoidal motions were not as smooth. This was as expected, as increasing the cut-off frequency means that higher frequencies were allowed to pass through, distorting the sinusoidal motion. The effect

of increasing the cut-off frequency is now visualised. Increasing the cut-off frequency helps to preserve detail, while lowering the cut-off frequency helps to filter out noise.
Lastly, a cut-off frequency of 8 Hz was applied (Figure 4.7). This was used as this is just below the frequency of the rotation of the blades. The 2 Hz sinusoidal motion looks very similar compared to the 2 Hz sinusoidal motion with the 10 Hz filter, meaning that it is still smooth and the effect of the rotation of the blade does not have that much effect. The 5 Hz sinusoidal motion looks slightly more sinusoidal relative to the 10 Hz filter. However, the amplitude is still very small, meaning it is still negligible.
To sum up, the different filters had the following impact on the data. The 10 Hz filter was able to smoothen the 2 Hz surge motion by excluding the higher frequencies. The 25 Hz filter caused the sinusoids to be less smooth as more noise was included, however more detail was present in these graphs. Lastly, the 8 Hz filter smoothened the sinusoids even further, as the frequency of the rotation of the blades was also excluded. From now on, the time averaged thrust and power plots will be filtered with an 8 Hz Butterworth filter.

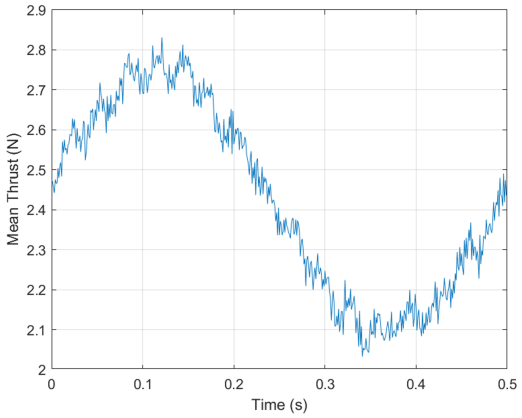

Figure 4.5: Thrust (time averaged over 240 cycles) measured at a downwind turbine located 1.75D downwind - Turbine 1 is moving with a 2 Hz surge motion - no filter is applied

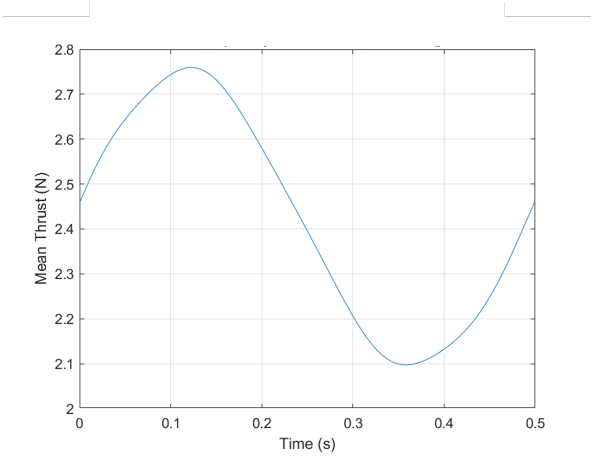

Figure 4.6: Thrust (time averaged over 240 cycles) measured at a downwind turbine located 1.75D downwind - Turbine 1 is moving with a 2 Hz surge motion - a 10 Hz low pass filter is applied

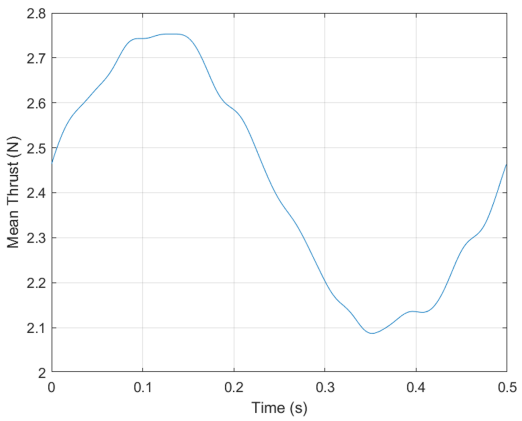

Figure 4.7: Thrust (time averaged over 240 cycles) measured at a downwind turbine located 1.75D downwind - Turbine 1 is moving with a 2 Hz surge motion - a 25 Hz low pass filter is applied

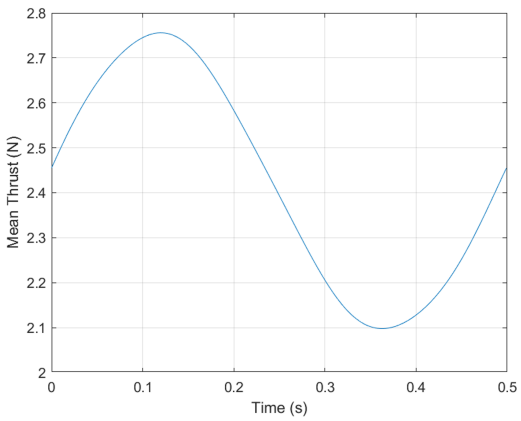

Figure 4.8: Thrust (time averaged over 240 cycles) measured at a downwind turbine located 1.75D downwind - Turbine 1 is moving with a 2 Hz surge motion - an 8 Hz low pass filter is applied

A different cut-off frequency was used for when the upstream is standing still. These two cases are different as there are no cycles, so they will not be averaged over the cycles. In Figure 4.9, the full signal is plotted. In Figure 4.10, a cut-off frequency of 8 Hz is used. In Figure 4.11, a cut-off frequency of 2.5 Hz is used, 2.5 Hz is chosen because it is just below the frequency of a single blade. The latter one shows the lowest amount of noise, this is why this cut-off frequency is chosen for the cases where the turbine is not moving.

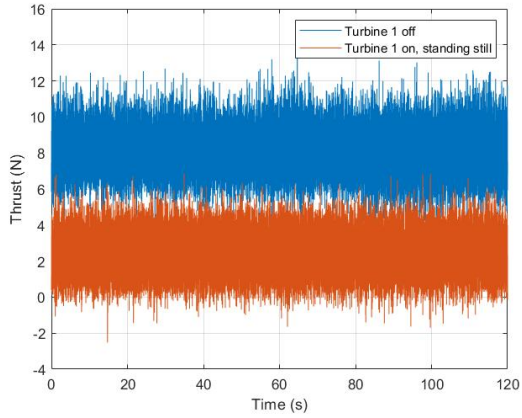

Figure 4.9: Thrust measured at a downwind turbine located 1.75D downwind - Turbine 1 is not moving - no filter is applied

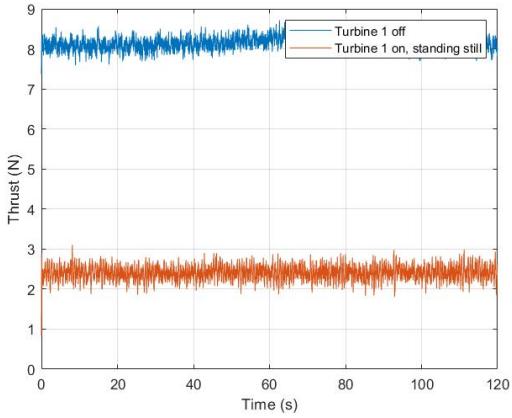

Figure 4.10: Thrust measured at a downwind turbine located 1.75D downwind - Turbine 1 is not moving - 8 Hz filter is applied

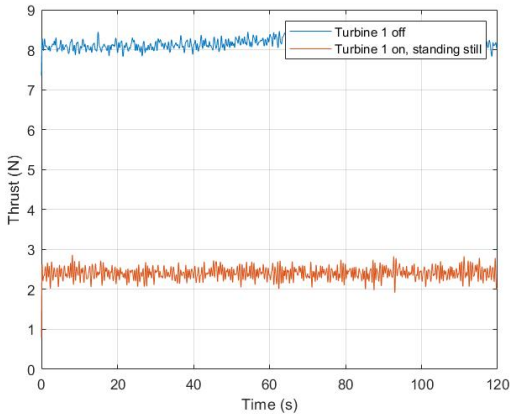

Figure 4.11: Thrust measured at a downwind turbine located 1.75D downwind - Turbine 1 is not moving - 2.5 Hz filter is applied

4.2.2. Thrust - various cases

The time averaged thrust for various cases is plotted in Figure 4.12 to Figure 4.14. The results are filtered with a low pass filter with a cut-off frequency of 8 Hz to remove the higher frequencies and focus on the frequencies of the applied motions.

When turbine 1 is not moving, the thrust is nearly constant. The purpose of these two situations, i.e. turbine 1 off and on, is to have a baseline when comparing it to the cases where the turbine is moving. The fact that the thrust is nearly constant, implies that the variation in the thrust force is now mostly influenced by sinusoidal motion of the upstream turbine.The thrust is much lower when the upstream turbine is on than compared to when it is off, as the deficit in the wake increases when the turbine is on.

When the upstream turbine is turned on, the thrust on the downstream turbine is significantly lower compared to when the upstream turbine is off. This happens because the deficit in the wake increases when the turbine is on. The rotating blades extract energy from the flow, leading to a lower incoming wind at the downstream turbine, which then causes the thrust force to be lower. When the upstream is turned on and moves with a 2 Hz sinusoidal motion, the sinusoidal motion is also visible in the thrust data. This indicates that the thrust force responds to the motion of the turbine. The effect is best visible in the surge and pitch motions, these are also the motions where the amplitude is the greatest. When the turbine is moving with a 2 Hz surge motion, the thrust data contains a clear and smooth sinusoidal motion, which was also found in literature [22]. Pitching the turbine has a similar effect to the thrust data as surging the turbine, as a sinusoidal motion becomes visible in the thrust as well. The amplitude and the mean thrust increases as well. In contrast, applying a 2 Hz yaw motion to the turbine causes the sinusoidal thrust motion to be less smooth. The motion is still present, however it is more irregular, meaning the yaw motion has a smaller impact on the thrust force measured. In general, the mean thrust is higher when the turbine moves with a 2 Hz motion compared to when it is standing still, irrespective of whether it is moving with surge, pitch, or yaw. When the turbine moves with a 5 Hz motion, the thrust is almost constant, indicating that the high frequency motion does not impact the thrust as much.

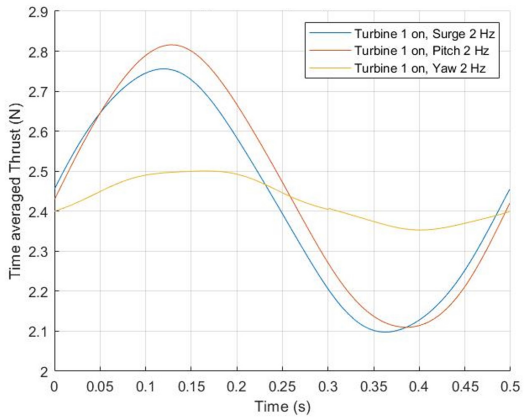

Figure 4.12: Thrust (time averaged over 240 cycles) measured at a downwind turbine located 1.75D downwind - 2 Hz cases

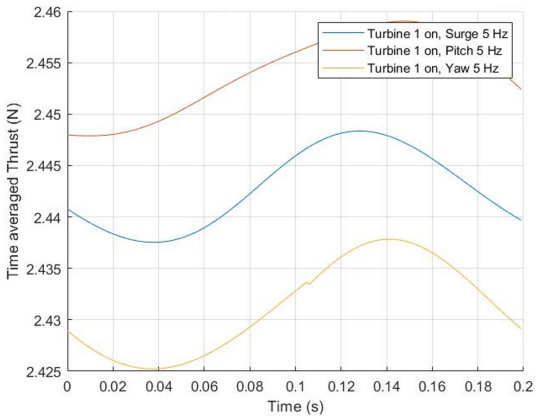

Figure 4.13: Thrust (time averaged over 240 cycles) measured at a downwind turbine located 1.75D downwind - 5 Hz cases

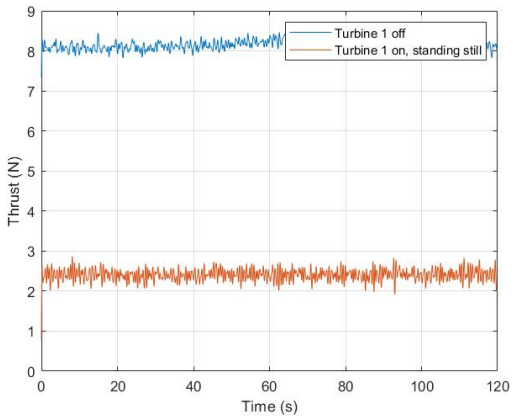

Figure 4.14: Thrust measured at a downwind turbine located 1.75D downwind - No motion cases

Next, the standard deviations are calculated and plotted. The standard deviation of the thrust measured at the downstream turbine when it is located at 1.75 D downstream is shown in Figure 4.15 and Figure 4.16. The standard deviations for the 5 Hz cases are the greatest. When looking at the 5 Hz thrust cases (Figure 4.13), it can be seen that the amplitudes of the visible sinusoids are indeed within the standard deviation range, meaning the thrust measured in the 5 Hz cases are indeed constant. When looking at thrust measured when the upstream turbine is moving with 2 Hz (Figure 4.12), the amplitudes do not fall within the standard deviation range, meaning, the sinusoidal motions here are indeed visible. The standard deviation for the case where the turbine is off and the case where the turbine is on but standing still are both 1.02 N.

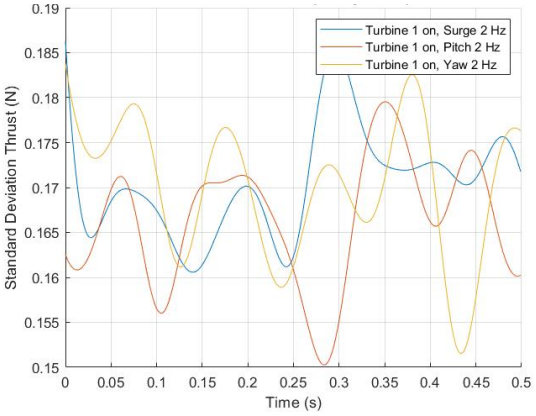

Figure 4.15: Standard deviation of the thrust (time averaged over 240 cycles) measured at a downwind turbine located 1.75D downwind - 2 Hz cases

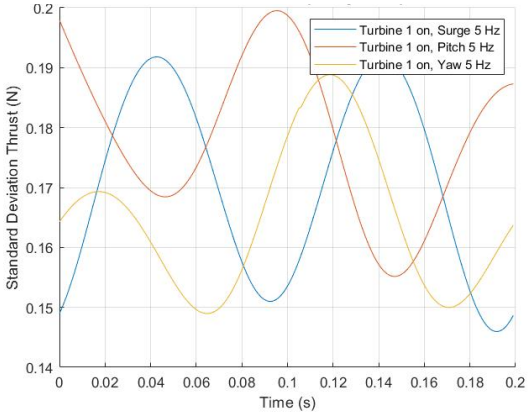

Figure 4.16: Standard deviation of the thrust (time averaged over 240 cycles) measured at a downwind turbine located 1.75D downwind - 5 Hz cases

After this, the PSD is calculated. When the upstream turbine is off and when it is on but standing still (Figure 4.17), there are peaks visible at 8 Hz and at multiples of 8 Hz. 8 Hz corresponds to an RPM of 480, which is the rotational speed of the turbine. For the latter case, the peaks are higher, as two turbines are rotating at this speed. The other peaks visible are multiples of 8 Hz.
When a surge or pitch motion with 2 Hz is applied, a peak at 2 Hz can be seen as well (Figure 4.18 to Figure 4.21). This is as expected because when looking at the thrust and torque cases, the sinusoidal motion was present at this low frequency. When a 2 Hz yaw (Figure 4.22 and Figure 4.23) motion is applied, almost no peak can be observed. This also corresponds to earlier findings, where the effect of the sinusoidal motion was less visible in yaw. When a 5 Hz motion is applied, no peaks are visible at 5 Hz. As no 5 Hz motions were visible in the time averaged plots, this was also expected.

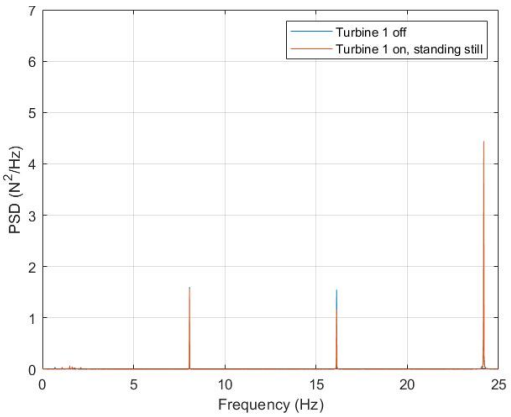

Figure 4.17: Power Spectral Density of the thrust - no motion Hz cases

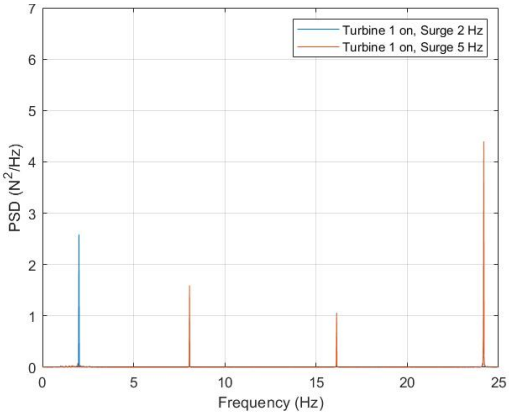

Figure 4.18: Power Spectral Density of the thrust - surge cases

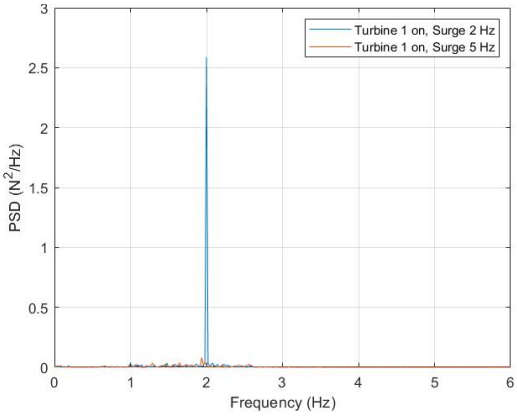

Figure 4.19: Power Spectral Density of the thrust - surge cases - zoomed in

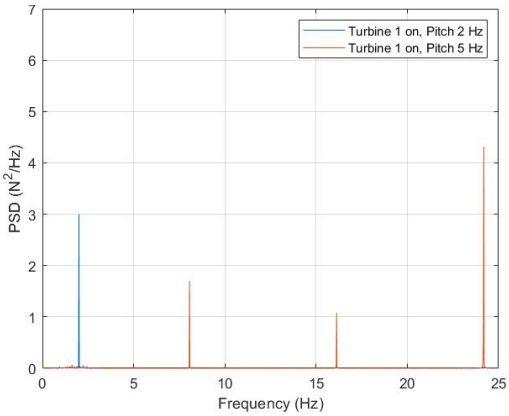

Figure 4.20: Power Spectral Density of the thrust - pitch cases

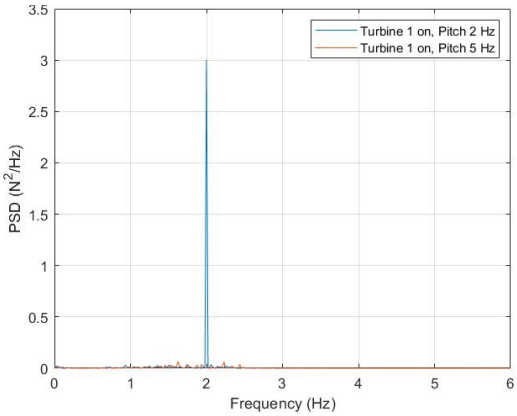

Figure 4.21: Power Spectral Density of the thrust - pitch cases - zoomed in

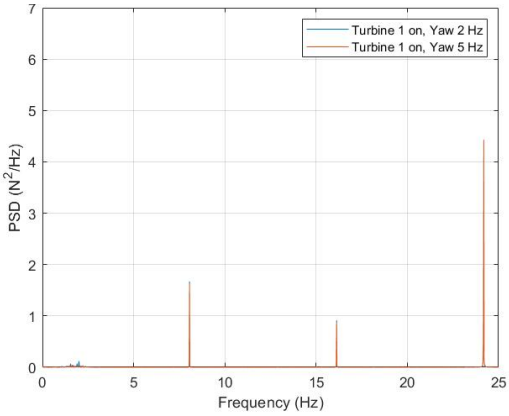

Figure 4.22: Power Spectral Density of the thrust - yaw cases

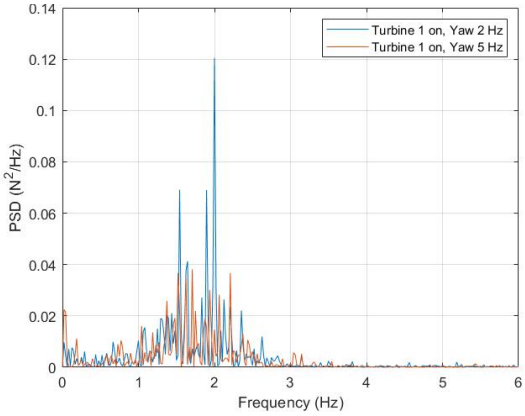

Figure 4.23: Power Spectral Density of the thrust - yaw cases - zoomed in

4.2.3. Thrust - various locations

Next, various locations are compared, to examine the behaviour of the thrust when the downstream turbine is placed at different locations. The surge 2 Hz motion is chosen for this comparison, as this has the

clearest sinusoidal motion to the thrust force (Figure 4.24). The thrust experienced by the downstream turbine increases as it is placed further away from the upstream turbine. This is because the turbine is placed further outside the wake and it thus encounters less wake deficit, meaning the incoming wind contains more energy. This increase demonstrates the effect of the wake on the thrust load on a turbine located downstream.

Likewise, the thrust experienced by the downstream turbine increases when the lateral distance increases. As the downstream turbine is placed further away from the centre, it moves further outside the wake of the upstream turbine. This has a similar effect to moving the turbine further downstream, as the incoming wind will contain more energy.

The sinusoidal motion of the thrust becomes less smooth when moving the turbine outside the wake. This is because the effect of the moving turbine on the incoming wind reduces with distance. When moving the turbine laterally, the incoming wind will be a combination of the free stream wind and the wake of the upstream turbine, causing the sinusoidal motion in the thrust to be less smooth. Additionally, the amplitude of the sinusoid becomes lower, also indicating the effect of the moving turbine on the flow reduces. The magnitude of the thrust at different locations is visualized in Figure 4.25. This figure depicts the height of the mean thrust at several locations, illustrating how the thrust experienced by the downstream turbine varies amongst various positions. The mean thrust at various downstream position when the upstream turbine is moving with a 2Hz surge motion is also shown in Table 4.1 and Table 4.2.

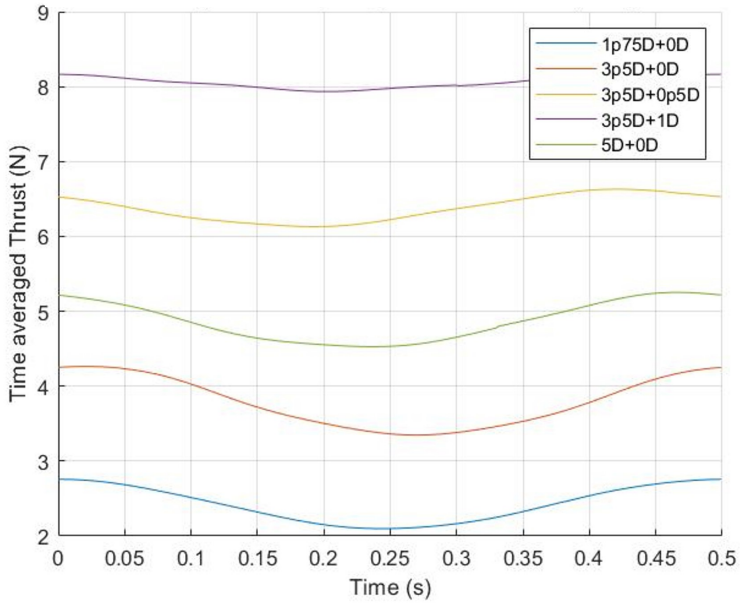

Figure 4.24: Thrust (time averaged over 240 cycles) measured at a downwind turbine located at several downwind positions while the upstream turbine is moving with a 2 Hz sinusoidal surge motion

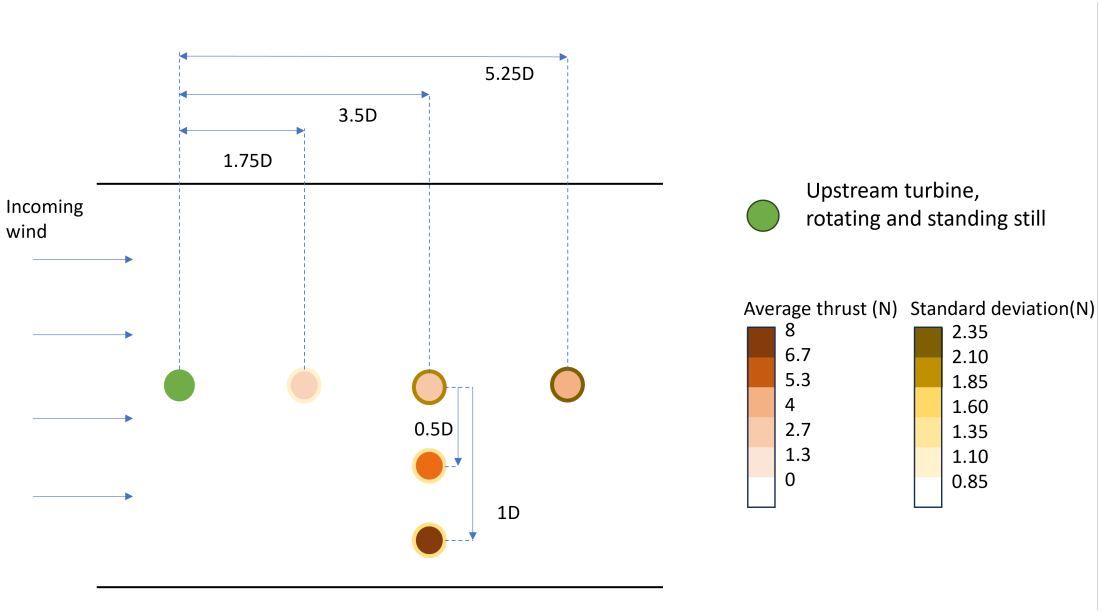

Figure 4.25: Top view of the wind tunnel. The green circle is the upwind turbine. The other circles present the downstream turbine, where the colour indicates the different magnitudes of the thrust. The upstream turbine is rotating and standing still.

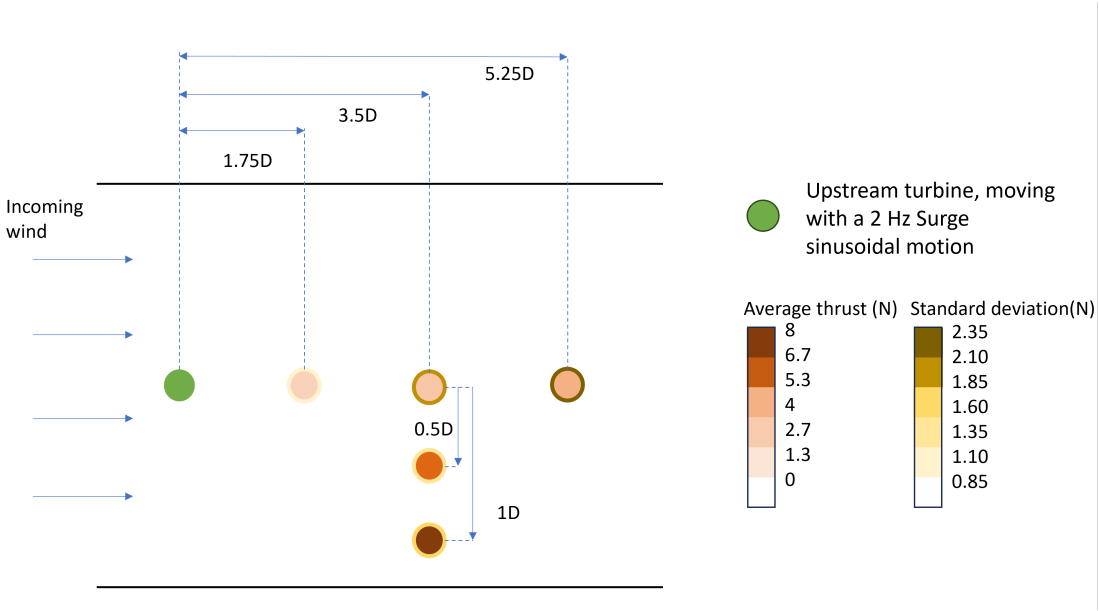

Figure 4.26: Top view of the wind tunnel. The green circle is the upwind turbine. The other circles present the downstream turbine, where the colour indicates the different magnitudes of the thrust. The upstream turbine is rotating and moving with a 2 Hz sinusoidal motion.

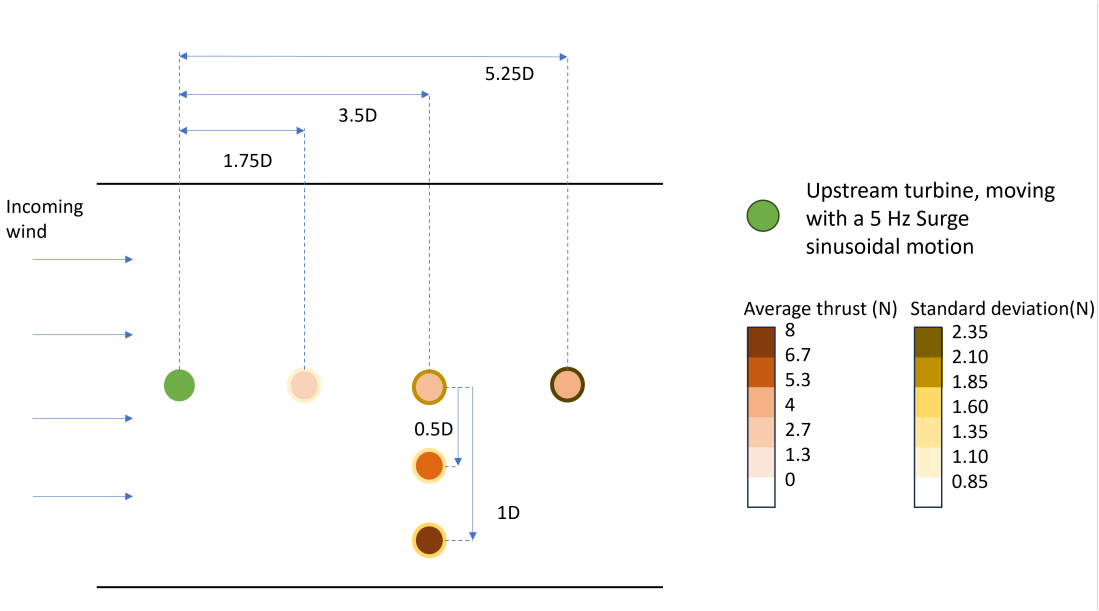

Figure 4.27: Top view of the wind tunnel. The green circle is the upwind turbine. The other circles present the downstream turbine, where the colour indicates the different magnitudes of the thrust. The upstream turbine is rotating and moving with a 5 Hz sinusoidal motion.

Table 4.1: Thrust (N) - measured at the downstream turbine at various downstream positions

Case	1.75D	3.5D	5D
Turbine 1 off	8.10 ±1.02	8.79 ±1.22	8.75 ±1.19
Turbine 1 on, standing still	2.41 ±1.02	3.67 ±1.87	4.89 ±2.27
Turbine 1 on, Surge 2 Hz	2.42 ±1.04	3.79 ±1.80	4.87 ±2.31
Turbine 1 on, Surge 5 Hz	2.44 ±1.06	3.69 ±1.82	4.91 ±2.45
Turbine 1 on, Pitch 2 Hz	2.45 ±0.98	3.87 ±1.88	4.97 ±2.28
Turbine 1 on, Pitch 5 Hz	2.45 ±1.01	3.69 ±1.82	4.83 ±2.25
Turbine 1 on, Yaw 2 Hz	2.43 ±1.00	3.82 ±1.87	4.89 ±2.42
Turbine 1 on, Yaw 5 Hz	2.43 ±0.97	3.74 ±1.79	4.88 ±2.35

Table 4.2: Thrust (N) measured at the downstream rotor located 3.5D downstream at various lateral positions

Case	3.5D + 0D	3.5D + 0.5D	3.5D + 1D
Turbine 1 off	8.79 ±1.22	9.24 ±1.07	7.68 ±1.46
Turbine 1 on, standing still	3.71 ±1.87	6.28 ±1.44	8.04 ±1.55
Turbine 1 on, Surge 2 Hz	3.79 ±1.80	6.37 ±1.46	8.06 ±1.63
Turbine 1 on, Surge 5 Hz	3.69 ±1.82	6.39 ±1.45	8.07 ±1.65
Turbine 1 on, Pitch 2 Hz	3.87 ±1.88	6.40 ±1.47	7.99 ±1.65
Turbine 1 on, Pitch 5 Hz	3.69 ±1.82	6.34 ±1.43	8.07 ±1.69
Turbine 1 on, Yaw 2 Hz	3.82 ±1.87	6.35 ±1.43	8.10 ±1.62
Turbine 1 on, Yaw 5 Hz	3.74 ±1.79	6.32 ±1.43	8.04 ±1.58

The other results are presented in the appendix.

4.3. Power

Next, the power of the downstream turbine is discussed. The power (time averaged over 240 cycles) at a downstream distance of 1.75D is shown in Figure 4.28 to Figure 4.30. The power is calculated by multiplying the torque with the rotational speed. The torque referred to in this section, is the torque on the rotor side (LSS). The power is negative, apart from the case where the upstream turbine is turned off. The negative values indicate that the downstream turbine is not generating power. This is because when the upstream turbine is on, more energy is taken from the wind meaning the incoming wind at the downstream turbine contains less energy, and it can thus convert less energy into power. Thus at rated wind speed, the downstream turbine, when located at 1.75D downstream, does not generate power when the upstream turbine is on. A sinusoidal motion is visible, however the amplitudes are very small. This means that the torque is almost constant, as expected, since the upstream turbine is not moving.

The sinusoidal motion is better noticeable when the upstream turbine is subjected to a 2 Hz pitch, surge or yaw motion (Figure 4.28). In the case where the upstream turbine is subjected to a 2 Hz pitch motion, the amplitude of the sinusoidal motion is the greatest. This demonstrates that the impact of pitch on the power generation is large. When the turbine is subjected to a 2 Hz surge motion, the amplitude of the sinusoid the power data generates is also significant, albeit smaller than when subjected to the pitch motion. This suggests that surge also affects the power, although it is not as impactful as the pitch motion. The 2 Hz yaw motion also causes the power to be a sinusoid, although the amplitude is lower than that of the other motion. This indicated that this degree of freedom has the least impact on power generation.
Although there are different amplitudes, all three cases display a 2 Hz sinusoidal motion, meaning that when the upstream turbine moves with a 2 Hz sinusoidal motion, the power of the downstream turbine responds.
In all 2 Hz motion cases, the sinusoidal power variations follow the 2 Hz frequency, as expected, reflecting the direct influence of the upstream turbine's motion on the downstream turbine's power response. In contrast, this motion is not visible when the upstream turbine moves with a 5 Hz motion (Figure 4.29). The fluctuations in the data are small, meaning that the power is practically constant. This suggests that the downstream turbine is not impacted much by the 5 Hz sinusoidal motion.

The power of the downstream turbine at several locations is visualised in Figure 4.36. When the downstream distance increases, the power also increases. This is as expected, as the downstream turbine will be less affected by the wake. When the lateral distance increases, the power increases as well. The power becomes positive when it is located at 3.5D downstream, and 1D in the lateral direction.
The magnitude of the power at different locations is visualized in Figure 4.33. This figure depicts the height of the mean power at several locations, illustrating how the power experienced by the downstream turbine varies amongst various positions. The mean power at various downstream positions when the upstream turbine is moving with a 2Hz surge motion is also shown in Table 4.3 and Table 4.4.

In literature, it was found that power increases when the platform was pitched [21]. In Table 4.4, it can be seen that the power also increases when the upstream turbine is subjected to pitch motion, however this is not visible at 1.75D and 5D downstream (Table 4.3). The power does however increase with an increasing distance between the turbines. Moreover, the power also fluctuates more in Figure 4.36 than when the upstream turbine is not moving (Figure 4.30). This was both also found in literature [22] and [24].

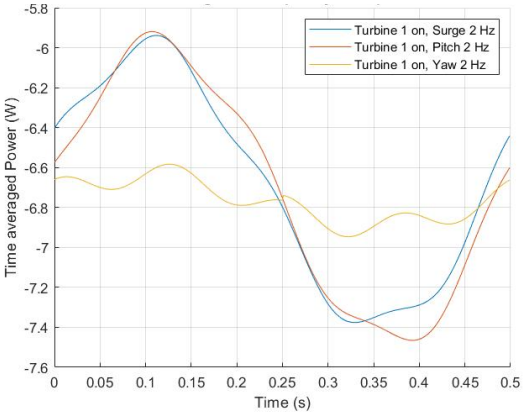

Figure 4.28: Power (time averaged over 240 cycles) measured at a downwind turbine located 1.75D downwind - 2 Hz cases

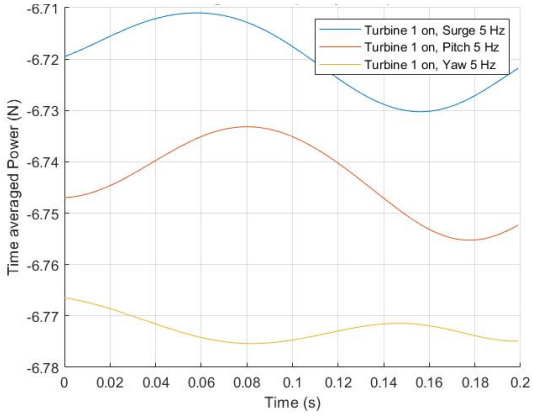

Figure 4.29: Power (time averaged over 240 cycles) measured at a downwind turbine located 1.75D downwind - 5 Hz cases

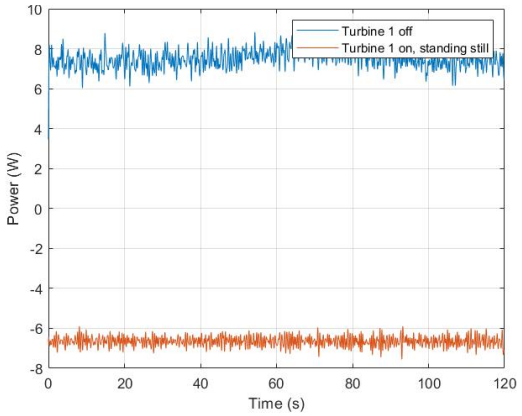

Figure 4.30: Power measured at a downwind turbine located 1.75D downwind - No motion cases

Next, the standard deviations are calculated and plotted. The standard deviations for the power measured at the downstream turbine when it is located at 1.75 D downstream are shown in Figure 4.31 and Figure 4.32. The standard deviations for the 5 Hz cases are the greatest. When looking at the 5 Hz power cases (Figure 4.13), it can be seen that the amplitudes of the visible sinusoids are indeed within the standard deviation range, meaning the power measured in the 5 Hz cases are indeed constant. When looking at power measured when the upstream turbine is moving with 2 Hz (Figure 4.12), the amplitudes do not fall within the standard deviation range, meaning, the sinusoidal motions here are indeed visible. The standard deviation for the case where the turbine is off and the case where the turbine is on but standing still are 0.07 and 0.06 W, respectively.

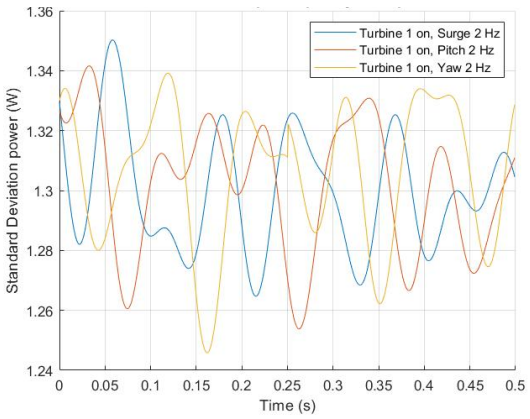

Figure 4.31: Standard deviation of the power (time averaged over 240 cycles) measured at a downwind turbine located 1.75D downwind - 2 Hz cases

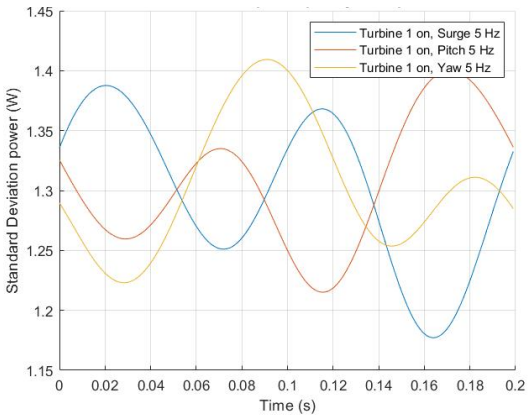

Figure 4.32: Standard deviation of the power (time averaged over 240 cycles) measured at a downwind turbine located 1.75D downwind - 5 Hz cases

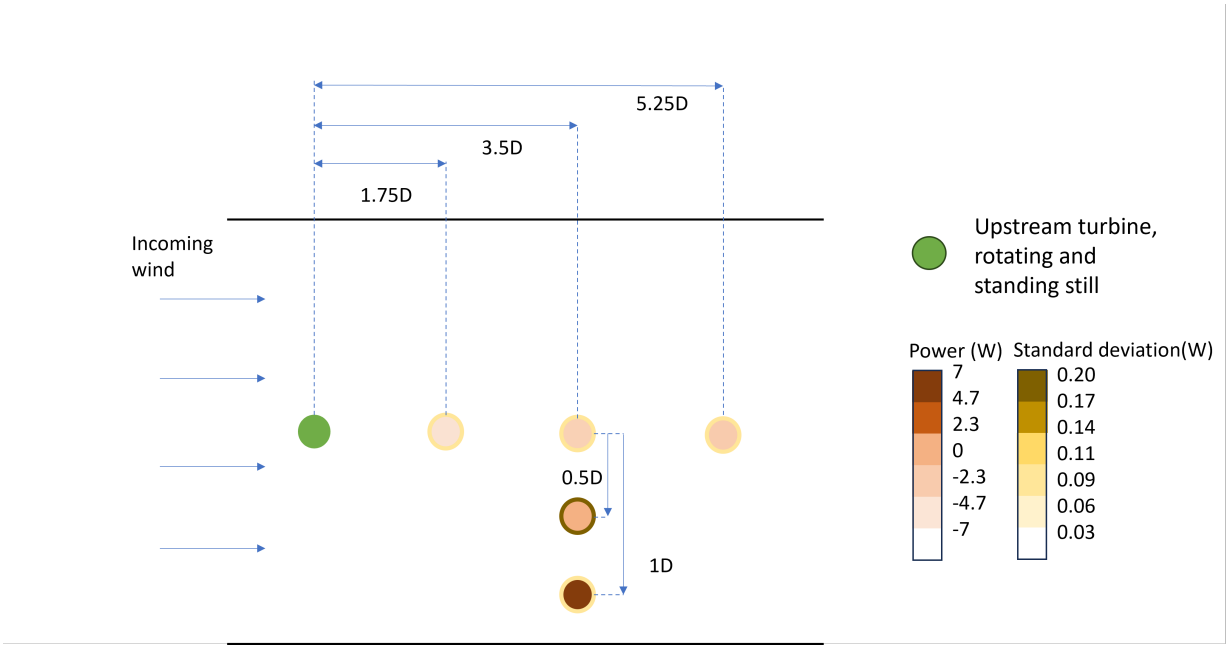

Figure 4.33: Top view of the wind tunnel. The green circle is the upwind turbine. The other circles present the downstream turbine, where the colour indicates the different magnitudes of the power. The upstream turbine is rotating and standing still

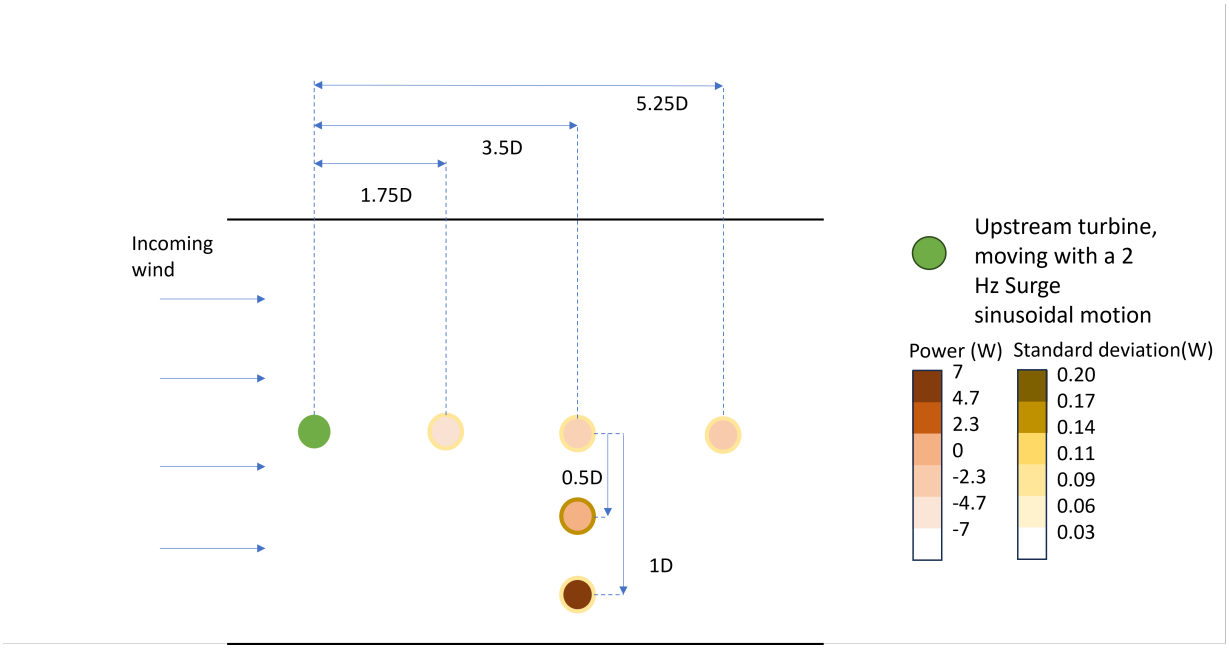

Figure 4.34: Top view of the wind tunnel. The green circle is the upwind turbine. The other circles present the downstream turbine, where the colour indicates the different magnitudes of the power. The upstream turbine is rotating and moving with a 2 Hz sinusoidal motion.

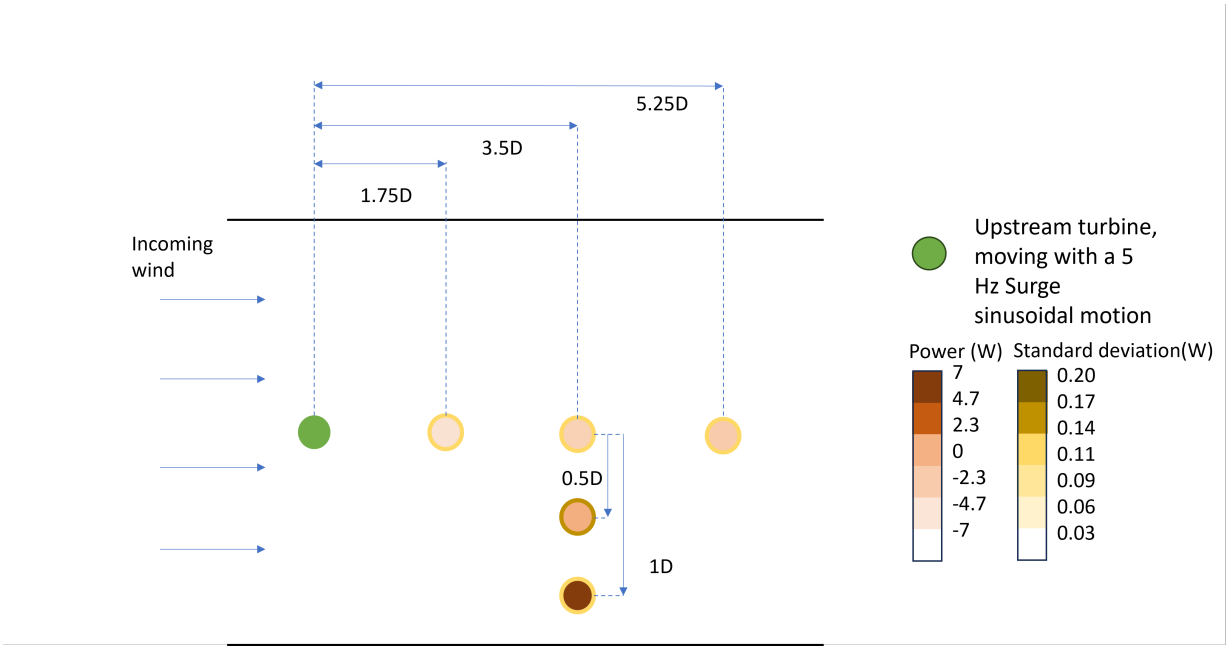

Figure 4.35: Top view of the wind tunnel. The green circle is the upwind turbine. The other circles present the downstream turbine, where the colour indicates the different magnitudes of the power. The upstream turbine is rotating and moving with a 5 Hz sinusoidal motion.

Table 4.3: Power (W) - measured at the downstream turbine at various downstream positions

Case	1.75D	3.5D	5D
Turbine 1 off	7.37 ±0.07	8.19 ±0.06	8.22 ±0.06
Turbine 1 on, standing still	-6.64 ±0.06	-5.58 ±0.06	-2.75 ±0.06
Turbine 1 on, Surge 2 Hz	-6.68 ±0.06	-5.39 ±0.06	-2.72 ±0.07
Turbine 1 on, Surge 5 Hz	-6.72 ±0.06	-5.76 ±0.06	-2.78 ±0.06
Turbine 1 on, Pitch 2 Hz	-6.72 ±0.06	-5.37 ±0.06	-2.92 ±0.07
Turbine 1 on, Pitch 5 Hz	-6.74 ±0.06	-5.86 ±0.06	-2.99 ±0.06
Turbine 1 on, Yaw 2 Hz	-6.76 ±0.06	-5.66 ±0.06	-2.80 ±0.06
Turbine 1 on, Yaw 5 Hz	-6.77 ±0.06	-5.81 ±0.06	-2.90 ±0.07

Table 4.4: Power (W) measured at the downstream rotor located 3.5D downstream at various lateral positions

Case	3.5D + 0D	3.5D + 0.5D	3.5D + 1D
Turbine 1 off	8.19 ±0.06	9.96 ±0.11	5.24 ±0.06
Turbine 1 on, standing still	-5.58 ±0.06	-0.44 ±0.20	6.26 ±0.06
Turbine 1 on, Surge 2 Hz	-5.39 ±0.06	-0.77 ±0.17	6.30 ±0.07
Turbine 1 on, Surge 5 Hz	-5.76 ±0.06	0.89 ±0.14	6.18 ±0.07
Turbine 1 on, Pitch 2 Hz	-5.37 ±0.06	-0.19 ±0.18	5.87 ±0.07
Turbine 1 on, Pitch 5 Hz	-5.86 ±0.06	-0.52 ±0.19	6.15 ±0.08
Turbine 1 on, Yaw 2 Hz	-5.66 ±0.06	-0.70 ±0.19	6.25 ±0.07
Turbine 1 on, Yaw 5 Hz	-5.81 ±0.06	-0.92 ±0.20	6.15 ±0.07

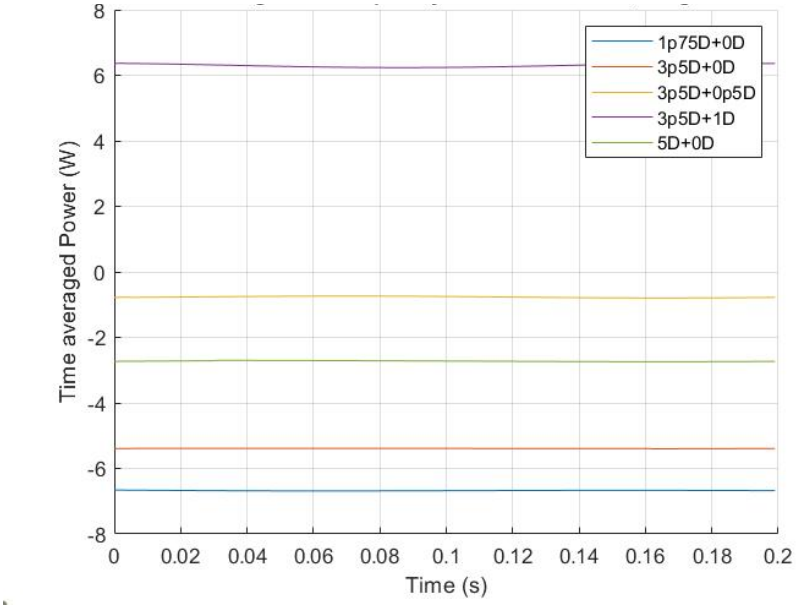

Figure 4.36: Power (time averaged over 240 cycles) measured at a downwind turbine located at several downwind positions while the upstream turbine is moving with a 2 Hz sinusoidal surge motion

When the load cell was used to measure the power, the values measured were higher than when the motor was used (Figure 4.37). This is because the motor measures after the transmission, i.e. the

transmission losses are also taken into account.

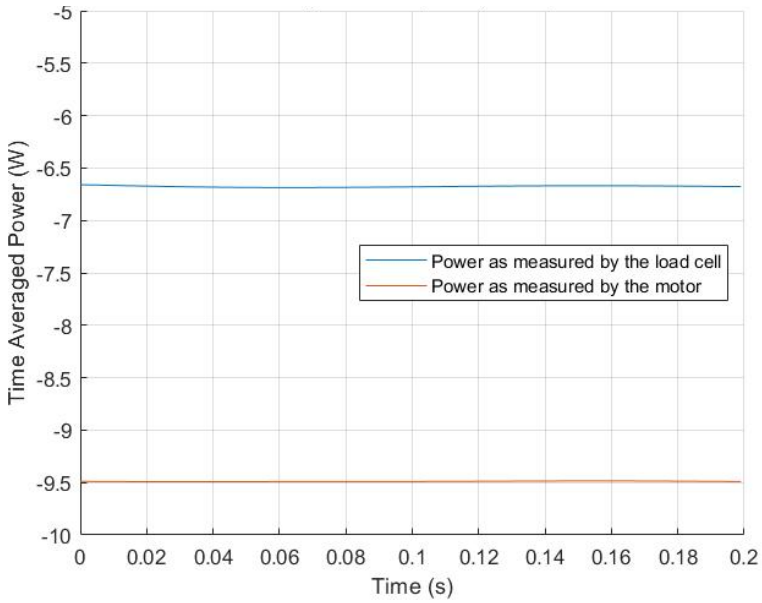

Figure 4.37: Time averaged torque per cycle at a downwind turbine located at 1.75D downwind while the upstream turbine is moving with a 2 Hz sinusoidal surge motion measured by the load cell compared to that measured by the motor.

Lastly, the power spectral density (PSD) was plotted. When the upstream turbine is off and when it is on but standing still (Figure 4.38), there are again peaks visible at 8 Hz and at multiples of 8 Hz, corresponding to the rotational speed of the turbine. When a surge or pitch motion with 2 Hz is applied, a peak at 2 Hz can be seen as well (Figure 4.39 to Figure 4.42). This is as expected because when looking at the thrust and torque cases, the sinusoidal motion was present at this low frequency.
When a 2 Hz yaw motion (Figure 4.43 to Figure 4.44) is applied, a very slight peak or no peak can be observed. This also corresponds to earlier findings, where the effect of the sinusoidal motion was less visible in yaw. When a 5 Hz motion is applied, no peaks are visible at 5 Hz. As no 5 Hz motions were present in the thrust and torque cases, this was also expected.

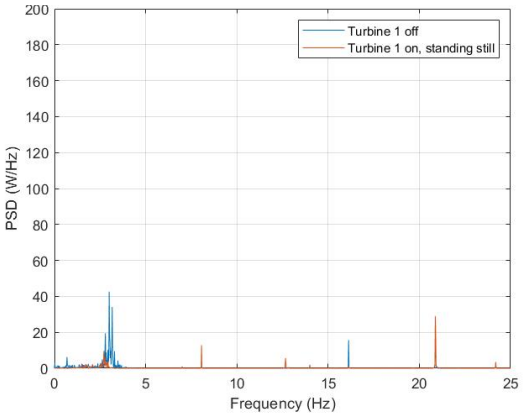

Figure 4.38: Power Spectral Density of the power - no motion Hz cases

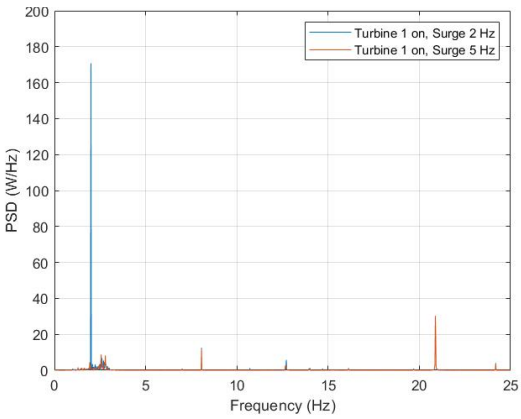

Figure 4.39: Power Spectral Density of the power - surge cases

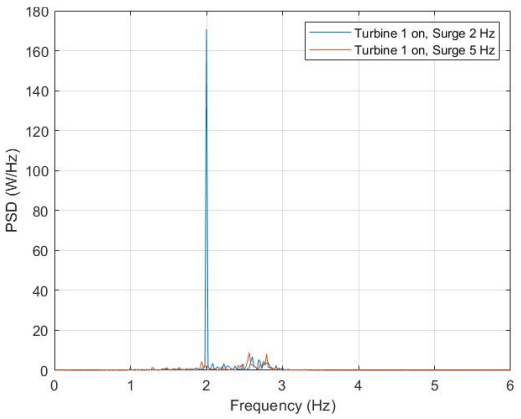

Figure 4.40: Power Spectral Density of the power - surge cases - zoomed in

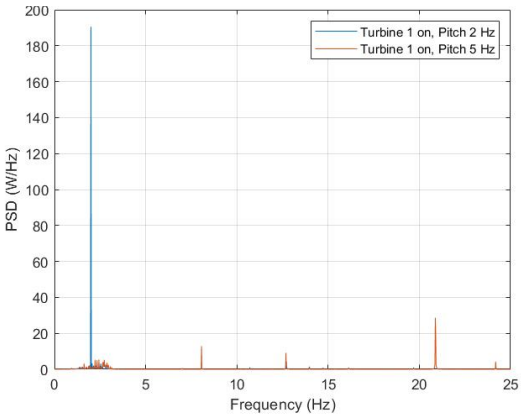

Figure 4.41: Power Spectral Density of the power - pitch cases

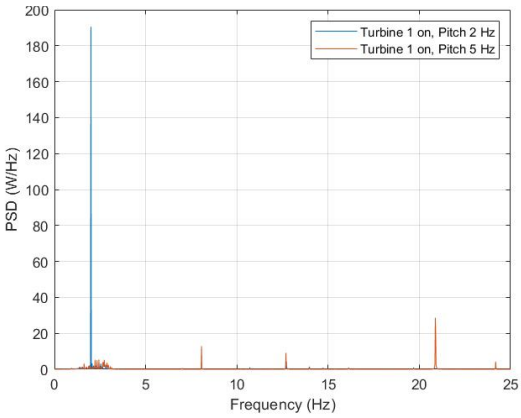

Figure 4.42: Power Spectral Density of the power - pitch cases - zoomed in

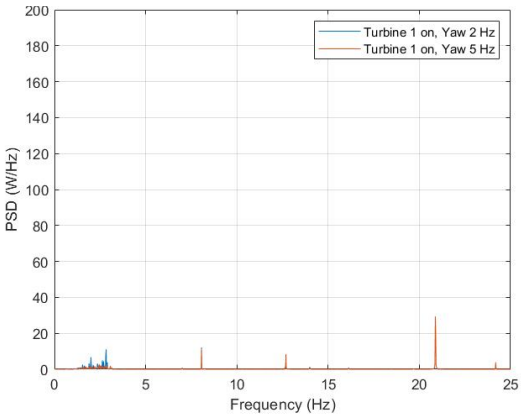

Figure 4.43: Power Spectral Density of the power - yaw cases

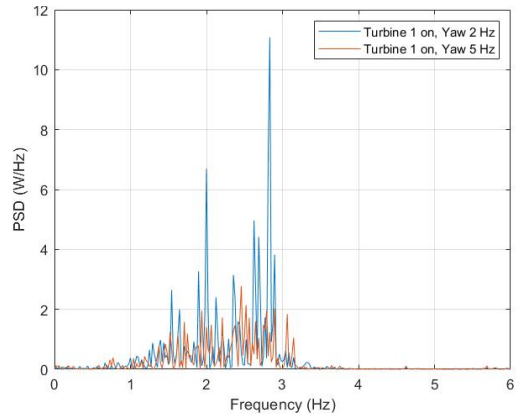

Figure 4.44: Power Spectral Density of the power - yaw cases - zoomed in

5

Conclusion and recommendations

In this section, the conclusion and recommendations of this thesis will be discussed. First, the aim and main objectives will be repeated. Next, the research questions will be answered. Lastly, some key takeaways will be given.
After the conclusions, some recommendations will be given regarding improving the tests, and further possible research will be suggested.

5.1. Conclusion

5.1.1. Aim and main objectives

The aim of this thesis is to investigate the effect of the turbine movements on the flow field in its wake as well as the effect on the loads experienced by a stationary downstream turbine positioned at various locations. This thesis is split into two main objectives:

1. The flow field is analysed using Particle Tracking Velocimetry (PTV) to study the flow field when the turbine is subjected to a surge or pitch motion. In particular, the mean velocity, vorticity, and power spectral density are analysed.
2. The subsequent effect of the wake on a stationary downstream turbine is then evaluated. This includes looking at the thrust, torque, and power experienced by the downstream turbine. The downstream turbine is positioned at different locations in the wake of the moving upstream turbine.

By investigating these two objectives, the thesis aims to provide an understanding of the wake and the effect of the wake of a moving turbine, which can be useful when designing and optimizing wind farms.

5.1.2. Research Questions

In this section, the research questions are repeated and answered.

1. **What does the flow field in the wake of a turbine look like when it is moving with a sinusoidal pitch or a sinusoidal surge motion?**

   To answer the first research question, a PTV setup was used. The turbine was placed onto a kinematic robot, which was able to move in all 6 DoF. HFSB were added to the flow as tracer particles,

and two LED lights were used to illuminate them. DaVIS10 was used for both the recording and post-processing of the tests.

(a) *How does the wake of a turbine compare when it is moving with a surge motion vs when it is moving with a pitch motion?*

- Pitch has more influence on the wake than surge. This is for instance demonstrated by the vorticity, where the magnitude of the vorticity is different between low and high frequency pitch, but not with low and high frequency surge. Moreover, the velocity in the wake of two surge cases are very similar and in the wake of the two pitch cases there is a difference. This all indicates that the pitch has a greater effect on the wake.

(b) *What is the difference between the velocity field behind the turbine when it is moving with low frequency (2 Hz) sinusoidal motion vs when it is moving with a high frequency (5 Hz) sinusoidal motion?*

- When comparing the low frequency with the high frequency, the velocity field of the pitch looks very different. The velocity when the frequency is high is much higher than when the frequency is low. This difference is not visible for the surge cases.
- Something else that can be noticed is that the vortices travel further when the frequency is high. Moreover, the areas where the vorticity is high are smaller when the frequency is high.

2. **How does applying surge, pitch, and yaw to the upstream turbine impact the loads on the downstream turbine?**

To answer the second research question, a second turbine was placed behind the original turbine. The second turbine was identical to the first turbine, but it was placed onto a static stand rather than a kinematic robot. The downstream location was varied between 1.75D, 3.5D, and 5.25D downstream of the upstream turbine. At 3.5D downstream, the lateral position was also varied between 0, 0.5D and 1D. The loads were measured with a load cell. The loads that were considered were the thrust force, the torque, and the power. The latter two were also measured by the motor itself, these values were compared to those measured by the load cell to examine the difference.

(a) *How do the loads on the downstream turbine change when the upstream turbine is moving with a low frequency (2 Hz) or a high frequency (5 Hz) motion?*

- The effect of low compared to high frequency motion was also examined. The low frequency motion had a far greater effect on the downstream turbine than the high frequency motion. In the case of low frequency surge and pitch, the amplitude of the thrust is around 0.7 N, the amplitude of the torque is around 0.03 Nm and the power 0.003 W. In the case of low frequency surge and pitch, the amplitude of the thrust is around 0.01 N, the amplitude of the torque is around 0.0004 Nm and the power 0.00006 W. Therefore, it can be concluded that the effect of the high frequency motion is not visible in the measured thrust, torque, and power.

(b) *How do the loads on the downstream turbine change when the downstream turbine is positioned at different locations in the downstream direction?*

- When moving the downstream turbine from 1.75D to 3.5D the thrust increases between 51% and 59%.
- When moving the downstream turbine from 1.75D to 3.5D the torque increases between 16% and 24%.
- When moving the downstream turbine from 1.75D to 3.5D the power increases between 15% and 25%.
- When moving the downstream turbine from 1.75D to 5.25D the thrust increases between 96% and 103%
- When moving the downstream turbine from 1.75D to 5.25D the torque increases between 137% and 158%
- When moving the downstream turbine from 1.75D to 5.25D the thrust increases between 25% and 46%
- This is for the cases where the upstream turbine is rotating, when the upstream turbine is off, there is not much of a difference. These findings correspond to literature [24] where the thrust and power also increase with increasing distance.

(c) *How do the loads on the downstream turbine change when the downstream turbine is positioned at different locations in the lateral direction?*

- When moving the downstream turbine from 0D to 0.5D the thrust increases between 65% and 73%. When moving the downstream turbine from 0D to 0.5D the thrust increases between 106% and 118%. As moving the turbine laterally shows a large increase in thrust while it is moved less far than moving it in the downstream direction, it shows that it is useful to not place turbines directly behind one another in a wind farm.

(d) *Difference between pitch, surge, and yaw*

- Pitch has more influence on the wake than surge. This is for instance demonstrated by the vorticity, where the magnitude of the vorticity is different between low and high frequency surge, but not with low and high frequency pitch. Moreover, the velocity in the wake of two surge cases is very similar and in the wake of the two pitch cases there is a difference. This all indicates that the pitch has a greater effect on the wake.

5.1.3. Key takeaways

- Pitch has the most influence on the wake of the upstream turbine, as well as on the measured loads on the downstream turbine. Surge only has slightly less effect on the downstream turbine, whereas yaw had much less effect.
- When placing the downstream turbine further downstream, the difference was smaller compared to when the turbine was varied in the lateral direction
- The effects of low frequency movement were well visible in the loads measured on the downstream turbine, whereas the effect of high frequency movement was not as visible.
- When doing PTV, the particles were not well distributed and located at the centre of each FOV as well as located in the low velocity areas.

5.2. Recommendations

5.2.1. Recommendations regarding PTV

Possible improvements to the tests

Several ways exist in which the tests could be improved. One thing that can be examined, is whether we are actually measuring what we think we are measuring. I.e. if a velocity of 3 m/s is measured using the PTV set-up, does this mean that the actual velocity of the flow is 3 m/s? A way to do this, is to measure the flow in the wind tunnel without the turbine present. When the wind speed in the wind tunnel was set to 4 m/s, this measurement was confirmed. By measuring the wind speed using the PTV set-up, the accuracy of the set-up can be confirmed. In the figures in the result setup, it could be seen that the helium filled soap bubbles were concentrated in the middle of each test section. Possible reasons for this included that the flow field pushed the bubbles to these locations and that the bubbles were spread more evenly, but the LED lights did not light the full test section, meaning that bubbles were not recorded due to a lack of light. By doing a test without the turbine present, the reason for this could be determined. If the particles are now evenly distributed, the first reason for the particle distribution is likely and if the particles are still concentrated in the middle of the test section, the latter reason is more likely. It may also be a combination of the two reasons.
The next test could be with the turbine, but turned off, and afterwards with the turbine turned on, but without movements by the hexapod. These can be used as base cases, with the current study only the difference between pitch and surge and low and high frequency can be determined. However, the effect of movement compared to a fixed turbine cannot be determined, even though this would be an interesting comparison.

Possible further research

Several things can be studied in the future.

- First, a larger part of the wake can be measured. Currently, only the wake behind the top blade is measured, but it would be interesting to capture the full wake behind the blades.
- Moreover, only the near wake is measured, while the far wake is also interesting and possibly more interesting as the downstream turbines will be placed in the far wake.
- To add, the wake could also be measured at a downstream turbine at various locations. This could provide insights on the effect of one turbine on another, which is crucial in understanding the wakes so that wind farm designs can be optimized.
- Furthermore, extending the DoF could be interesting. Now only a surge and pitch motion are applied. Combining DoF or wave cases could be interesting too.
- Lastly, the tests could be supplemented by doing CFD for verification.

Relevance of the results

The results of these tests are useful for understanding the wakes of floating wind turbines. Understanding the wake is useful to determine a wind farm layout. Moreover, it is useful to determine the location of floating wind farms. These results show that when the turbine is pitched, the velocity in the wake is higher. Therefore, it could be useful to place a wind farm in a location where the waves will mostly cause a pitch motion. More research should be done to exactly determine this.

5.2.2. Recommendations regarding the loads test

Possible further research

Further research that could be done, is positioning the downstream turbine at more locations, both downstream and lateral. I.e. $5D$, $7.5D$ downstream and also varying in the lateral direction at those places. To add to this, more DoF could be tested, as well as wave cases.
Additionally, the fixed downstream turbine could be altered to a moving downstream turbine.
Moreover, the loads on upstream and downstream turbine could be compared.

Relevance of the results

The results could be used to determine a layout of a wind farm. It can be seen that moving the turbine further downstream increases the thrust, torque, and power. The same can be achieved when moving the turbine in the lateral direction, meaning that when creating a lay-out for a floating wind farm, it is beneficial to not place the turbines directly behind each other.
Additionally, when adding a low frequency pitch or surge motion, the average thrust, torque, and power of the downstream rotor increases. However, the fluctuations are also greater, which negatively affects the grid

References

[1] Abdolrahim Rezaeiha et al. “Wake interactions of two tandem floating offshore wind turbines: CFD analysis using actuator disc model”. In: *Renewable Energy* 179 (Dec. 2021), pp. 859–876.

[2] UNFCCC. *The Paris Agreement*. unfcc.int. https://unfccc.int/process-and-meetings/the-paris-agreement (accessed Jan. 26, 2024).

[3] Beatriz Dromant Bellver. *AN EU STRATEGY TO HARNESS THE POTENTIAL OF OFFSHORE RENEWABLE ENERGY FOR A CLIMATE NEUTRAL FUTURE*. 2020. URL: https://roderic.uv.es/rest/api/core/bitstreams/12845a51-dbd8-4d9a-96e3-e9d57dd16754/content.

[4] Delphine De Tavernier et al. *AE4W31 – FLOATING OFFSHORE WIND ENERGY lecture 1*. 2023.

[5] M Capaldo et al. “Influence of cracks on the buckling of wind turbine towers”. In: *Journal of Physics: Conference Series* (2020).

[6] *Park Effect*. June 2003.

[7] Magnus K. Vinnes et al. “The far wake of porous disks and a model wind turbine: Similarities and differences assessed by hot-wire anemometry”. In: *J. Renewable Sustainable Energy* 14 (2 Mar. 2022).

[8] N. Moskaleno Kluth et al. “Study of wake effects for offshore wind farm planning”. In: *Modern Electric Power Systems (MEPS)* (Oct. 2010).

[9] Phillip McKay et al. “Turbine Wake Dynamics”. In: *Advances in Wind Power* (Nov. 2012).

[10] ALexander Piqué et al. “Laboratory investigation of the near and intermediate wake of a wind turbine at very high Reynolds numbers”. In: *Experiments in Fluids* 63 (106 June 2022).

[11] Michael Sherry et al. “The interaction of helical tip and root vortices in a wind turbine wake”. In: *Physics of Fluids* 25 (Dec. 2013), pp. 1–16.

[12] Bernhard Stoevesandt et al. *Handbook of Wind Energy Aerodynamics*. Springer Cham, 2022.

[13] Adam S. Wise et al. “Wake meandering effects on floating wind turbines”. In: *Wiley* (2019).

[14] Wei Yu. *Wind farm wake reducing concepts*. 2023.

[15] Martin Hansen. *VeryBasicAero Slides*. URL: https://learn.inside.dtu.dk/d2l/le/content/125591/viewContent/495947/View.

[16] Martin Hansen. *BEM - slides*. URL: https://learn.inside.dtu.dk/d2l/le/content/125591/viewContent/499058/View.

[17] Hansen Martin O L. *Aerodynamics of wind turbines*. Routledge, 2015.

[18] CJ Simao Ferreira. *Programming a BEM model*. URL: https://www.tudelft.nl/en/student/education/brightspace/.

[19] Suzanne Hendriks et al. *Assignment 1: BEM*. Tech. rep. TU Delft, 2023.

[20] Hakjin Lee et al. “Effects of platform motions on aerodynamic performance and unsteady wake evolution of a floating offshore wind turbine”. In: *Renewable Energy* (143 Dec. 2019).

[21] Binrong Wen et al. “The power performance of an offshore floating wind turbine in platform pitching motion”. In: *Energy* (154 July 2018).

[22] Abdolrahim Rezaeiha et al. “CFD Simulation of Two Tandem Floating Offshore Wind Turbines in Surge Motion”. In: *Journal of Physics: Conference Series* (2020).

[23] Huang Yang et al. “Numerical Study of Wake Interactions between Two Floating Offshore Wind Turbines”. In: *Proceedings of the International Offshore and Polar Engineering Conference* (June 2018), pp. 541–548.

[24] Lei Xue et al. “Wake Interactions of Two Tandem Semisubmersible Floating Offshore Wind Turbines Based on FAST.Farm”. In: *J. Mar. Sci. Eng* 10 (12 Dec. 2022).

[25] Alireza Arabgolarcheh et al. “Modelling of two tandem floating offshore wind turbines using an actuator line model”. In: *Renewable Energy* 216 (2023), p. 119067. DOI: https://doi.org/10.1016/j.renene.2023.119067. URL: https://www.sciencedirect.com/science/article/pii/S0960148123009813.

[26] Navid Belvasi et al. “Far-Wake Meandering of a Wind Turbine Model with Imposed Motions: An Experimental S-PIV Analysis”. In: *Energies* 15.20 (2022). DOI: 10.3390/en15207757. URL: https://www.mdpi.com/1996-1073/15/20/7757.

[27] Alessandro Fontanella et al. “UNAFLOW: a holistic wind tunnel experiment about the aerodynamic response of floating wind turbines under imposed surge motion”. In: *Wind Energy Science* (Sept. 2019).

[28] Alessandro Fontanella et al. “Wind tunnel investigation of the wake-flow response for a floating turbine subjected to surge motion”. In: *Journal of Physics: Conference Series* (2022).

[29] Stanislav Rockel et al. “Experimental Study on Influence of Pitch Motion on the Wake of a Floating Wind Turbine Model”. In: *Energies* 7 (4 Mar. 2014), pp. 1954–1985.

[30] William B. Walcott. *Study of Parachute scale effects*. Tech. rep. Flight Accessories Laboratory Aeronautical Systems Division Air Force Systems Command Wright-Patterson Air Force Base, Jan. 1963.

[31] Michael F. Kerho et al. “Neutral buoyant bubbles used as flow tracers in air”. In: *Experiments in Fluids* 16 (1994), pp. 393–400.

[32] Matthias Kühn et al. “Large-scale tomographic particle image velocimetry using helium-filled soap bubbles”. In: *Experiments in Fluids* 50 (4 Apr. 2011), pp. 929–948.

[33] Johannes Bosbach et al. “Large scale particle image velocimetry with helium filled soap bubbles”. In: *Experiments in Fluids* 46 (Mar. 2009), pp. 539–547. DOI: 10.1007/s00348-008-0579-0.

[34] Fulvio Scarano. “On the use of helium-filled soap bubbles for large-scale tomographic PIV in wind tunnel experiments.” In: *Exp Fluids 56, 42* (2015).

[35] Giuseppe Carlo Alp Caridi et al. “Helium□filled soap bubbles for vortex core velocimetry”. In: *Exp fluids* 58 (130 Aug. 2017).

[36] David Engler Faleiros et al. “Helium-filled soap bubbles tracing fidelity in wall-bounded turbulence”. In: *Experiments in Fluids* 59 (56 Feb. 2018).

[37] Daan van der Hoek. *Advances in actuation techniques for wind darm control*. Tech. rep. TU Delft, 2023.

[38] D. Engler Faleiros. *Soap bubbles for large-scale PIV*. Tech. rep. TU Delft, 2021.

[39] Fulvio Scarano. *AE4-180 reader 2013 rev 11-02-13*. 2013.

[40] Suzanne Hendriks et al. *Determination of the Flow Distribution Around a NACA-0012 Airfoil at Varying Angles of Attack*. Tech. rep. TU Delft, 2023.

[41] Gerrit Einte Elsinga. *Tomographic particle image velocimetry and its application to turbulent boundary layers*. Tech. rep. TU Delft, 2008.

[42] Andreas Schröder Daniel Schanz Sebastian Gesemann. “Shake□The□Box: Lagrangian particle tracking at high particle image densities”. In: *Experiments in Fluids* (2016).

[43] *Open Jet Facility*. TU Delft.nl. https://filelist.tudelft.nl/LR/Organisatie/Afdelingen/ AerodynamicsWindEnergyFlightPerformanceandPropulsion/OJFboek.pdf (accessed Jan. 19, 2024).

[44] Federico Taruffi et al. “An experimental study on the aerodynamic loads of a floating offshore wind turbine under imposed motions”. In: (2023). DOI: 10.5194/wes-2023-86. URL: https://doi.org/10.5194/wes-2023-86.

[45] *Photron | FASTCAM SA1.1*. URL: https://techimaging.com/products/legacy/legacy-high-speed/product/photron-fastcam-sa1-1.

[46] *LED Illumination Units*. URL: https://www.lavision.de/en/applications/materials-testing/system-components/illumination/.

[47] *Mini45-E Transducer*. URL: https://www.ati-ia.com/products/ft/ft_models.aspx?id=mini45.

[48] Knud Erik Meyer. *Error Analysis - slides*. URL: https://learn.inside.dtu.dk/d2l/le/content/142652/viewContent/543646/View.

A

Thrust

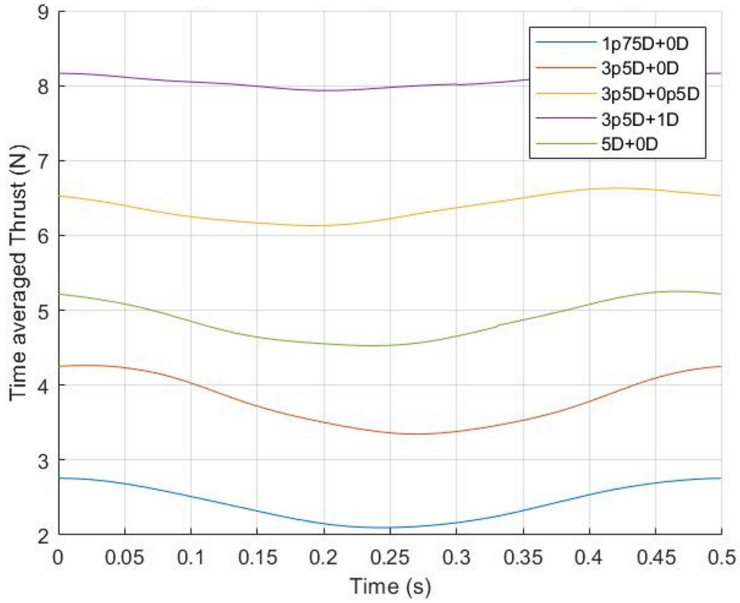

Figure A.1: Time averaged thrust per cycle at a downwind turbine located at various distances downwind while the upstream turbine is moving with a 2 Hz sinusoidal surge motion measured by the load cell - 8 Hz low pass filter.

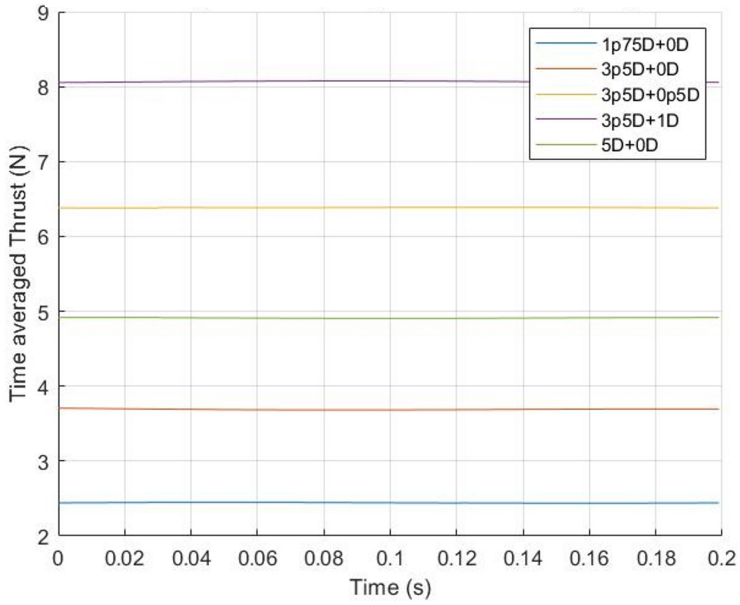

Figure A.2: Time averaged thrust per cycle at a downwind turbine located at various distances downwind while the upstream turbine is moving with a 5 Hz sinusoidal surge motion measured by the load cell - 8 Hz low pass filter.

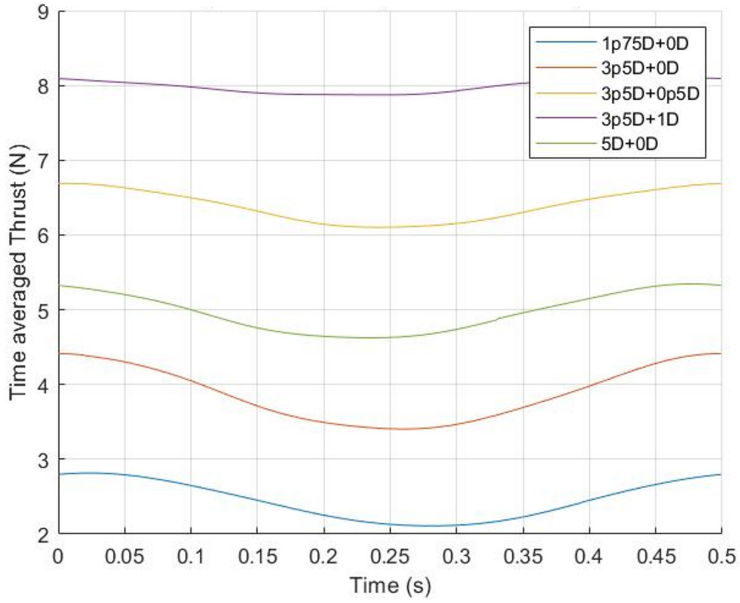

Figure A.3: Time averaged thrust per cycle at a downwind turbine located at various distances downwind while the upstream turbine is moving with a 2 Hz sinusoidal pitch motion measured by the load cell - 8 Hz low pass filter.

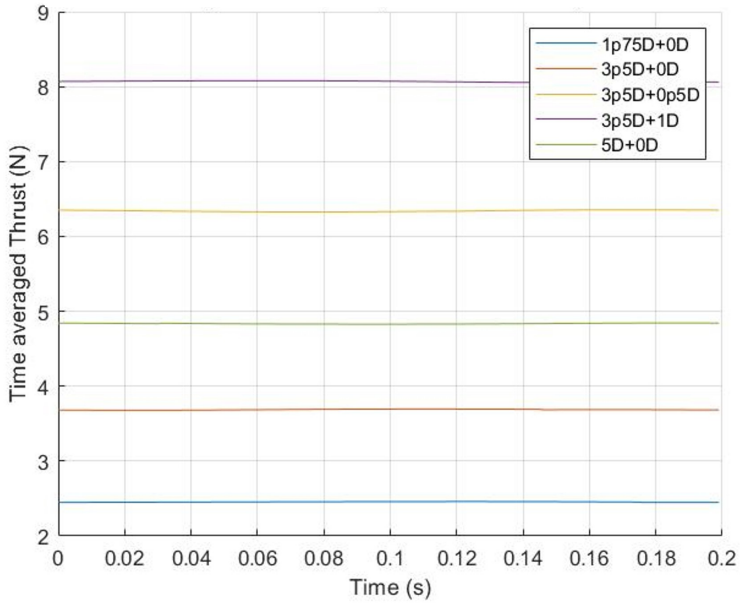

Figure A.4: Time averaged thrust per cycle at a downwind turbine located at various distances downwind while the upstream turbine is moving with a 5 Hz sinusoidal pitch motion measured by the load cell - 8 Hz low pass filter.

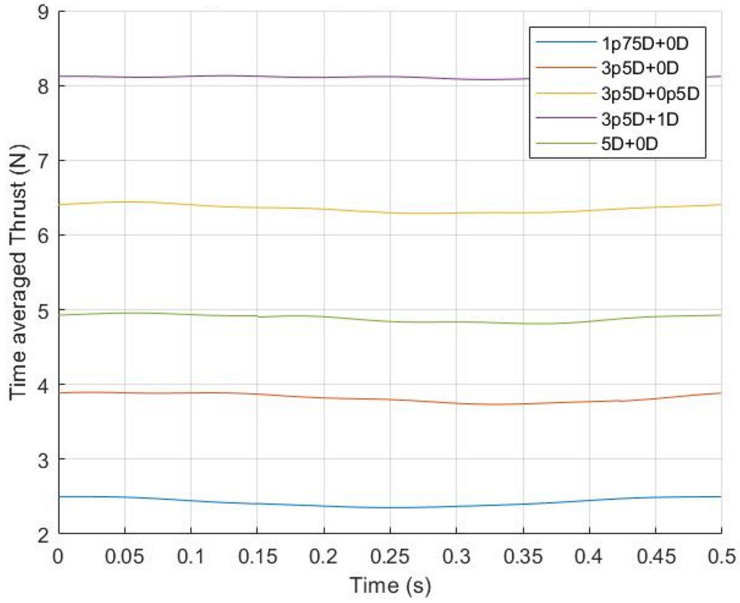

Figure A.5: Time averaged thrust per cycle at a downwind turbine located at various distances downwind while the upstream turbine is moving with a 2 Hz sinusoidal yaw motion measured by the load cell - 8 Hz low pass filter.

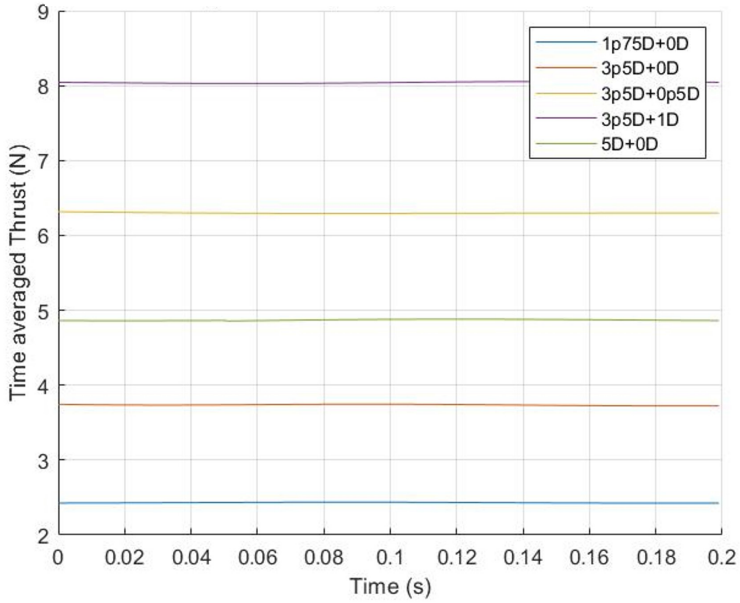

Figure A.6: Time averaged thrust per cycle at a downwind turbine located at various distances downwind while the upstream turbine is moving with a 5 Hz sinusoidal yaw motion measured by the load cell - 8 Hz low pass filter.

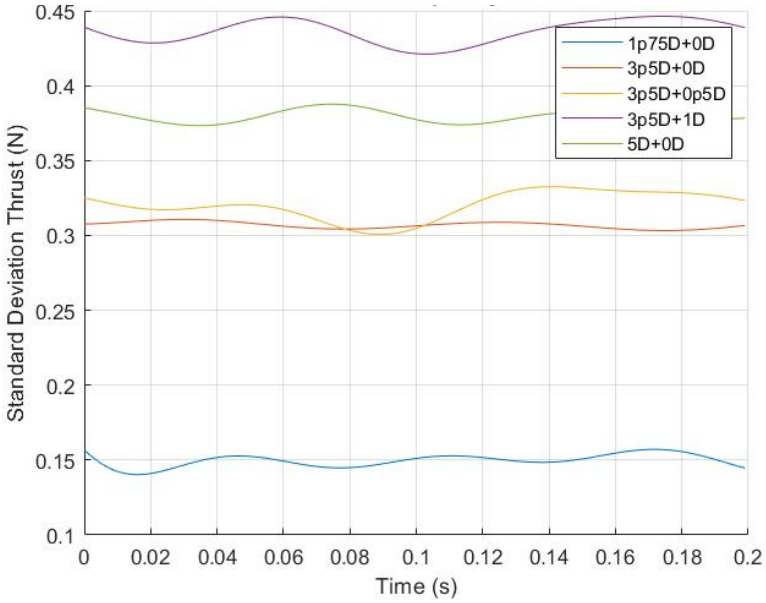

Figure A.7: Standard deviation of the thrust per cycle at a downwind turbine located at various distances downwind while the upstream turbine is turned off measured by the load cell - 8 Hz low pass filter.

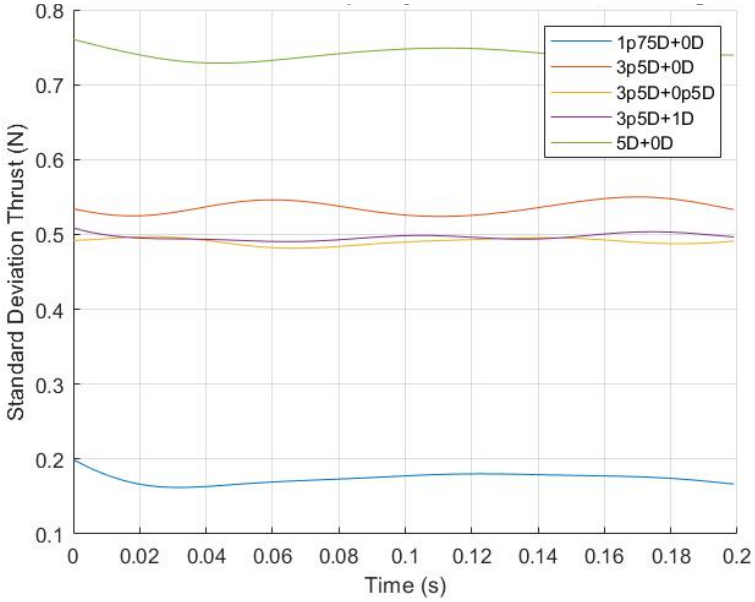

Figure A.8: Standard deviation of the thrust per cycle at a downwind turbine located at various distances downwind while the upstream turbine is moving but standing still measured by the load cell - 8 Hz low pass filter.

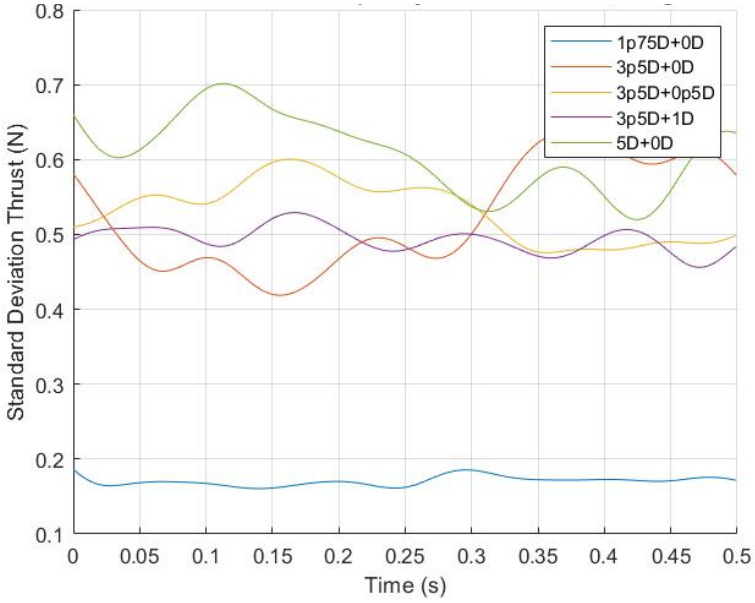

Figure A.9: Standard deviation of the thrust per cycle at a downwind turbine located at various distances downwind while the upstream turbine is moving with a 2 Hz sinusoidal surge motion measured by the load cell - 8 Hz low pass filter.

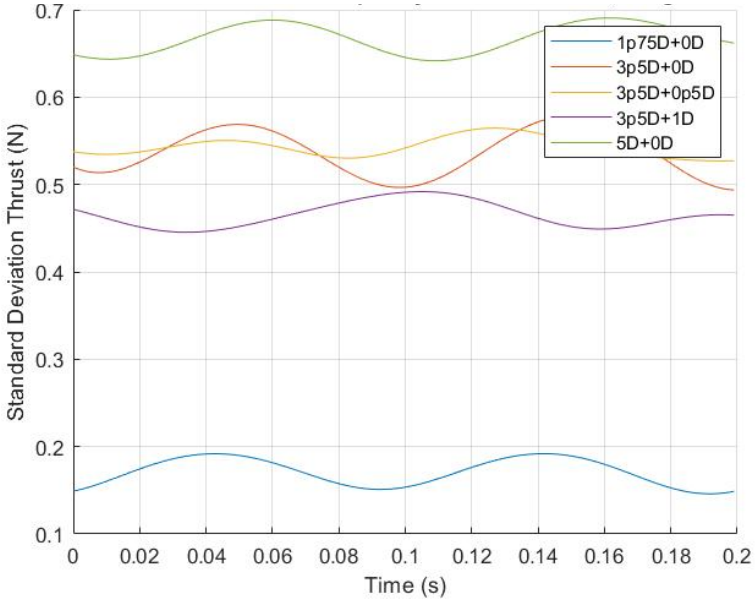

Figure A.10: Standard deviation of the thrust per cycle at a downwind turbine located at various distances downwind while the upstream turbine is moving with a 5 Hz sinusoidal surge motion measured by the load cell - 8 Hz low pass filter.

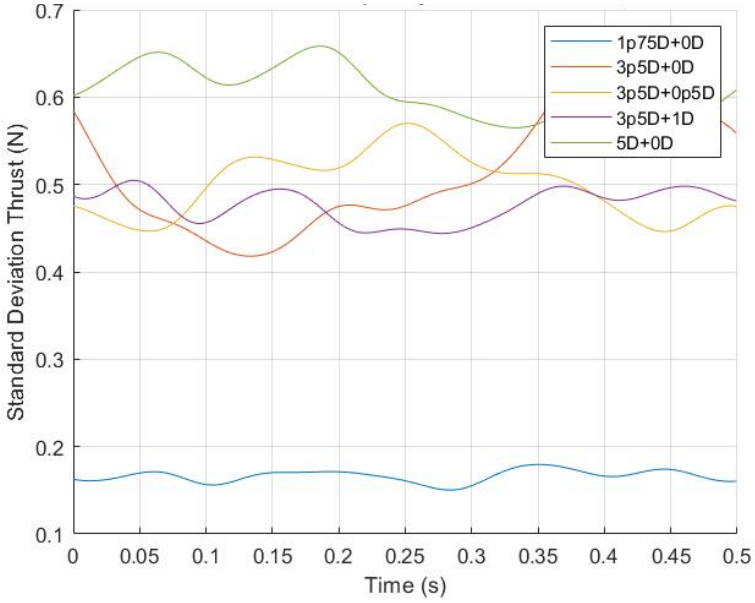

Figure A.11: Standard deviation of the thrust per cycle at a downwind turbine located at various distances downwind while the upstream turbine is moving with a 2 Hz sinusoidal pitch motion measured by the load cell - 8 Hz low pass filter.

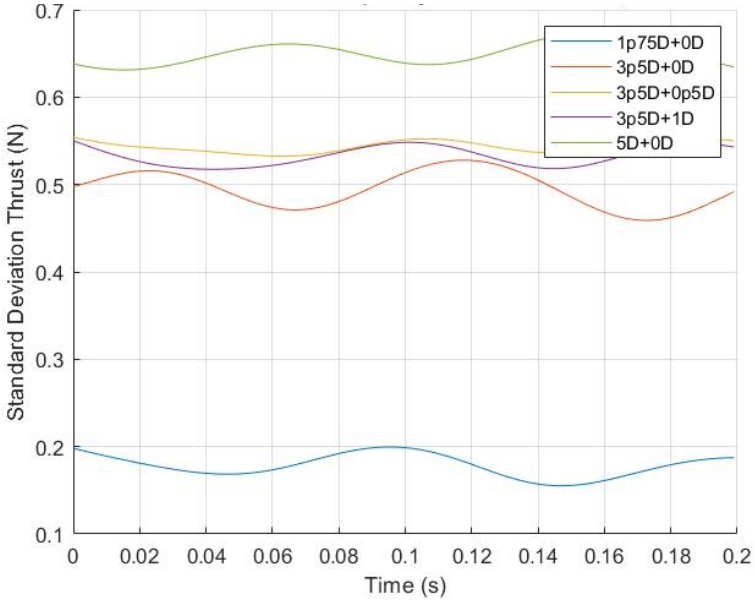

Figure A.12: Standard deviation of the thrust per cycle at a downwind turbine located at various distances downwind while the upstream turbine is moving with a 5 Hz sinusoidal pitch motion measured by the load cell - 8 Hz low pass filter.

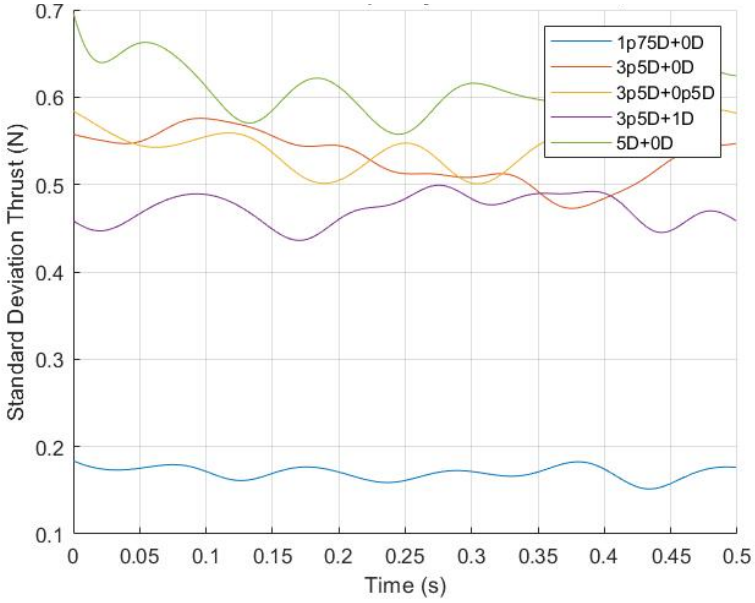

Figure A.13: Standard deviation of the thrust per cycle at a downwind turbine located at various distances downwind while the upstream turbine is moving with a 2 Hz sinusoidal yaw motion measured by the load cell - 8 Hz low pass filter.

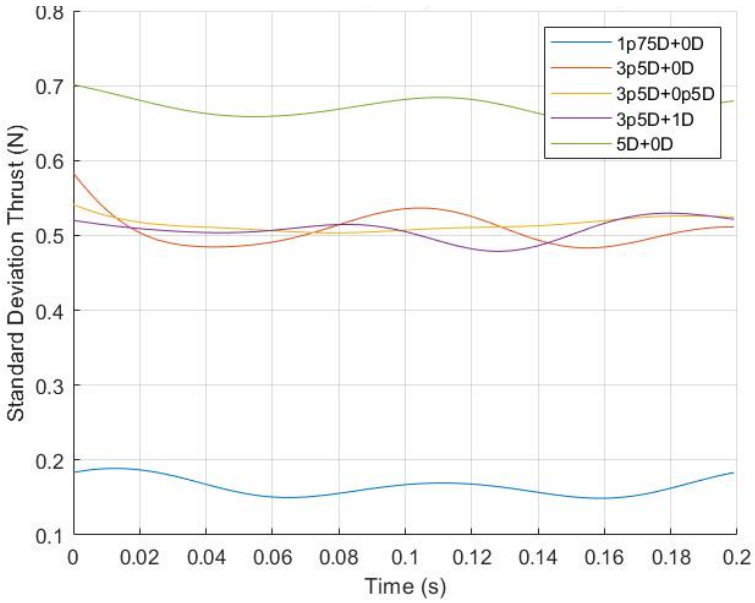

Figure A.14: Standard deviation of the thrust per cycle at a downwind turbine located at various distances downwind while the upstream turbine is moving with a 5 Hz sinusoidal yaw motion measured by the load cell - 8 Hz low pass filter.

B

Power

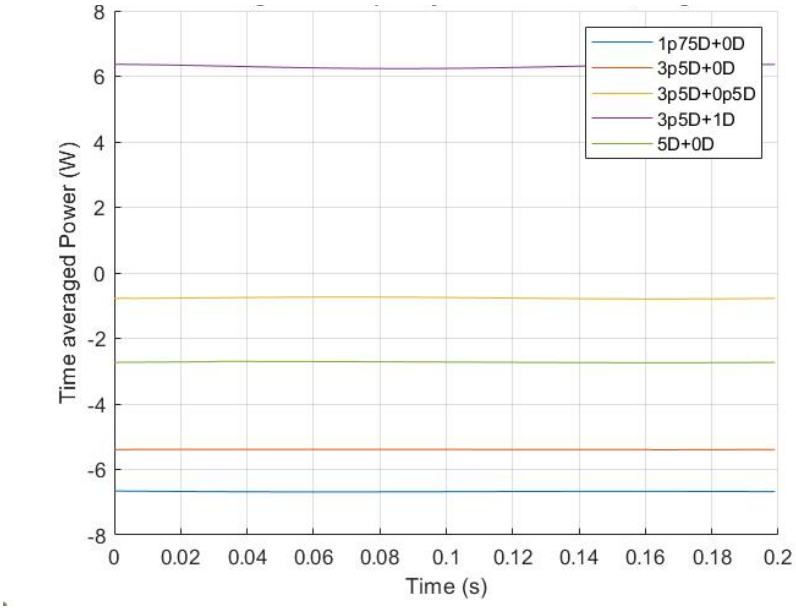

Figure B.1: Time averaged power per cycle at a downwind turbine located at various distances downwind while the upstream turbine is moving with a 2 Hz sinusoidal surge motion measured by the load cell (LLS) - 8 Hz low pass filter.

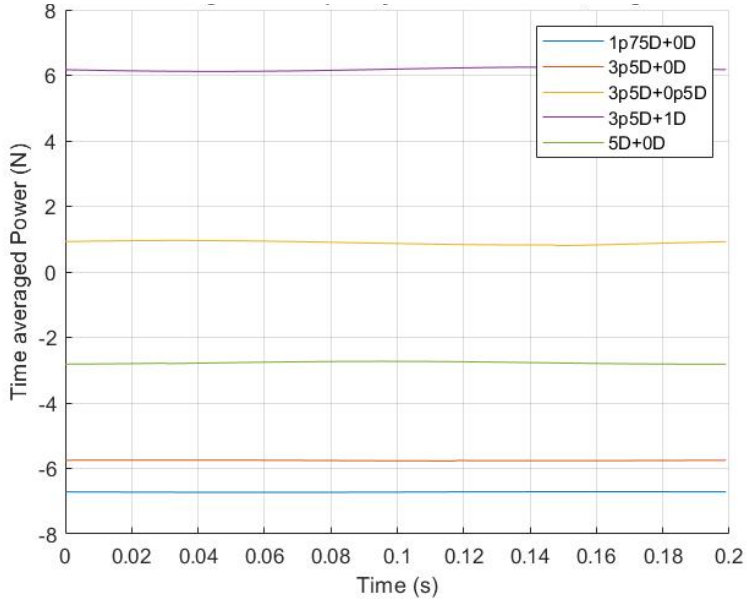

Figure B.2: Time averaged power per cycle at a downwind turbine located at various distances downwind while the upstream turbine is moving with a 5 Hz sinusoidal surge motion measured by the load cell (LLS) - 8 Hz low pass filter.

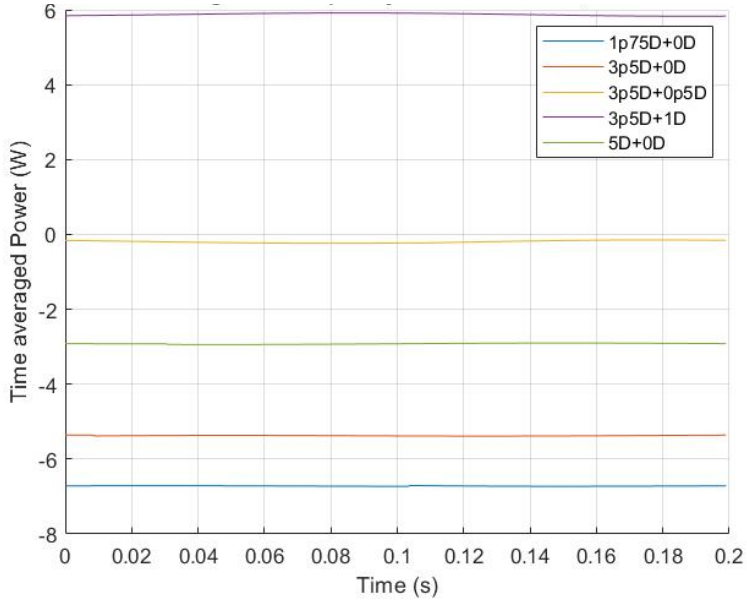

Figure B.3: Time averaged power per cycle at a downwind turbine located at various distances downwind while the upstream turbine is moving with a 2 Hz sinusoidal pitch motion measured by the load cell (LLS) - 8 Hz low pass filter.

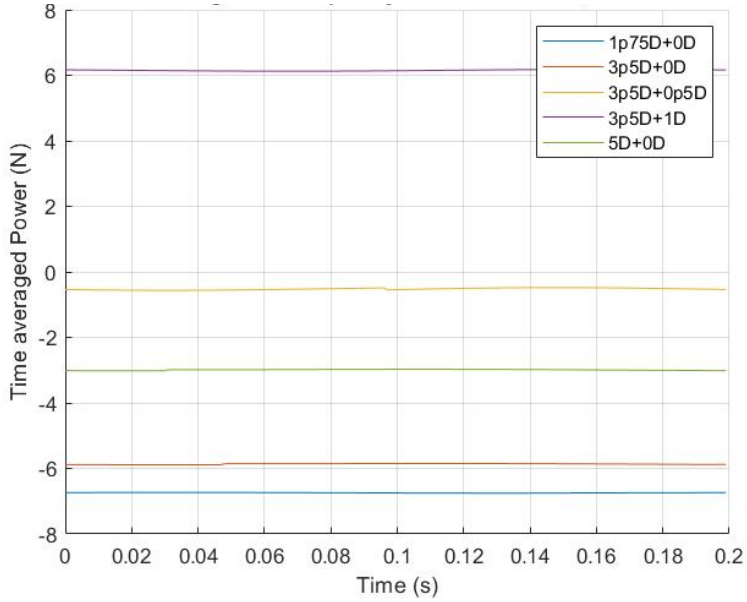

Figure B.4: Time averaged power per cycle at a downwind turbine located at various distances downwind while the upstream turbine is moving with a 5 Hz sinusoidal pitch motion measured by the load cell (LLS) - 8 Hz low pass filter.

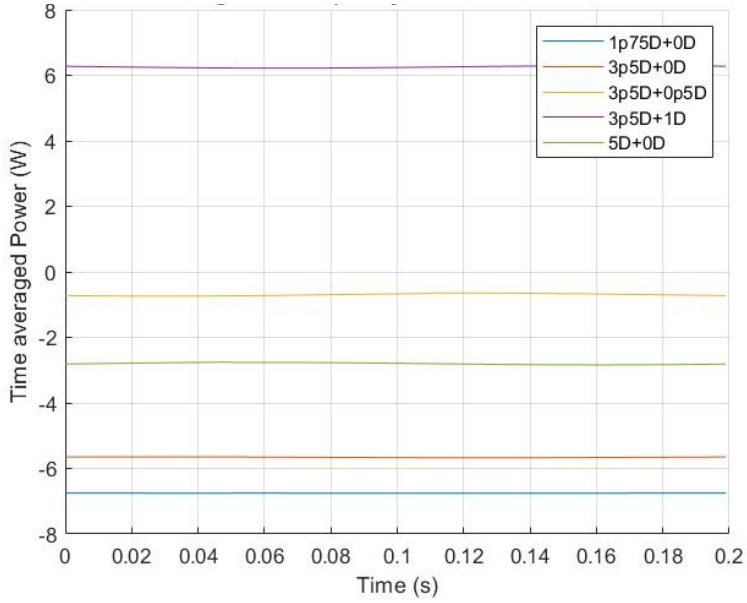

Figure B.5: Time averaged power per cycle at a downwind turbine located at various distances downwind while the upstream turbine is moving with a 2 Hz sinusoidal yaw motion measured by the load cell (LLS) - 8 Hz low pass filter.

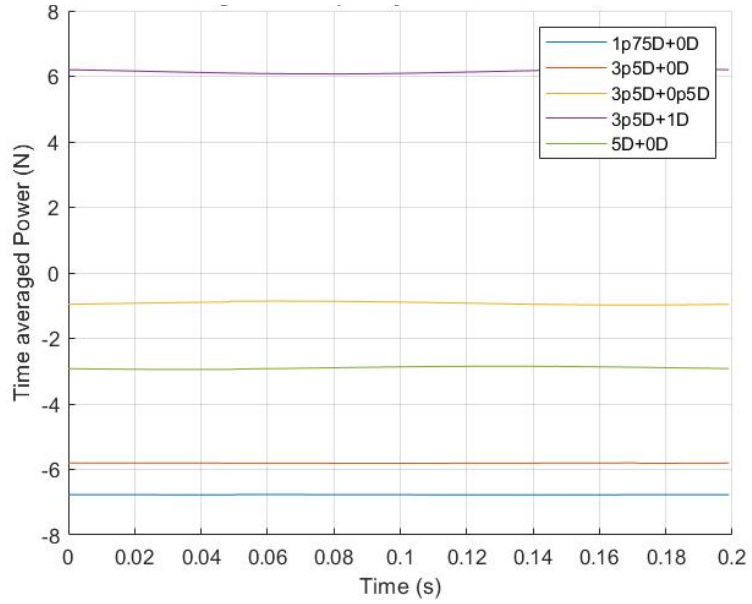

Figure B.6: Time averaged power per cycle at a downwind turbine located at various distances downwind while the upstream turbine is moving with a 5 Hz sinusoidal yaw motion measured by the load cell (LLS) - 8 Hz low pass filter.

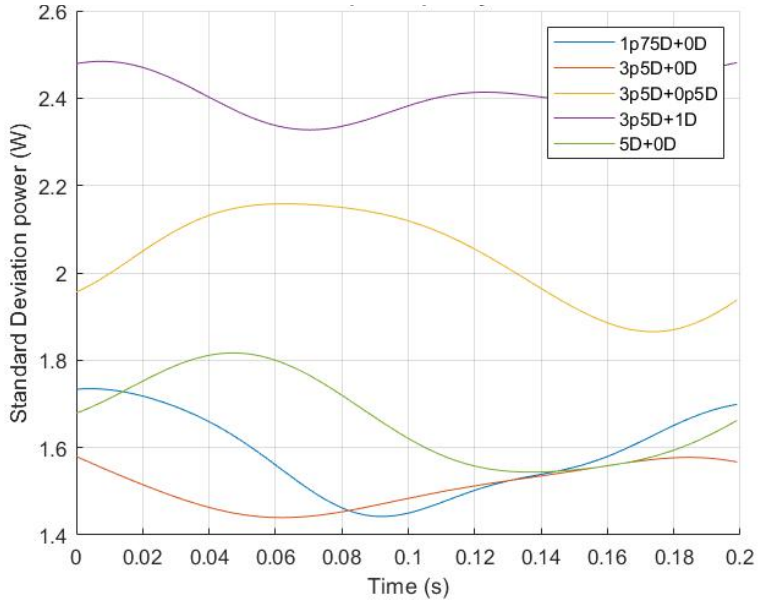

Figure B.7: Standard deviation of the power per cycle at a downwind turbine located at various distances downwind while the upstream turbine is turned off measured by the load cell (LLS) - 8 Hz low pass filter.

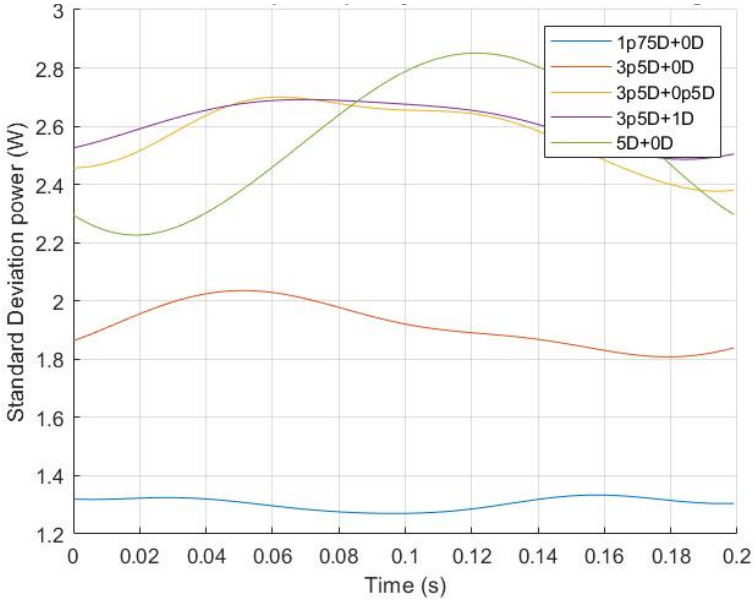

Figure B.8: Standard deviation of the power per cycle at a downwind turbine located at various distances downwind while the upstream turbine is moving but standing still measured by the load cell (LLS) - 8 Hz low pass filter.

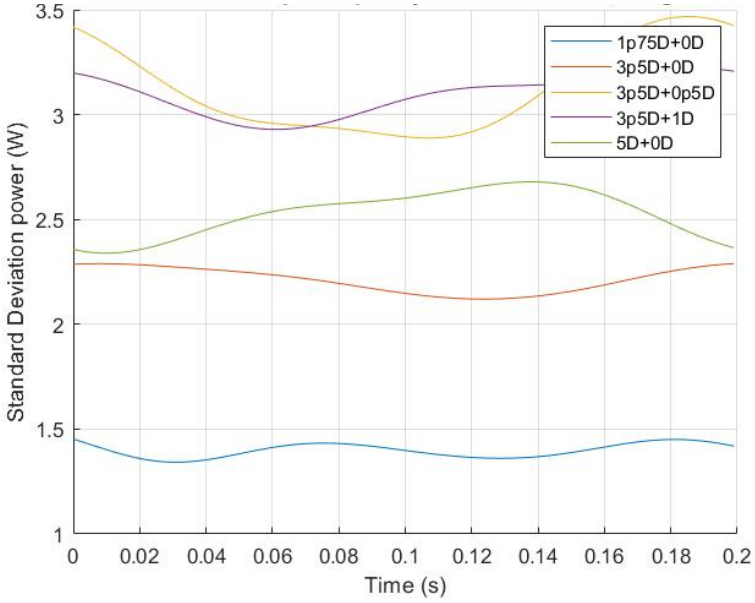

Figure B.9: Standard deviation of the power per cycle at a downwind turbine located at various distances downwind while the upstream turbine is moving with a 2 Hz sinusoidal surge motion measured by the load cell (LLS) - 8 Hz low pass filter.

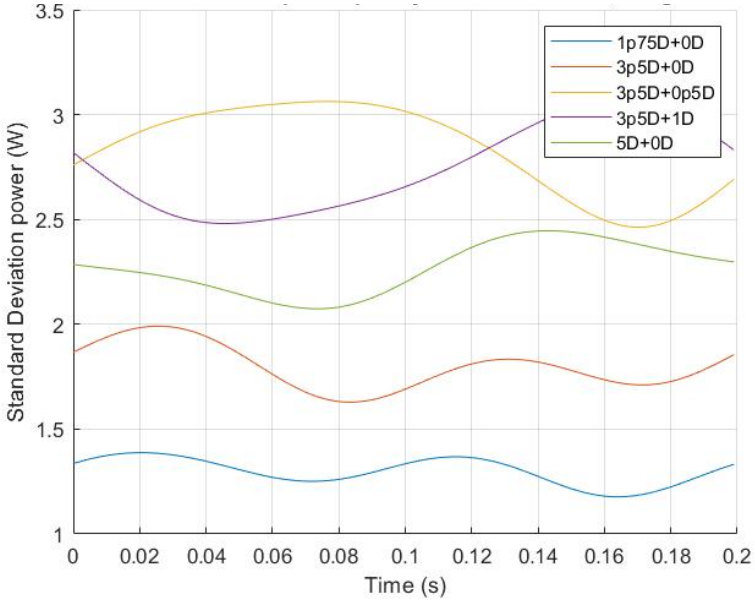

Figure B.10: Standard deviation of the power per cycle at a downwind turbine located at various distances downwind while the upstream turbine is moving with a 5 Hz sinusoidal surge motion measured by the load cell (LLS) - 8 Hz low pass filter.

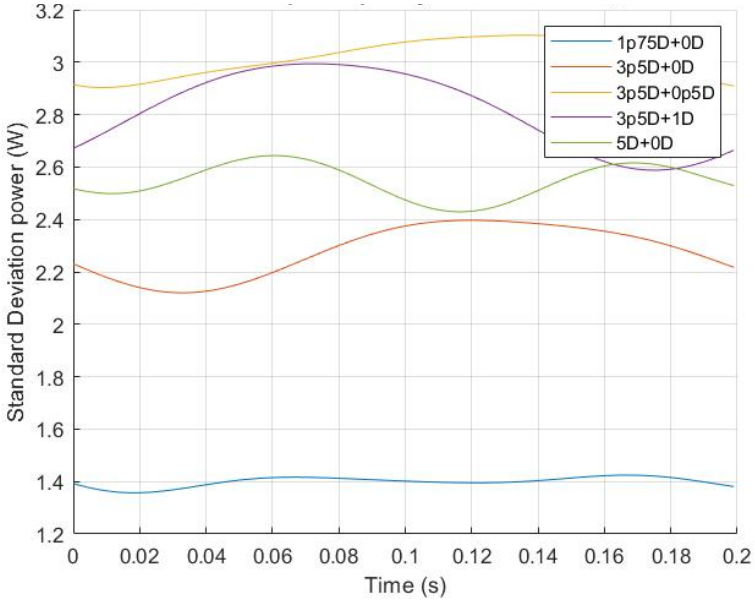

Figure B.11: Standard deviation of the power per cycle at a downwind turbine located at various distances downwind while the upstream turbine is moving with a 2 Hz sinusoidal pitch motion measured by the load cell (LLS) - 8 Hz low pass filter.

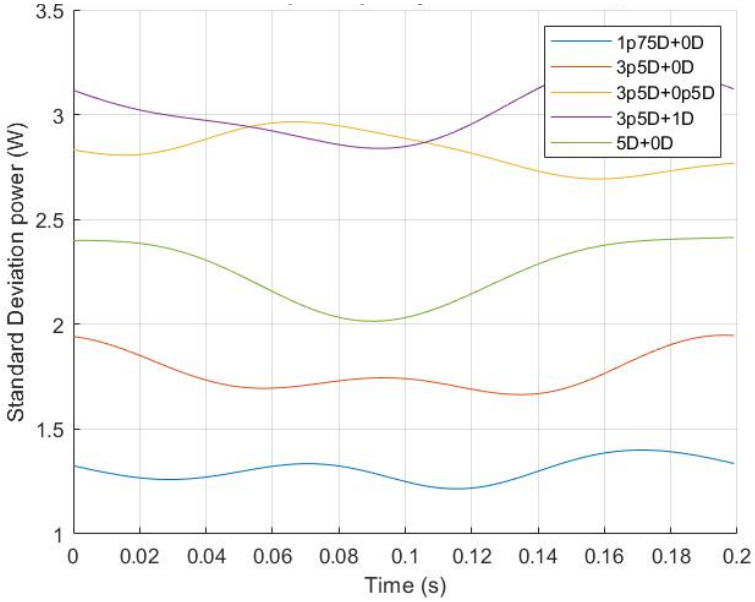

Figure B.12: Standard deviation of the power per cycle at a downwind turbine located at various distances downwind while the upstream turbine is moving with a 5 Hz sinusoidal pitch motion measured by the load cell (LLS) - 8 Hz low pass filter.

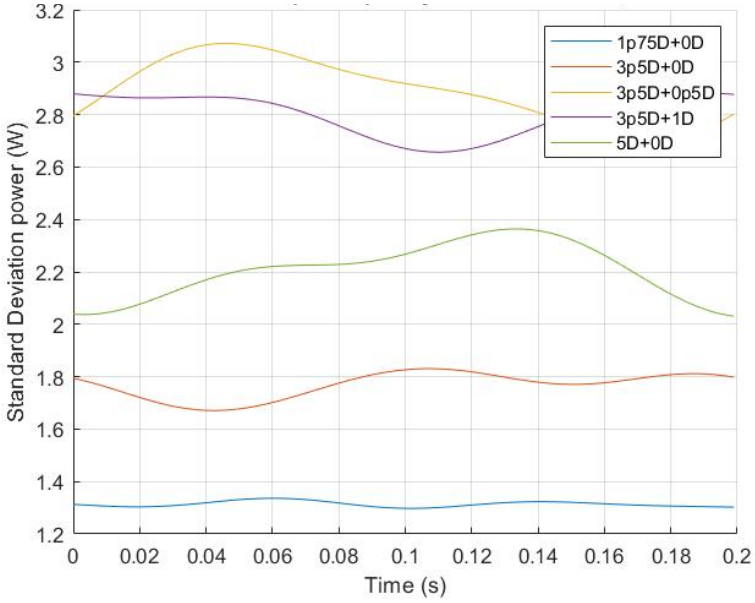

Figure B.13: Standard deviation of the power per cycle at a downwind turbine located at various distances downwind while the upstream turbine is moving with a 2 Hz sinusoidal yaw motion measured by the load cell (LLS) - 8 Hz low pass filter.

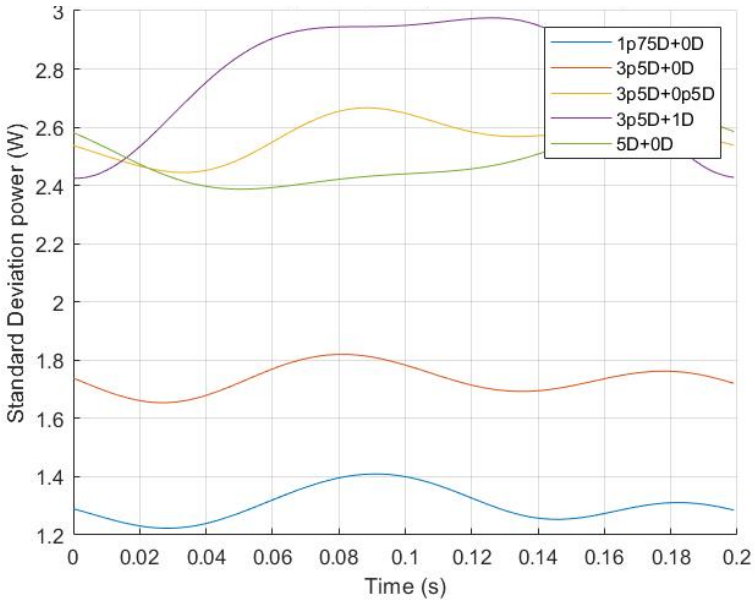

Figure B.14: Standard deviation of the power per cycle at a downwind turbine located at various distances downwind while the upstream turbine is moving with a 5 Hz sinusoidal yaw motion measured by the load cell (LLS) - 8 Hz low pass filter.

C

Torque

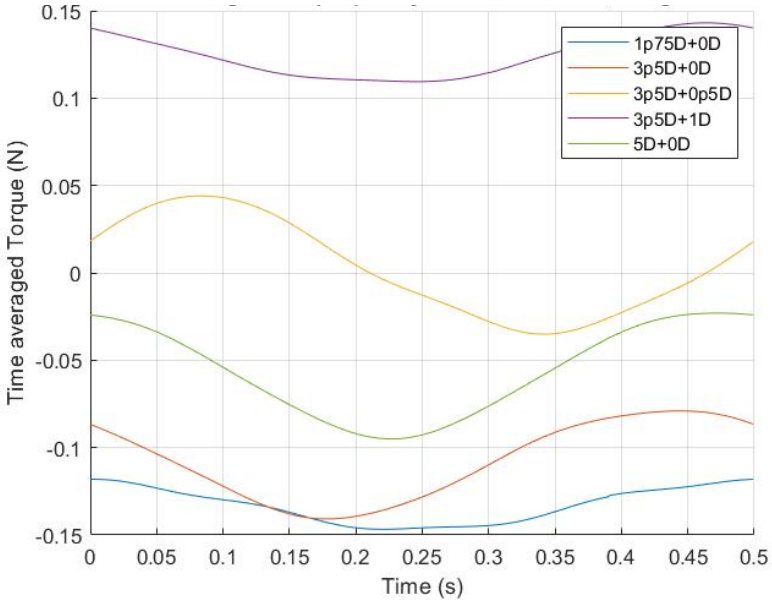

Figure C.1: Time averaged torque per cycle at a downwind turbine located at various distances downwind while the upstream turbine is moving with a 2 Hz sinusoidal surge motion measured by the load cell (LLS) - 8 Hz low pass filter.

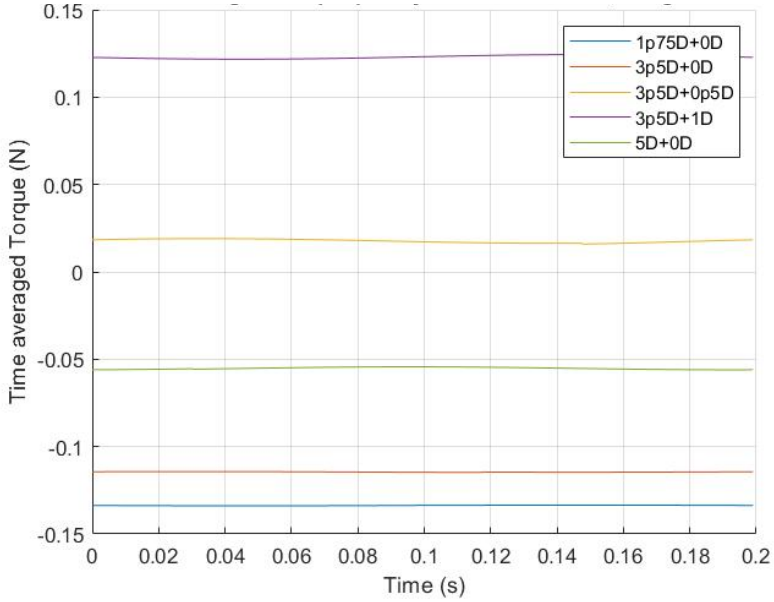

Figure C.2: Time averaged torque per cycle at a downwind turbine located at various distances downwind while the upstream turbine is moving with a 5 Hz sinusoidal surge motion measured by the load cell (LLS) - 8 Hz low pass filter.

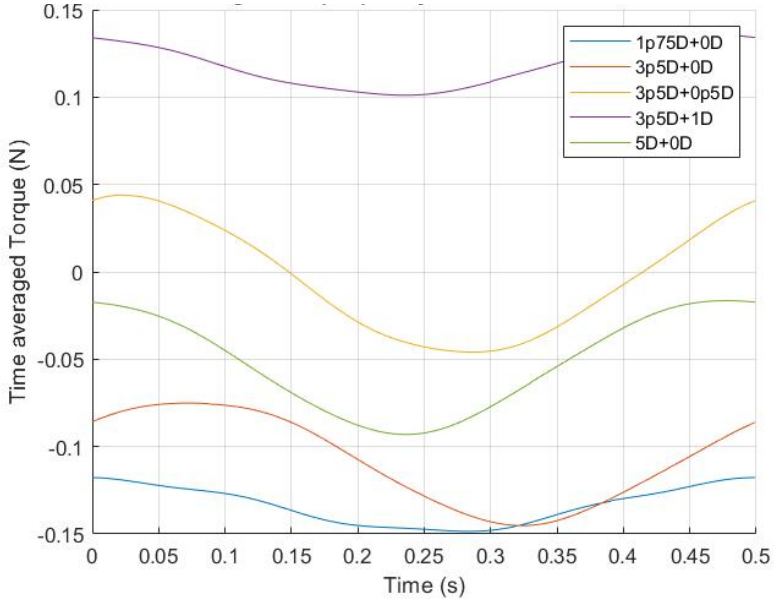

Figure C.3: Time averaged torque per cycle at a downwind turbine located at various distances downwind while the upstream turbine is moving with a 2 Hz sinusoidal pitch motion measured by the load cell (LLS) - 8 Hz low pass filter.

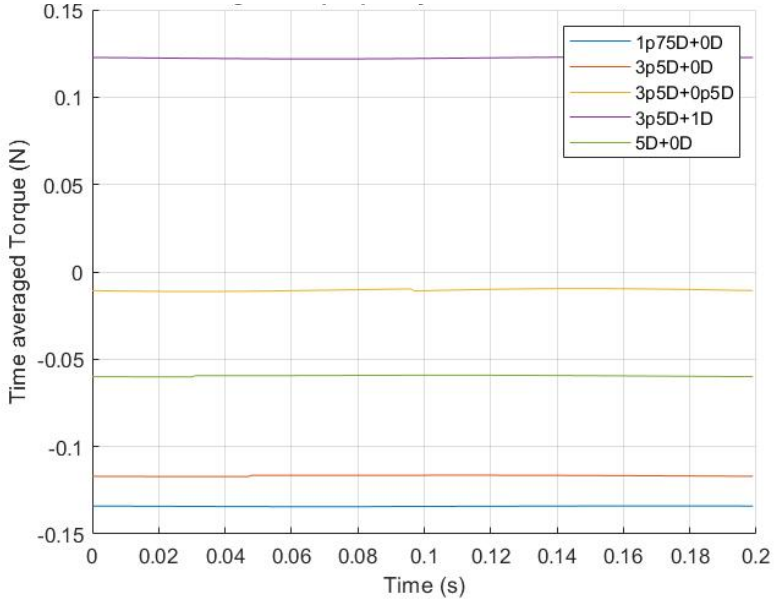

Figure C.4: Time averaged torque per cycle at a downwind turbine located at various distances downwind while the upstream turbine is moving with a 5 Hz sinusoidal pitch motion measured by the load cell (LLS) - 8 Hz low pass filter.

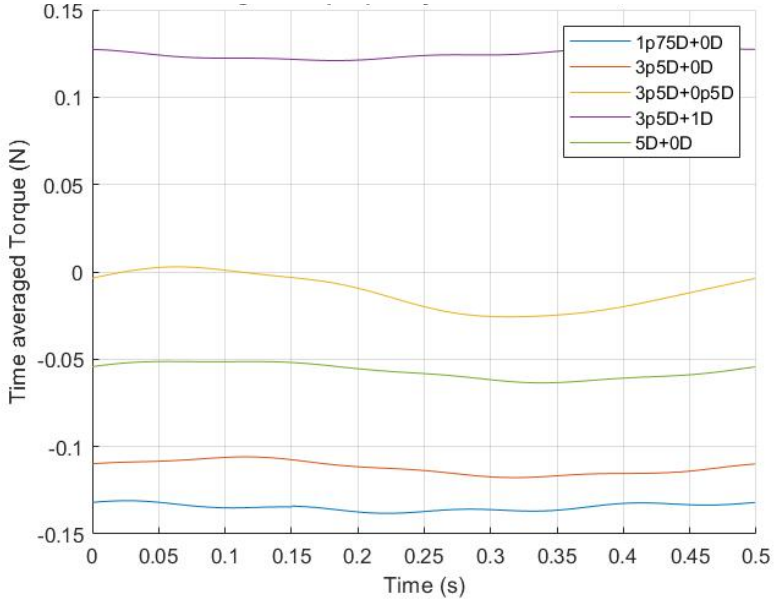

Figure C.5: Time averaged torque per cycle at a downwind turbine located at various distances downwind while the upstream turbine is moving with a 2 Hz sinusoidal yaw motion measured by the load cell (LLS) - 8 Hz low pass filter.

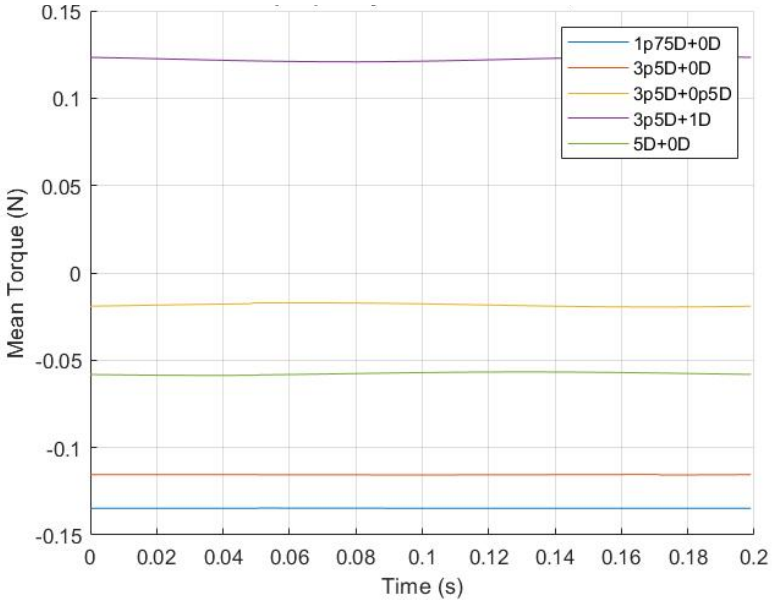

Figure C.6: Time averaged torque per cycle at a downwind turbine located at various distances downwind while the upstream turbine is moving with a 5 Hz sinusoidal yaw motion measured by the load cell (LLS) - 8 Hz low pass filter.

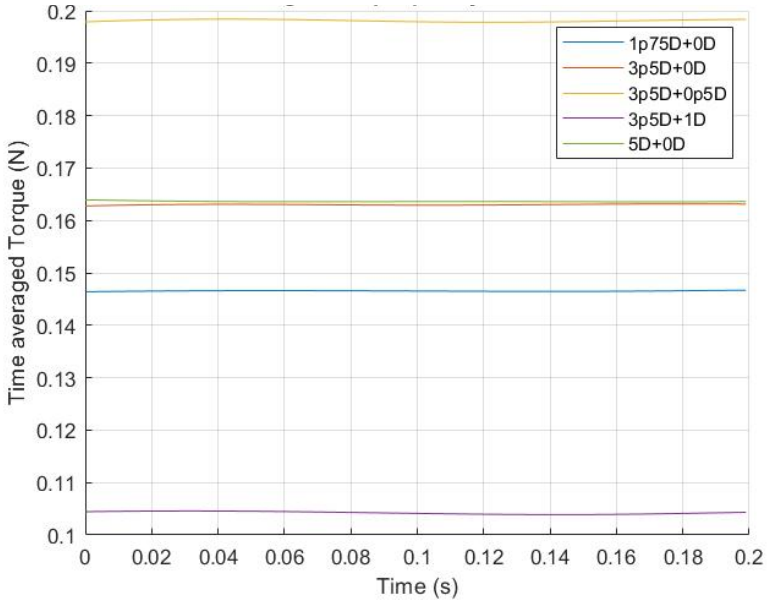

Figure C.7: Standard deviation of the torque per cycle at a downwind turbine located at various distances downwind while the upstream turbine is turned off measured by the load cell (LLS) - 8 Hz low pass filter.

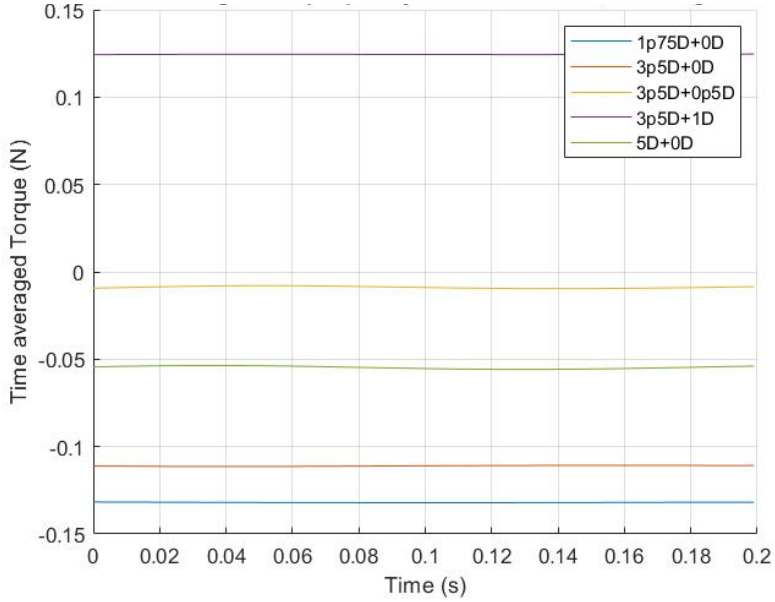

Figure C.8: Standard deviation of the torque per cycle at a downwind turbine located at various distances downwind while the upstream turbine is moving but standing still measured by the load cell (LLS) - 8 Hz low pass filter.

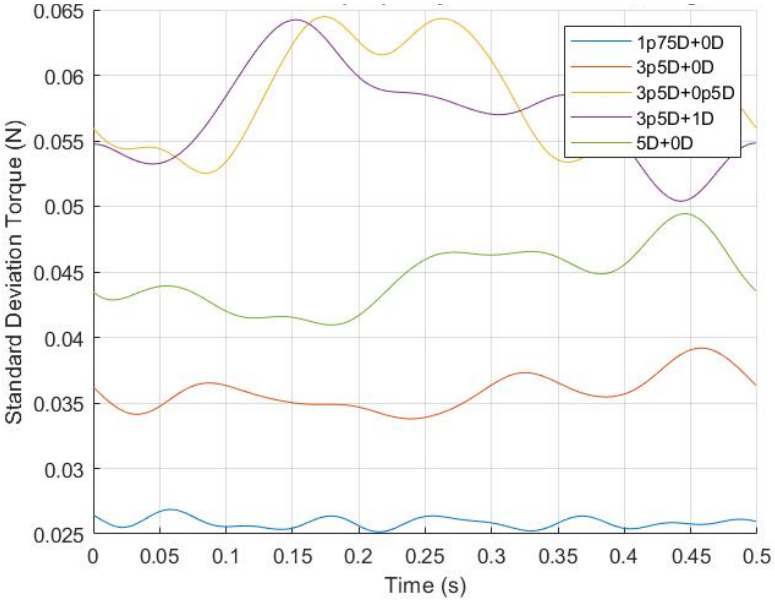

Figure C.9: Standard deviation of the torque per cycle at a downwind turbine located at various distances downwind while the upstream turbine is moving with a 2 Hz sinusoidal surge motion measured by the load cell (LLS) - 8 Hz low pass filter.

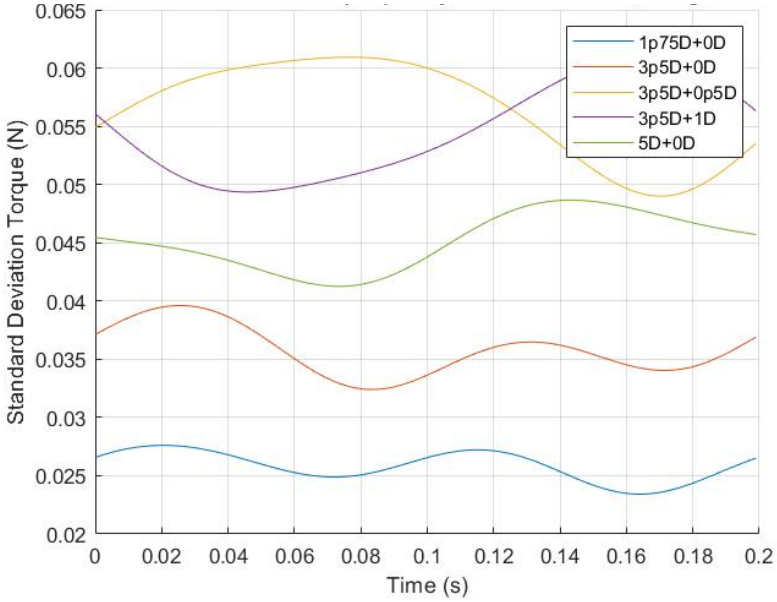

Figure C.10: Standard deviation of the torque per cycle at a downwind turbine located at various distances downwind while the upstream turbine is moving with a 5 Hz sinusoidal surge motion measured by the load cell (LLS) - 8 Hz low pass filter.

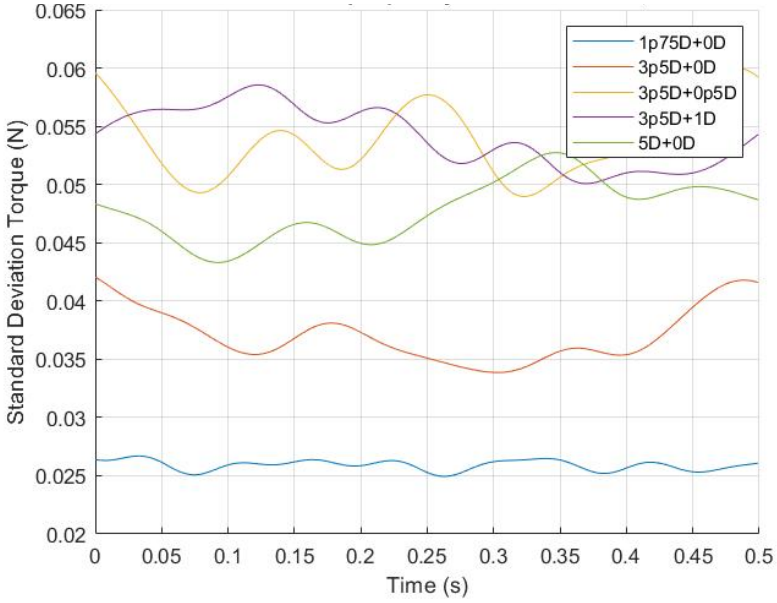

Figure C.11: Standard deviation of the torque per cycle at a downwind turbine located at various distances downwind while the upstream turbine is moving with a 2 Hz sinusoidal pitch motion measured by the load cell (LLS) - 8 Hz low pass filter.

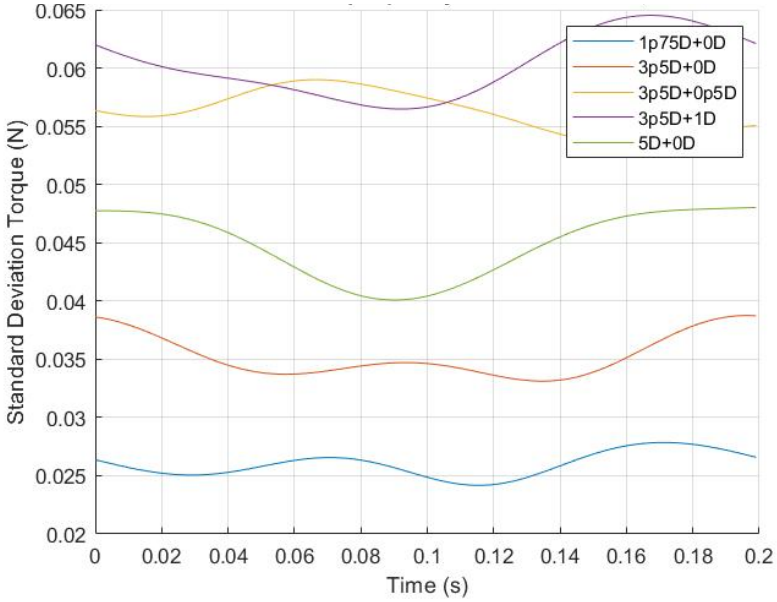

Figure C.12: Standard deviation of the torque per cycle at a downwind turbine located at various distances downwind while the upstream turbine is moving with a 5 Hz sinusoidal pitch motion measured by the load cell (LLS) - 8 Hz low pass filter.

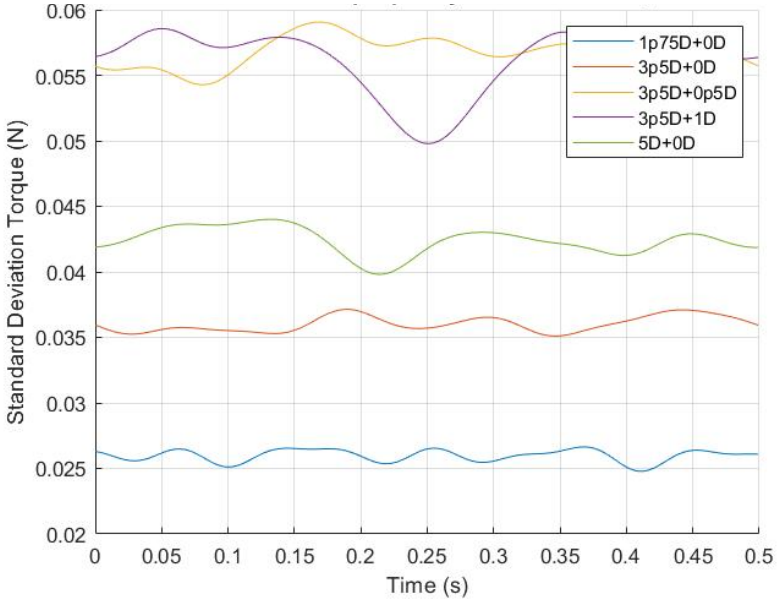

Figure C.13: Standard deviation of the torque per cycle at a downwind turbine located at various distances downwind while the upstream turbine is moving with a 2 Hz sinusoidal yaw motion measured by the load cell (LLS) - 8 Hz low pass filter.

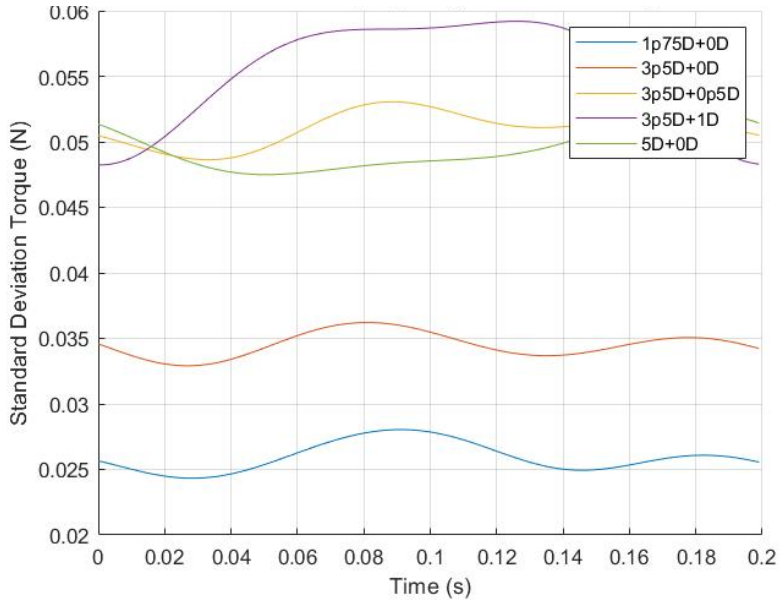

Figure C.14: Standard deviation of the torque per cycle at a downwind turbine located at various distances downwind while the upstream turbine is moving with a 5 Hz sinusoidal yaw motion measured by the load cell (LLS) - 8 Hz low pass filter.